

**High resolution analysis of mitotic metaphase chromosomes with scanning
electron microscopy:**

**Localizing histone H3 modifications with immunogold labeling in barley
(*Hordeum vulgare*)**

Dissertation
from the
Department of Biology I
Electron Microscopy
Ludwig-Maximilians-Universität München

Submitted by
Elizabeth Schroeder-Reiter

August 2004

1. Referee: Prof. Dr. G. Wanner

2. Referee: Prof. Dr. P. Dittrich

Date of oral defense: 22 October, 2004

Table of Contents

| | |
|--|-----------|
| Abbreviations | 4 |
| Introduction | 6 |
| Materials and Methods | 9 |
| <i>Preparation of plant material</i> | 9 |
| <i>Enzymatic tissue dissociation</i> | 10 |
| <i>Laser marked slides</i> | 10 |
| <i>Drop/Cryo fixation and isolation technique for chromosomes</i> | 10 |
| <i>Alternative isolation technique with "suspension preparation"</i> | 11 |
| <i>Enzymatic treatment for removal of nucleoplasm</i> | 11 |
| <i>DNA staining</i> | 12 |
| <i>Immunolabeling</i> | 12 |
| <i>Fluorescent light microscopy</i> | 13 |
| <i>Metallo-enhancement of Nanogold[·]-labeled specimens</i> | 14 |
| <i>Scanning electron microscopy</i> | 15 |
| <i>3D Analysis</i> | 15 |
| <i>Sections of Enterococcus faecalis</i> | 15 |
| <i>Image processing</i> | 16 |
| <i>Quantification</i> | 16 |
| <i>SDS PAGE Western blot and silver staining analysis</i> | 16 |
| | |
| Results | 19 |
| Chromosome Structure | 19 |
| Drop/CryoTechnique applied to different plant and animal species | 19 |
| Isolation of human and chicken chromosomes | 25 |
| Phosphorylated histone H3 (ser10) signal distribution on barley chromosomes as detected by LM | 29 |
| H3P signal distribution on chromosomes of other plant species | 30 |
| | |
| Optimization of immunolabeling procedure for SEM investigation | 33 |
| Shrinkage due to critical point drying | 33 |
| Immunogoldlabeling with different gold markers | 35 |
| Optimizing enhancement time | 38 |
| Influence of protocol steps on labeling efficiency | 39 |
| Influence of post-fixation on chromosome ultrastructure | 45 |
| Effect of fixation technique on labeling efficiency | 46 |
| Quantifying signal distribution | 49 |
| SEM detection of H3P distribution in <i>Hordeum vulgare</i> (barley) | 49 |
| SEM detection of H3P distribution in <i>Luzula sylvatica</i> | 52 |
| Correlative LM and SEM microscopy with Alexa Fluor[®] 488-Nanogold[®] | 55 |
| Effects of Nanogold[·] and fixation technique on H3P signal number and distribution | 57 |
| Immunogold labeling of other histone modifications | 59 |
| | |
| 3D SEM analysis | 66 |
| Depth perception with back-scattered electron BSE signals | 66 |
| Optimizing parameters with an alternative specimen | 70 |
| High resolution localization of signals to chromosome structure with SEM .. | 74 |
| High resolution 3D images of signal distribution | 76 |

| | |
|--|------------|
| Discussion | 79 |
| Universal applicability of drop/cryo chromosome isolation technique | 79 |
| Structural preservation | 83 |
| Immunogold marker size | 85 |
| Metalloenhancement of Nanogold | 88 |
| Theoretical considerations for correlative LM and SEM microscopy | 89 |
| Structure and signal detection in three dimension | 90 |
| Phosphorylated histone H3 (ser10) | 92 |
| H3P“signal gap” at the centromere of barley metaphase chromosomes | 94 |
| Dimethylated histone H3 on lysine 4 and lysine 9 | 94 |
| | |
| Conclusion | 97 |
| Summary | 98 |
| Zusammenfassung | 102 |
| References | 106 |
| Acknowledgements | 114 |
| Appendix | 115 |
| | |
| <i>Curriculum vitae</i> | 116 |

Abbreviations:

| | |
|-----------------|---|
| 3D | Three dimensional |
| ACA | Aminocaproic acid |
| AFM | Atomic force microscope |
| Ag | Silver |
| ADP | Adenine diphosphate |
| ANG | AlexaFluor®488-Nanogold® |
| AP | Alkaline phosphatase |
| APM | O-methyl-O(2-nitrotolyl)-N-isopropyl-phosphoramidothioat, amiprophosmethyl |
| APS | Ammonium peroxodisulfate |
| Au | Gold |
| BciP | 5'-brom-4'-chloro-3-indolyl phosphate disodium salt |
| bp | Base pairs |
| BSA | Bovine serum albumin |
| BSE | Back-scattered electron |
| CCD | Cacodylate buffer |
| CENP | Centromere protein |
| CPD | Critical point drying |
| Cy3 | Indocarbocyanin |
| DAPI | 4', 6-diamidino-2-phenylindol |
| DIC | Differential interference contrast |
| DIN A4 | "Deutsche Industrie Norm" (German paper standard 20.99 x 29.7 cm) |
| DMF | Dimethyl formamid |
| DMSO | Dimethyl sulfoxide |
| DNA | Desoxyribonucleic acid |
| EDX | Energy dispersive X-ray |
| Fab' | Fragment (antigen binding) (of immunoglobulin) |
| FESEM | Field emission scanning electron microscope |
| FITC | Fluorescein isothiocyanate |
| FNG | Fluorescein-Nanogold® |
| GFP | Green fluorescent protein |
| H3M (K4) | Dimethylated histone H3 (at lysine postion 4) |
| H3M (K9) | Dimethylated histone H3 (at lysine postion 9) |
| H3P | Phosphorylated histone H3 (at serine position 10) |
| HP | Heterochromatin protein |
| IgG | Immunoglobulin class G |
| IPK | Institute of Plant genetics and Crop Plant Research |
| ISH | <i>In situ</i> hybridization |
| LM | Light microscope (also microscopy, microscopic) |
| LMU | Ludwig-Maximilians-Universität (Munich, FRG) |
| MTC | Microtubule organizing center |
| NBT | p-nitroblue tetrazolium chloride |
| NG | Nanogold® |
| PAA | polyacrylamide |
| PBS | Phosphate buffered saline |
| Pt blue | (CH ₃ CN) ₂ Pt Bis(Acetonitrile)-platinum oligomere = platinum blue |
| RT | Room temperature |

| | |
|--------------------|---|
| RNA | Ribonucleic acid |
| SDS PAGE | Sodium dodecyl sulfate poly amide gel electrophoresis |
| SE | Secondary electron |
| SEM | Scanning electron microscope (also microscopy, microscopic) |
| SMC | Structural maintenance of chromosome (protein family) |
| SSC | Saline sodium citrate |
| TBST | Tris buffer salt + Tween |
| TCA | Trichloroacetic acid |
| TEM | Transmission electron microscopy |
| TEMED | N,N,N',N'-Tetramethylethylenediamine |
| TPII | Topoisomerase II |
| Tris | Ethylenediaminetetraacetic acid |
| TritonX-100 | Alkylphenyl polyethylenglycol |
| Tween | Polyoxyethylenesorbitan monolaurate |
| YAG | Yttrium aluminum garnet |

Introduction

Chromosomes have been a source of intense study since the end of the nineteenth century, from which time they have been characterized with light microscopy and with extensive cytological and molecular techniques. They are composed of approximately equal parts of DNA, histone proteins and non-histone proteins (EARNSHAW, 1991). It is generally accepted that the basic unit of chromatin, the nucleosome, is formed by a stretch 146 bp of DNA wrapping around a histone octamer core (ARENTS *et al.*, 1991). Since the DNA molecule is considered continuous for each chromosome, serial nucleosomes form a 10 nm elementary fibril that coils to form a solenoid, manifested as a 30 nm fibril (RATTNER & LIN, 1988). Although there are several models postulated, there is no consensus on the higher order of chromosome structure (DUPRAW, 1965; MANUELIDIS & CHEN, 1990; COOK, 1995; WANNER & FORMANEK, 2000; STACK & ANDERSON, 2001; WOODCOCK & DIMITROV, 2001). It has become evident that consensus can be reached when data from different areas of research converge, which emphasizes the importance of correlative approaches.

In addition to structural analysis of chromosomes, much research has been focused on functional analysis. An area of recent interest in chromosome function concerns histone proteins. It is postulated that histones play an important role in control of gene expression by regulating access to DNA. Histone amino-termini protrude from the nucleosome core and are subject to a variety of post-translational modifications – acetylation (on lysines), phosphorylation (on serines and threonines), methylation (on lysines and arginines), ubiquitination (on lysine) ADP-ribosylation (on glutamic acid residues) (PEREZ-BURGOS *et al.*, 2004). These modifications have been proposed to form a "histone code" that contributes to regulation of gene expression and to chromatin remodelling (JENUWEIN & ALLIS, 2001). Because of the intimate contacts between histones and DNA, these histone modifications are believed to alter chromatin structure and, in turn, play important regulatory roles in many DNA-templated processes.

It is surprising, given the resources available, that the current light microscopic achievements for functional investigations of chromosomes with labeling techniques (*e.g.* using *in situ* hybridization, confocal microscopy, M-FISH, chromosome painting) have only been accompanied by few SEM studies (JACK *et al.*, 1985; PELLING & ALLEN, 1993; MARTIN *et al.*, 1995; WANNER & FORMANEK, 1995). A major challenge in investigation of chromosomes and nuclear architecture is interpreting data in context. This is the aim of *in situ* investigation, but any microscopic assay is accompanied by both advantages and disadvantages in colocalizing

molecular and cytological details to overall structure. To this end, combining scanning electron microscopy (SEM) and fluorescent light microscopy (LM) techniques has great potential. In LM, chromosomes can be visualized by various DNA-specific counterstains or with GFP-labeled chromatin, with the considerable (if elusive) advantage of monitoring nuclear dynamics with live cell specimens. Only fluorescent structures can be visualized in LM, but multiple labeling is possible. LM resolution is currently limited to 250 nm, allowing three dimensional visualization chromosomes within a nucleus, but not of individual chromosomes. SEM has a 100-fold increase in resolution and can visualize structures down to the range of the DNA molecule on fixed chromosomes. In SEM, whole 3D structures can be visualized, but the composition of these structures must be determined by specific labeling.

In the past two decades high resolution scanning electron microscopy (SEM) has provided considerable information about chromosome ultrastructure down to nanometer scale (HARRISON *et al.*, 1982; ALLEN *et al.*, 1986; SUMNER, 1991; WANNER *et al.*, 1991; WANNER & FORMANEK, 1995, 2000). SEM investigations of chromosomes were limited for a long time by chromosome preparation methods; the classical chromosome drop technique developed for mammalian chromosomes involves an air-drying step that leads to artificial surface layers (ALLEN *et al.*, 1988; SUMNER, 1991). This was largely improved with the establishment of the drop/cryo technique for plant chromosomes (MARTIN *et al.*, 1994). Although well-preserved barley chromosome preparations are routinely established in our lab, specific protein and DNA sequence detection with immunolabeling for SEM has proved unsatisfactory for many years because of drastically low marking efficiency. Since immunolabeling has been successfully applied for detection of surface proteins for a variety of bacteria (RUHLAND *et al.*, 1993; GALLI *et al.*, 1989; JAURIS-HEIPKE *et al.*, 1999), we suspected that lack of labels on chromosomes could be due to sterical hindrance of the rather large gold-labeled antibody into the densely packed chromatin. Nanogold® products, developed in the early 1990s, showed promise of improved marking efficiency and stability because of their small covalently bound gold markers. In addition, digital recording of SEM images, a relatively recent acquisition in our lab, greatly facilitates 3D imaging and parallel experimental assays.

The aim of the present investigation was to test applicability of the drop/cryo technique for fixation and isolation of chromosomes of different plant and animal species, and to establish an alternative "suspension" technique to test its applicability for SEM investigation of chromosome structure. In addition, a goal was to optimize immunolabeling techniques on bar-

ley chromosomes for high resolution detection of specific proteins in SEM. For good comparison and signal correlation of LM and SEM results, immunolabeling was based on detection of phosphorylated histone 3 at serine position 10 (H3P), as its behavior is well documented for barley chromosomes (HOUBEN *et al.* 1999; MANZANERO *et al.*, 2000; MANZANERO *et al.*, 2002). The main goal was to colocalize histone H3 functional modifications with structural elements of chromosomes.

Materials and Methods

Preparation of plant material

Plant material that was available as seeds (Table 1) were sown in petri dishes on filter paper moistened with *aqua dest*, and were kept undisturbed in the dark 4°C for 2 days. Hydrated seeds were then exposed to room temperature for 6 hours until the primary root was visible. Sprouted seeds were incubated for 18 h in petri dishes moistened with hydroxyurea (1.25 mM) for synchronization, *i.e.* accumulation of chromosomes in the S-phase of the cell cycle. Sprouts were rinsed three times with *aqua dest*, and subsequently incubated for 2-4 h in petri dishes moistened with a 1:20 diluted (in *aqua dest*) solution of amiprophosmethyl (APM, 4 μ M stock solution dissolved in DMSO) for interruption of spindle assembly and arrestation of mitosis. Sprouts were washed three times in *aqua dest*, after which the root tips (at this point ranging in length between 5-10 mm) were removed with tweezers and incubated in ice water overnight to prevent aggregation of chromosomes and to impede polymerization of tubulin in the mitotic spindle. Root tips harvested from mature plant material (Table 1) were also incubated overnight in ice water. Root tips were fixed in 3:1 (ethanol:acetic acid, v/v) and stored in fixative at -20°C.

Table 1 Sources of plant and animal material for chromosome isolation

| <i>Species name</i> | common name | Source |
|---|-------------|--|
| <i>Hordeum vulgare</i> | barley | Seed (var. Steffi), BayWa AG, Perlach |
| <i>Vicia faba</i> | field bean | isolated chromosomes courtesy of Dr. Andreas Houben from IPK, Gatersleben |
| <i>Arabidopsis thaliana</i> | thale cress | root tips courtesy of Dr. Ute Vogelknecht, LMU Dept. I Biologie, München from wild type plant cultures |
| <i>Secale cereale</i> | rye | Seed (var. Sorum) courtesy of PD Dr. Uwe Hohmann |
| <i>Glycine max</i> | soybean | seeds courtesy of Dr. Christian Lindermayr, LMU Dept. I Biologie München |
| <i>Ozoroë biflora</i> (Ruiz & Pav) Speta* | | Seeds and root tips from cultivated plants from Chile courtesy of Prof. J. Grau, LMU Dept. I Biologie, München |
| <i>Luzula sylvatica</i> | wood rush | root tips from cultivated plants from Botanical Gardens, München |
| <i>Gallus gallus</i> | chicken | Fixed (3:1 v/v methanol, acetic acid) cell suspensions from DT40 cell cultures courtesy of Dr. Irina Solovei, LMU Dept. II Biologie, München |
| <i>Homo sapiens</i> | human | Fixed (3:1 v/v methanol, acetic acid) cell suspensions from fibroblast cell cultures courtesy of Dr. Irina Solovei, LMU Dept. II Biologie, München |

* described in GUAGLIANONE and ARROYO-LEUENBERGER, 2002, formerly *Camassia biflora*

Enzymatic tissue dissociation

Prior to enzymatic tissue dissociation for isolation of chromosomes, fixed root tips were washed in *aqua dest* 30-45 min. Meristematic tips (approx. 2 mm each) were separated from roots and dissected into smallest possible sections, taking care to avoid drying. Root-tip sections were then macerated in a 200 µl mixture of 2% pectolyase and 2% cellulase (w/v in lyase buffer: 75 mM KCl, 7.5 mM EDTA in *aqua dest*) for 70-110 min, depending on the species, tempered at 30°C in an immersion bath. To promote tissue dissociation, the mixture was periodically rigorously churned with a spatula. Progression of digestion was monitored with LM. The mixture was then filtered through a 100 µm gauze, and then hypotonically treated for 5 min in approx. 5 ml 75 mM KCl. This suspension was centrifuged for 7 min 20°C at 760 rpm/75 g. The supernatant was discarded, the precipitate was resuspended in 10 ml 3:1 fixative, and was centrifuged for 7 min at 760 rpm /75 g at 20°C. This was repeated 5 times. The after discarding the supernatant from the final wash, the resulting pellet was resuspended in 200 – 500 µl 3:1 fixative (depending on size of pellet). This cell suspension could be stored over a period of up to several months, and was used for chromosome isolation with the “drop/cryo” technique.

Laser marked slides

Laser marked slides (Laser Marking, Fischen, Germany) were rinsed and wiped under running tap water. The slides were then submerged in chromosulfuric acid for at least 24 h, were subsequently washed under running water, rinsed 3 times with *aqua dest*, rinsed 2 times in ethanol, and air dried. Clean slides were stored at –20°C.

Laser-marked slides were used to facilitate location of chromosomes in SEM. Chromosomes were located in phase contrast LM, and their position “mapped“ manually and with a video camera on the coordinate system etched on the glass slides.

“Drop/ Cryo” isolation of metaphase spreads

The „drop/cryo“ technique, a chromosome spread isolation method especially appropriate for SEM analysis, was performed according to Martin *et al.* (1994). Briefly, approx. 20 µl of a cell suspension in 3:1 fixative was dropped from a height of 60 cm onto an ice-cold moistened laser marked glass slide. Just as the fixative evaporates (as visible with the naked eye), one drop of 45% acetic acid was applied to the areal of the dropped cell suspension. A cover slide

(same size as the marked region of interest, 24 x 32 mm) was immediately applied, and the whole slide was laid, coverslip-side down, on dry ice. After 15 min the coverslip was pried off, and the glass slide was immediately immersed a fixative solution of 2.5% glutaraldehyde in 75 mM cacodylate buffer (CCD, 75 mM dimethylarsenic acid, 2 mM MgCl₂, pH 7.0). This fixation step was omitted prior to immunolabeling; in this case slides were temporarily incubated in phosphate buffered solution (PBS, 0.13 M NaCl, 7 mM Na₂HPO₄, 3mM NaH₂PO₄, pH 7.0 with 0.1% Tween 20) before blocking.

Alternative isolation technique with “suspension preparation”

Alternatively, barley chromosomes were isolated according to a slightly modified version of the method published by Schubert *et al.*(1993). In short, root tips from synchronized and arrested barley sprouts were soaked overnight in ice water, and were then fixed in 2% formaldehyde v/v in Tris/HCl buffer (10 mM Tris, 10 mM Na₂EDTA, 100 mM NaCl, pH 7.5) for 20 min in ice water (5°C) and were subsequently washed 2 x 5 min in Tris. Sections of meristematic tissue were dissected from the root tips in isolation puffer (15 mM Tris, 2 mM Na₂EDTA, 0.5 mM Spermin, 80 mM KCl, 15 mM mercaptoethanol, 0.1% v/v Triton X-100, pH 7.5), and were homogenized with a Polytron hand homogenizer (Kinematica, Luzern, Switzerland) 15 000 rpm for 50 sec. The resulting suspension was filtered through a 50 µm Falcon cell strainer (round-bottom tube), transferred to a 200 µl Eppendorf tube with an enlarged polyurethane tip, and centrifuged for 3 min at 29 000 g to increase density of suspended particles (including chromosomes). 20 µl of the suspension were applied to laser-marked slides mounted on “cyto-spin” slide-holders (Hettich, Tuttlingen, Germany) and were “dry-spun” for 2 min at 89 g at RT. Slides were immediately immersed in 2.5% glutaraldehyde in cacodylate buffer (for structural analysis only) or in PBS/Tween (for immunolabeling specimens).

Enzymatic treatment for removal of nucleoplasm

In experiments in which it was attempted to remove the concealing nucleoplasmic layer, human and chicken metaphase spreads were treated with various proteases by submersion in enzyme solution after to drop/cryo preparation of chromosomes (Table 2). For all concentrations, specimens were tested both prior and subsequent to 2.5% glutaraldehyde (v/v in CCD buffer, pH 7.0) fixation. Pepsin, cathepsin and rennin were diluted in 0.1 N HCl (pH 2.0). Immediately after specimens were treated, the pH of the enzyme solution was measured to ensure that the pH of the respective solution had remained stable.

Table 2 Proteolytic enzymes applied for digestion of nucleoplasmic layer to human and chicken chromosomes

| Enzyme | Enzyme type | pH optimum | Concentrations w/v and times applied | |
|----------------------------------|----------------------------|------------|--------------------------------------|-------------------------|
| Trypsin (Merck, FRG) | serine-protease | 7-9 | 0.1% 30 min | |
| Pepsin (Sigma, FRG) | aspartate/carboxy protease | 1.5 - 4 | 0.01% 30 min | 0.001% 15 and 30 min |
| Cathepsin (Sigma, FRG) | aspartate/carboxy protease | 3 | 0.001% 15 and 30 min | |
| Rennin (Sigma, FRG) | aspartate/carboxy protease | 2 | 0.01% 30 min | 0.001% 15 and 30 min |

DNA staining

For preparations involving fluorescent immunolabeling, chromosomes were counterstained by incubating slides in a 0.5 mg/ml DAPI solution in PBS for 15 min. Slides were washed under running *aqua dest*, briefly drip-dried (not allowed to totally air-dry) and then covered with the anti-fading agent Vectashield[®] (Vector Laboratories, Burlingame, CA, USA) and a coverslip. These specimens were stored at 4°C prior to LM.

For visualization of DNA with SEM, chromosomes were stained for 30 min at room temperature with platinum blue (Pt-blue, 10 mM dissolved in distilled H₂O, pH 7.2; WANNER & FORMANEK, 1995), then washed 3 times in *aqua dest*.

Immunolabeling

Slides for immunolabeling were incubated in phosphate buffered solution (PBS, 0.13 M NaCl, 7 mM Na₂HPO₄, 3mM NaH₂PO₄, pH 7.0 with 0.1% Tween 20). All labeling procedures were carried out at room temperature; all wash steps were three times 10 min each. Slides were incubated in a blocking solution (1% bovine serum albumin in PBS) for 30 min. Antibodies were diluted in blocking solution at the ratios given in Table 3. Primary antibodies were applied and incubated for 1 h. The slides were washed in PBS/Tween. The secondary antibody, either anti-rabbit-Cy3, anti-rabbit 10 nm gold, anti-rabbit-Fluoronanogold[™] or anti-rabbit-Nanogold[®], was then applied and incubated for 1 h. The slides were subsequently washed in PBS/Tween. Specimens were routinely post-fixed with 2.5% glutaraldehyde in PBS (without Tween 20); for comparison 2% formaldehyde in PBS was also used. Preparations with fluores-

cent secondary antibodies were incubated for 15 min in a 4',6-diamidino-2-phenylindole (DAPI, 0.5 mg/ml diluted in PBS), rinsed with *aqua dest*, mounted in Vectashield® (Vector, Burlingame, CA, USA) and stored at 4°C prior to fluorescent light microscopy.

Table 3 Antibodies used for immunolabeling

| Primary antibodies | dilution [◊] | Secondary antibodies | dilution [◊] |
|---|-----------------------|---|-----------------------|
| us 06-570 IgG Polyclonal anti-phosphorylated histone H3 (serine 10) in rabbit Upstate, Lake Placid, NY, USA | 1:250 | IgG polyclonal anti-rabbit-10 nm gold Sigma, Saint Louis, MO, USA | 1:10 |
| ab7766 IgG Polyclonal anti-dimethylated histone H3 (lysine 4) in rabbit Abcam, Cambridge, UK | 1:250 | IgG polyclonal anti-rabbit-Cy3 Jackson ImmunoResearch, West Grove, PA, USA | 1:250 |
| us07-212 IgG Polyclonal anti-dimethylated histone H3 (lysine 9) in rabbit Upstate, Lake Placid, NY, USA | 1:250 | IgG polyclonal anti-goat-Cy3 Jackson ImmunoResearch, West Grove, PA, USA | 1:250 |
| NA14 IgG monoclonal anti-topoisomerase II (Ab-1) in mouse Oncogene Research Products, Boston, MA, USA | 1:20 | Fab' polyclonal anti-rabbit-Nanogold® (1.4 nm)* | 1:20 |
| | | Fab' polyclonal anti-mouse-Fluoronanogold® (FITC) * | 1:10 |
| | | Fab' polyclonal anti-rabbit-FluoroNanogold® (FITC)* | 1:20 |
| | | Fab' polyclonal anti-rabbit-Alexa Fluor® 488-Nanogold®* | 1:20 |

*All Nanogold® products were purchased from Nanoprobes, Yaphank, NY, USA

◊Antibodies were diluted in blocking solution (PBS/Tween + 1% w/v BSA)

Fluorescent light microscopy

Fluorescent light microscopy was performed on a Zeiss Axioplan equipped with a 100 W mercury lamp, manually switched filter blocks (Carl Zeiss, Göttingen, Germany) (Table 4) appropriate for the fluorochromes applied (Table 5), and a cooled black and white CCD Camera Series 200 (Photometrics, Roper Scientific, Germany). Separate images were captured using IPLab imaging software (Signal Analytics, Vienna, VA USA). Specimens labeled with Fluoronanogold or AlexaNanogold were washed to remove the anti-fading reagent Vectashield™ 3 X 10 min in 100% ethanol (p.A.), then immersed in *aqua dest* prior to silver or gold enhancement.

Table 4 Zeiss Filter sets for specific detection of fluorochromes in LM

| | Excitation filter | Beamsplitter | Emmission filter | Applied fluorochrome |
|---------------|--------------------------|---------------------|-------------------------|-----------------------------|
| Filter Set 01 | BP 365/12 | FT 395 | LP 397 | DAPI |
| Filter Set 15 | BP 546/12 | FT 580 | LP 590 | Cy3 |
| Filter Set 17 | BP 485/20 | FT 510 | BP 515-565 | FITC Alexa Fluor® 488 |

BP band pass

FT "Farbteiler"(German) = beamsplitter

LP long pass

Table 5 Wavelengths of fluorescent markers

| Fluorescent marker | Excitation wavelength (λ_{ex}) | Emission wavelength (λ_{em}) |
|---------------------------|--|--|
| DAPI | 358 | 461 |
| FITC | 492 | 520 |
| Cy3 | 553 | 575 |
| Alexa Fluor® 488 | 488 | 520 |

Metallo-enhancement of Nanogold®-labeled specimens

Nanogold-labeled specimens were washed with *aqua dest* and either gold- or silver-enhanced according to manufacturer's instructions (Goldenhance® kit; HQ Silver™ enhancer kit, Nanoprobes, NY, USA; for review of enhancement procedure see HAINFELD *et al.*, 1999; HAINFELD & POWELL, 2000). For gold enhancement, equal proportions of the four components of gold enhancement kit were mixed at room temperature, 80 μ l of the mixture applied to each slide, and covered with a 24 x 32 mm coverslip for 6 or 10 min. Silver enhancement is light-sensitive and must be performed under darkroom conditions; equal proportions of three components were mixed and applied to each slide for 6 min (unless otherwise indicated for a specific experiment) as with gold enhancement. The coverslips were subsequently removed, and the slides were washed in *aqua dest* 3 x 10 min.

After the final wash, the slides were dehydrated for 3 x 10 min in 100% acetone and critical point dried (Fisons Instruments, VG Microtech, East Sussex, UK). It was essential for preservation of three dimensional chromosome ultrastructure and for viewing access of the metaphases with SEM that the slides were at no point allowed to air dry. Chromosomes were first

mapped to the coordinated system on laser-marked slides with LM in phase contrast mode, trimmed to approximately 15 x 15 mm² and mounted with double-sided tape to aluminium stubs fit to the SEM specimen platform. Slides were first controlled with LM in phase contrast mode.

Scanning electron microscopy

Preparations exclusively examined in the secondary electron (SE) mode were sputter-coated with platinum to a layer of 3-5 nm; preparations for backscattered electron (BSE) detection (Pt-blue stained and immunolabeled specimens) were carbon-coated by evaporation, also to a layer of 3-5 nm with a Magnetron SCD 050 (Balzers, Liechtenstein) and examined at an accelerating voltage of 8 kV (for exclusively SE images) or 12-30 kV (for simultaneous SE and BSE imaging) with a Hitachi S-4100 field emission scanning electron microscope equipped with a YAG-type BSE-detector (Aurata). SE and BSE images were recorded simultaneously with Digiscan™ hardware and processed with Digital Micrograph 3.4.4 software (Gatan, Inc., Pleasanton, CA USA). Element analysis by energy dispersive X-ray analysis (EDX) was performed with a Noran “Vantage” system equipped with a light element silicon detector (Pioneer) and an ultra-thin window.

3D Analysis

3D micrographs were constructed by tilting specimen table and capturing images from one location at an angle difference of 3°. Corresponding images were then mounted either as stereoscopic pairs (for instructions to stereo viewing see Appendix) or superimposed in separate color channels (in Adobe® Photoshop) resulting in an anaglyph image (to be viewed with 3D bicolor glasses).

Sections of Enterococcus faecalis

Embedded specimens of the immunogold-labeled bacterium *Enterobacter faecalis* were available from archived material from earlier studies (GALLI *et al.*, 1989; WANNER *et al.*, 1989). *Enterococcus faecalis* bacteria were indirectly labeled for a cell surface aggregate protein with 10 nm gold IgG, contrasted with uranyl acetate and embedded in carbon-based epoxy resin. Sections with area of approximately 5 mm² of different thickness (1, 2, 3, 4, 5 and 6 µm) were cut with a pyramitome (LKB, Bromma, Sweden), applied in a drop of *aqua dest* on a glass slide, and heated on a hotplate until the water droplet evaporated and the sections spread and

adhered to the slide. The glass slide with specimen was subsequently “trimmed” to an area of approximately 15 x 15 mm², mounted and C-evaporated for SEM investigation.

Image processing

Images were Tiff-formatted in their respective softwares of origin (IP Lab for fluorescent LM and Digital Micrograph for SEM), and further processed in Adobe® Photoshop. QuarkX-Press (Quark, USA) was used for layout of figures and color plates.

Quantification

Signals in SEM were quantified by counting gold signals from a BSE image (at a magnification of approximately 20 000 fold). Signal distribution could be quantified by counting the number of signals in defined transverse sections, averaging the counts per section for all chromosomes in a particular assay, and plotting the averages in terms of signal number and relative length of chromosome. Transverse sections were defined by tracing 1 cm segments on full-page (DIN A4) print-outs of BSE images. The number of signals was counted per segment, and documented in an Excel (Microsoft Office 98) spreadsheet. Quantification units were signal number per chromosome segment.

SDS PAGE Western blot and silver staining analysis

Cell suspensions from barley root tips of different fixations were prepared: root tips fixed for 20 min in 2% v/v formaldehyde (in Tris buffer: 10 mM Tris, 10 mM Na₂EDTA, 100 mM NaCl, pH 7.5), root tips treated with ice water and subsequently fixed in 3:1 (v/v ethanol/acetic acid) and stored overnight at -20°C, and unfixed root tips. Meristematic tissue from (fixed) root tips were dissected into smallest possible sections in Tris buffer, then buffer was exchanged for Tris with 5% v/v glycerin, and the sections were sonified/homogenized in a 2 ml Eppendorf vial for 50 s at 15 000 rpm with a Polytron hand homogenizer (Kinematica, Luzern, Switzerland). The resulting suspension was passed through a 50 µm cell strainer and centrifuged for 10 min at 12 100 g. For 3:1 fixation, no pellet developed, and the entire suspension was used for subsequent protein isolation; for the other two fixations, the supernatant and precipitate, to which 20 µl Tris/5% glycerin was added, were separated and stored at -20°C. Protein content was determined using a Bio-Rad Protein Assay kit (Bio-Rad Laboratories, Hercules, CA, USA) by spectrometry at a wavelength of 595 nm using the Bradford assay (BRADFORD, 1976). Dried protein pellets were resuspended in 20 µl loading buffer (0.1 M

NaCO₃, 2% w/v SDS, 0.2 M DTT, 5% w/v glycerol, 0.001% w/v bromophenol blue), denatured for 5 min at 100°C, applied to a polyacrylamide gel (PAA: 17% w/v acrylamide, 0.369 M Tris HCl pH 8.8, 0.1% w/v SDS, 0.065% w/v APS, 0.1% v/v TEMED) and electrolysed (25 mA/gel, BioRad PowerPac 300, Bio-Rad Laboratories, Hercules, CA) for 1.5 h according to the SDS-PAGE technique (LAEMMLI, 1970). Proteins were isolated from each fraction by precipitating with 10% v/v trichloroacetic acid (TCA). Fractions were subsequently centrifuged at 29 000 g for 5 min at 4°C. The supernatant was discarded, the pellet was washed twice with 100 µl acetone (100%), and centrifugation was repeated. The precipitate was air dried on a heating element at 40°C for approximately 15 min.

For Western blotting, the PAA gel was layered between filter paper soaked in buffers of different ionic strengths (4 filters in anode buffer I: 300 mM Tris, 20% v/v methanol; 3 filters in anode buffer II: 25 mM Tris, 20% v/v methanol; 4 filters in cathode buffer: 40 mM ACA, 0.01% w/v SDS, 20% v/v methanol) and a nitrocellulose membrane. These layers were assembled between anode and cathode plates of the blotting apparatus in the following order: anode I, anode II, nitrocellulose, gel, cathode. A current of 80 mA (0.8 mA / cm² Gel) was applied for approx. 1.5 h. The membrane was washed in distilled H₂O and used for immunolabeling tests; the PAA gel was silver-stained to control whether proteins remained on the gel (see below).

Prior to immunolabeling, the blotted membrane was incubated in blocking buffer (0.25% w/v gelatine in 150 mM NaCl, 5 mM EDTA pH 8.0, 50 mM Tris pH 7.5, 0.05% v/v TritonX-100), then incubated in 20 ml of a 1:2 000 solution of rabbit anti-dimethylated histone H3 (lysine 9) in blocking buffer (see above) overnight at 4°C. This primary antibody was then washed away first 10 min with TBST (0.1% v/v Tween 20 in 50 mM Tris/HCl pH 7.8, 150 mM NaCl, 2mM MgCl₂) then two subsequent 10 min washes with the same solution (with Tween 20 omitted). The membrane was then incubated in 20 ml of a 1:20 000 solution of anti-rabbit IgG alkaline phosphatase conjugate for 1 h at room temperature, washed as with the primary antibody, and then treated with 5 ml of developing solution (AP buffer, 16.5 µl 5'-Brom-4'-chloro-3-indolylphosphat-disodium salt [BciP] 50 mg/ml in 100% dimethylformamid [DMF], 16.5 µl p-Nitrobluetetrazoliumchloride [NBT] 100 mg/ml in 70% v/v DMF) until bands were visible, and then washed thoroughly with distilled H₂O. The Western blot was air dried and then digitally acquired (Snapscan 1236, Agfa, Germany) for documentation.

Prior to silver staining of the proteins in the PAA, the PAA gel was incubated over night in 50% v/v methanol. The methanol was then discarded, the gel washed 2 x in *aqua dest*, and subsequently incubated for 15 min in 30 ml of the silver staining solution (according to WRAY *et al.*, 1981: in short, 0.6 ml of a 1.4 mM AgNO₃ solution added dropwise to “solution 2” and

filled to a volume of 30 ml; solution 2: 284 μ l 2N NaOH in 420 μ l 30% w/v NH_4OH). After discarding the silver staining solution, the gel was washed 2x 5 min with distilled H_2O , then incubated in a developing solution (500 μ l 1% w/v citric acid, 50 μ l 38% v/v formaldehyde in 100ml distilled H_2O) until bands were visible. The gel was generously washed with distilled H_2O , after which a stop-solution (40% v/v ethanol, 10% v/v acetic acid) was applied. The PAA gel was dried and laminated, and digitally acquired (Snapscan 1236, see above) for documentation.

Results

Chromosome structure

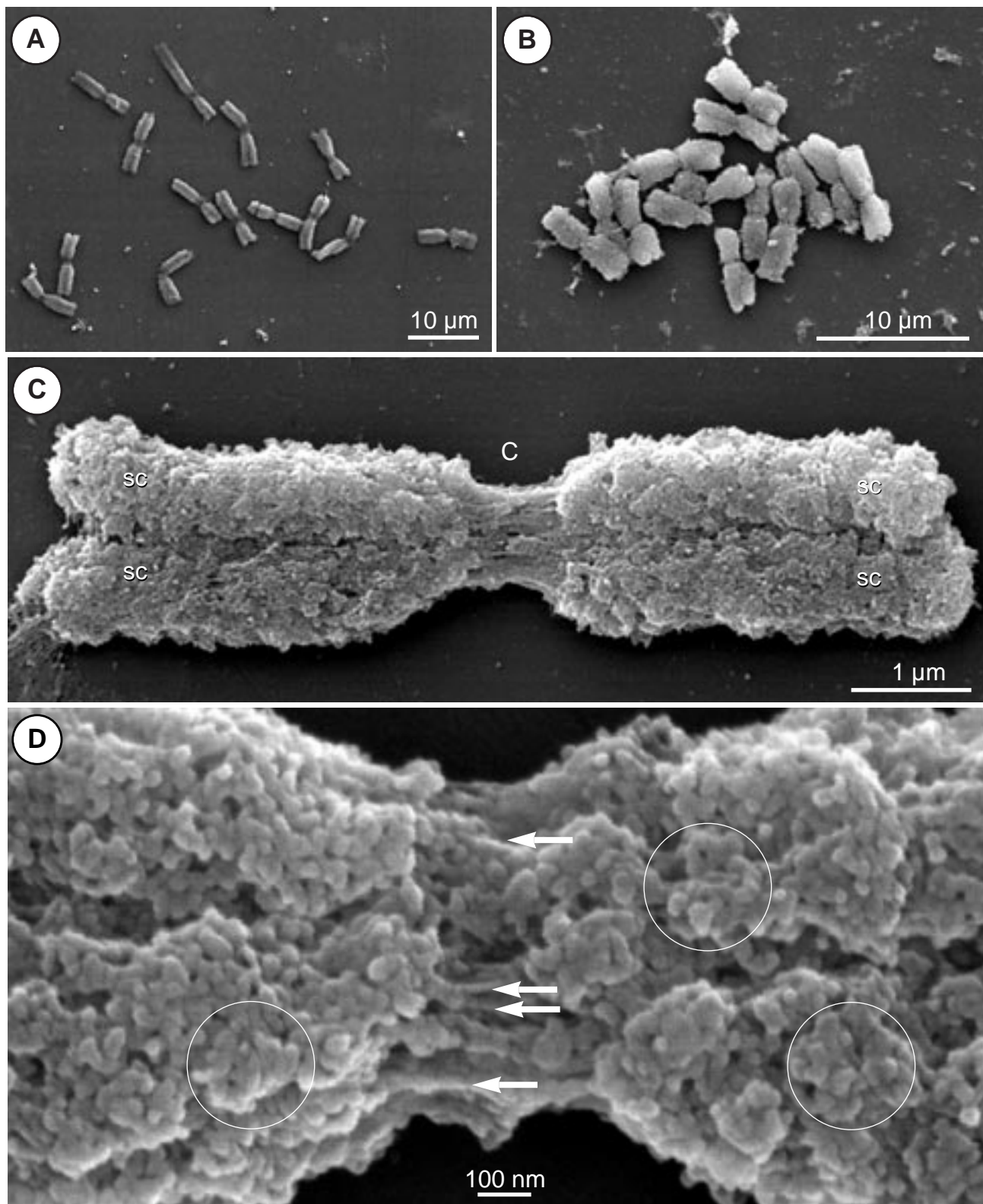
Drop/Cryo Technique applied to various plant and animal species

The well-established drop/cryo method (MARTIN *et al.*, 1994) for fixation and isolation of barley mitotic metaphase chromosomes was applied to other plant and animal species to test its applicability as a routine universal chromosome preparative method and to establish the scope of this study. Criteria for applicability were based on the well-characterized ultrastructure of barley chromosomes and were as follows: (i) chromosome groups (in future referred to as „metaphase spreads“) exposed after dropping of cell suspension and bursting on glass slide impact are largely nucleoplasm-free (Figure 1 A, B); (ii) structural chromosomal features, such as sister chromatids, primary constriction at the centromere and three dimensional preservation of the chromosome, are recognizable at low magnifications (1 000-5 000 fold) (Figure 1 C); (iii) basic structural elements of chromatin, chromomeres and parallel fibrils, as described by Wanner and Formanek (2000), should be recognizable at moderate magnification (5 000-15 000 fold) (Figure 1 D). Species for chromosome isolation were chosen by merit of availability, representative variations in genome and chromosome sizes, and diversion in kingdoms (inclusion of two animal species) and (plant) families (Table 6).

Table 6 Plant and animal species investigated for chromosome structure

| Kingdom | Family | Species | Common name | Chromosome number (2n) | Genome size (1C)* |
|----------|---------------|--|-------------|------------------------|----------------------|
| Plantae | Poaceae | <i>Hordeum vulgare</i> | barley | 14 | $5 \cdot 10^9$ bp |
| Plantae | Fabaceae | <i>Vicia faba</i> | field bean | 12 | $2 \cdot 10^{10}$ bp |
| Plantae | Brassicaceae | <i>Arabidopsis thaliana</i> | thale cress | 10 | $1 \cdot 10^8$ bp |
| Plantae | Poaceae | <i>Secale cereale</i> | rye | 14 | $5 \cdot 10^9$ bp |
| Plantae | Fabaceae | <i>Glycine max</i> | soybean | 40 | $1 \cdot 10^9$ bp |
| Plantae | Hyacinthaceae | <i>Oziroë biflora</i> (Ruiz & Pav) Speta | none | 32/34 | unknown |
| Plantae | Juncaceae | <i>Luzula sylvatica</i> | wood rush | 12 | $8 \cdot 10^8$ bp |
| Animalia | Phasianidae | <i>Gallus gallus</i> | chicken | 77/78 | $1.2 \cdot 10^9$ bp |
| Animalia | Hominidae | <i>Homo sapiens</i> | human | 46 | $3 \cdot 10^9$ bp |

* plant species according to BENNET *et al.*, 2000 and SINGH, 2002; For animal species according to the website "Chromosome numbers for selected organisms"

**Figure 1**

SE micrographs of barley chromosomes fixed and isolated with the drop/cryo method. Criteria for standard well-preserved chromosome structure were: exposed metaphase spread that are largely free of nucleoplasm (A and B); chromosomal features, such as distinguishable sister chromatids (sc), primary constriction at centromere (C) and three dimensional preservation visible at low magnifications (C); basic structural elements (D, detail of centromeric region of a barley chromosome), chromomeres (circled areas) and parallel fibers (arrows), are recognizable at higher magnifications. Note separation of sister chromatids at the distal regions of the chromosome arms (C), a characteristic feature for barley, but not a universal feature for all species in this study.

Chromosomes of various plant species were examined (Figure 2 A-G): *Hordeum vulgare* (barley), *Secale cereale* (rye), *Glycine max* (soybean), *Vicia faba* (field bean), *Arabidopsis thaliana* (thale cress), *Ozoroë biflora*, and *Luzula sylvatica* (wood rush) (Table 6). Barley, which has medium sized chromosomes and are metacentric, was the routine specimen for this study (Figure 2 A). Rye could be isolated routinely with the drop/cryo technique, has metacentric chromosomes and, as has been reported in other studies (ZOLLER *et al.* 2004A), does not have distinguishable sister chromatids (Figure 2 B). Mitotic *G. max* chromosomes are 1-2 μm in length; *A. thaliana* chromosomes measure only 1 μm (Figure 2 C, D). *G. max* and *A. thaliana* preparations resulted in metaphase spreads which were not routinely well-spread and nucleoplasm-free (Figure 3). Chromosomes were recognizable in some metaphase spreads in spite of a nucleoplasmic residue (Figure 3 A-C), but at higher magnification structural chromosome details could not be satisfactorily distinguished from the surrounding milieu (Figure 3 D). Exceptions were chromosomes which were separated from their complements (Figure 3 B). Medial centromeric constrictions were rarely recognized on the small chromosomes for *G. max* chromosomes and *A. thaliana*, depending on their isolation from nucleoplasm and how they spread on the glass slide (see Figure 2 C, D). DNA staining for SEM with platinum blue (Pt-blue) stained chromosomes, but not residual nucleoplasm, indicating that the nucleoplasm contains negligible DNA and/or RNA (Figure 3 C, D). Moderate resolution BSE images of Pt-blue stained *A. thaliana* chromosomes shows areas of less dense DNA distribution, whereas the SE image shows the surface structure of all components of chromatin (Figure 3 D).

V. faba chromosomes were available as suspension preparations, and have large chromosomes with various centromeric orientations (meta-, acro-, and telocentric). Sister chromatids are clearly distinguishable, sometimes even separated (Figure 2 E). *O. biflora* chromosome spreads could be isolated with the routine drop/cryo method, and vary remarkably in size, ranging from 1- 12 μm (Figures 2F, 4 A-E). Chromosomes showed good three dimensional preservation, and primary constrictions were visible on all but the smallest of the chromosomes, which in late metaphase appear spherical rather than cylindrical in shape (Figure 4 , arrow). Sister chromatids were not distinguishable; an invagination along the longitudinal axis, however, could be observed occasionally on medium-sized (2 μm) chromosomes (Figure 4 D). Isolation of *L. sylvatica* chromosomes with the drop/cryo method required modification of duration of enzymatic tissue dissociation (110 min), and resulted in

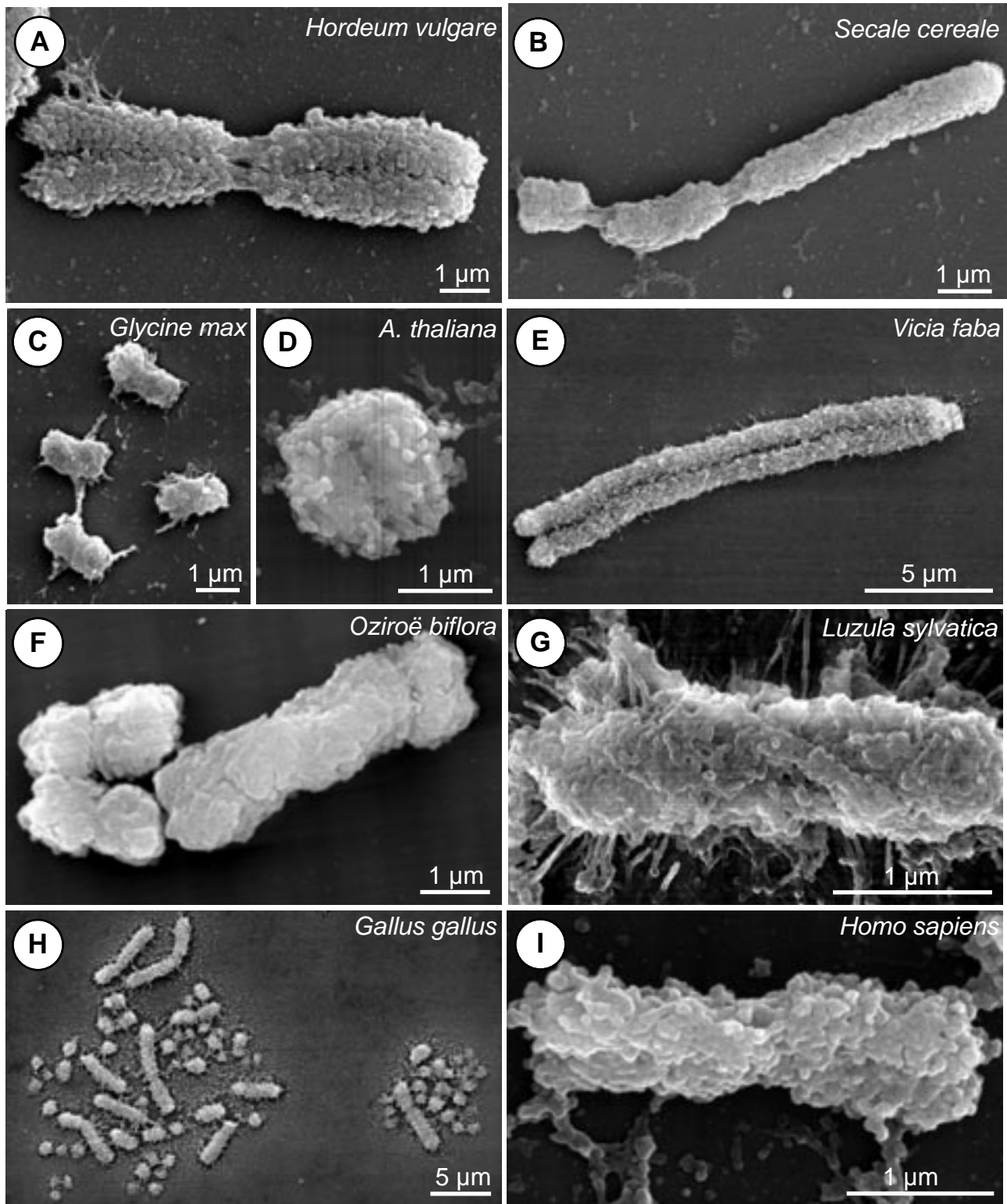


Figure 2

SE micrographs of chromosomes of different plant and animal species showing a survey of representative mitotic chromosome structures. **A** *Hordeum vulgare* (barley), **B** *Secale cereale* (rye), **C** *Glycine max* (soybean), **D** *Arabidopsis thaliana* (thale cress), **E** *Vicia faba* (field bean), **F** *Oziroë biflora* (new species), **G** *Luzula sylvatica* (wood rush), **H** *Gallus gallus* (chicken), **I** *Homo sapiens* (human). All chromosomes were fixed and isolated by the drop/cryo method, with exception of *V. faba* (**E**), which was isolated by the suspension method. Metaphase spreads of *Glycine max*, *Arabidopsis thaliana*, *Gallus gallus* and *Homo sapiens* could not be routinely isolated without nucleoplasm. A common feature on all chromosomes studied is the compact and “soft-lobed” surface structure.

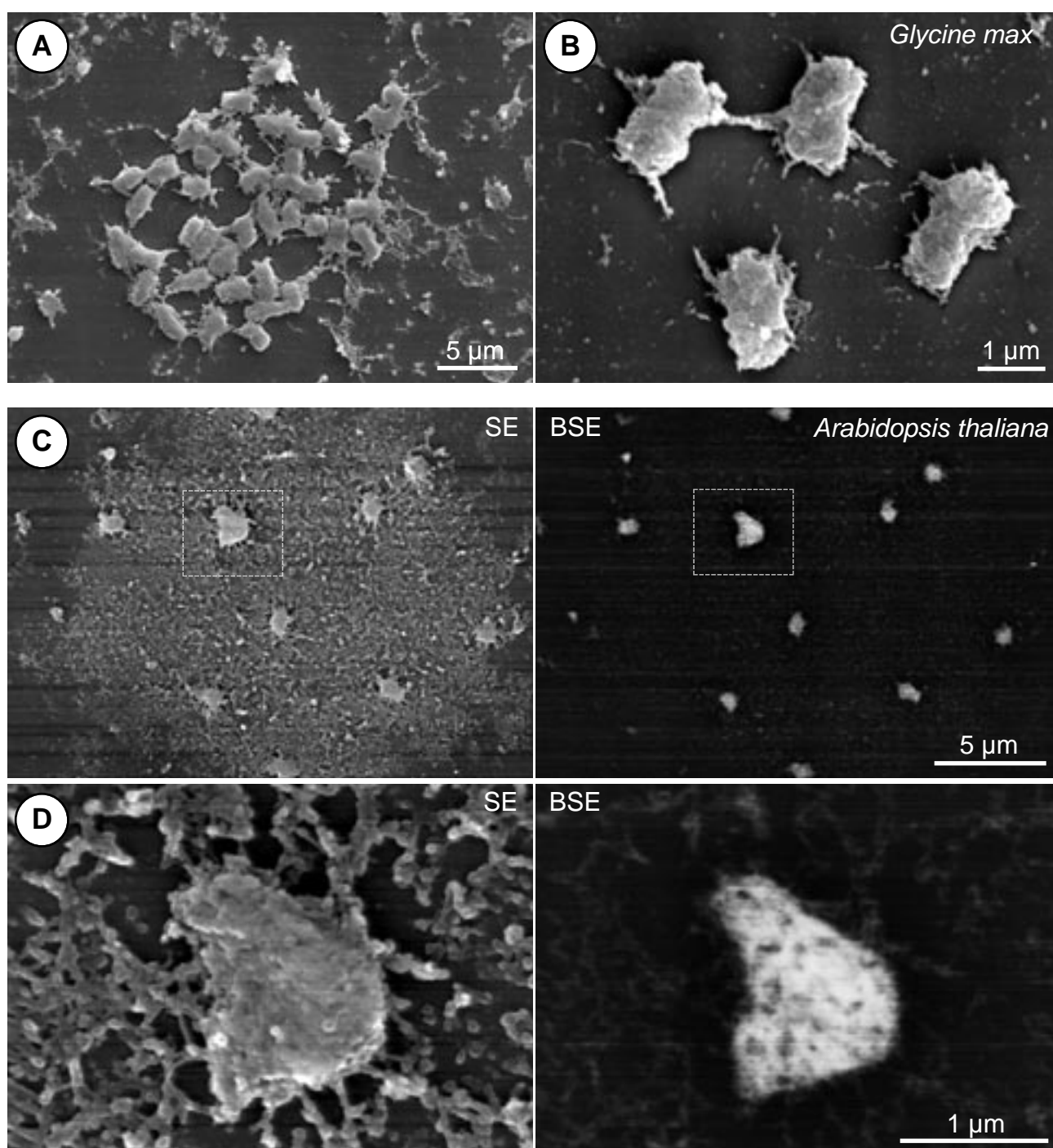


Figure 3

SEM micrographs of *Glycine max* (soybean, **A,B**) and *Arabidopsis thaliana* (thale cress, **C, D**) metaphase chromosomes. Spreading and isolation from nucleoplasm was inconsistent for these plant species with small chromosomes (**A**) SE image of soybean chromosomes show that chromosomes are recognizable at low magnification, despite obvious nucleoplasmic residue. At higher magnification, chromosomes that are separated from their complement show discernable primary constrictions and chromosome surface structure (**B**). SE image of *Arabidopsis thaliana* stained with Pt-blue also shows nucleoplasmic residue through which chromosomes are easily discernible at low magnification (**B**); simultaneous BSE image shows strong Pt-blue signals from chromosomes recognizable in SE, but not from the nucleoplasmic residue, indicating that it does not contain DNA or RNA (**B**, image on right). Detail of framed area from B, shows that at higher magnifications surface structure of chromosome can be recognized, but structural details cannot be adequately distinguished from those of surrounding nucleoplasm (**C**, left image). Simultaneous BSE image of Pt-blue signal shows that chromosome, but not nucleoplasm, are stained with areas of varying signal intensity, indicating unhomogenous DNA distribution (**C**, image on right).

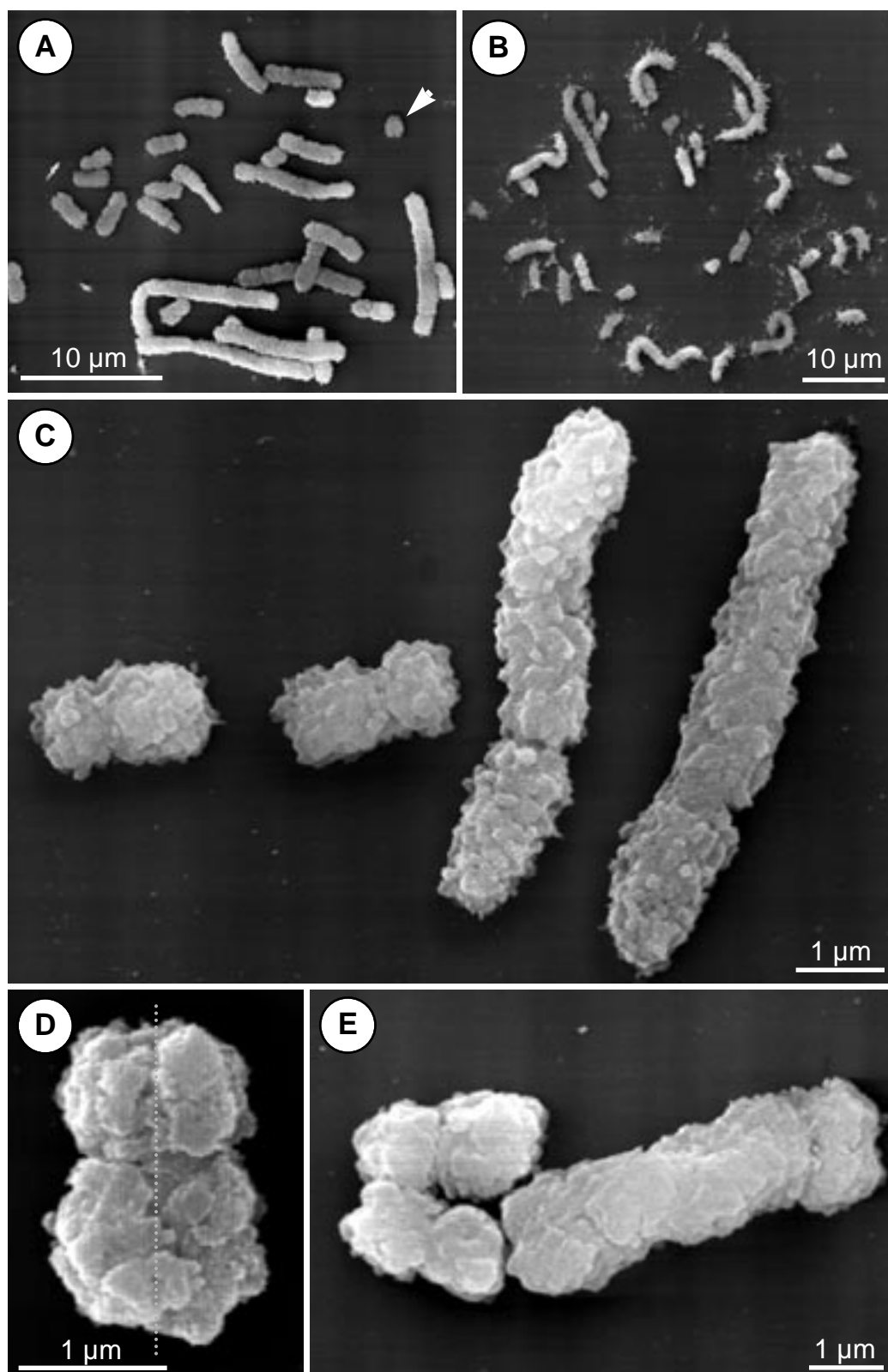


Figure 4

SE micrographs of chromosomes from *Orizoë biflora*. (A) Late metaphase chromosomes isolated from synchronized and arrested root tips from seedlings, and (B) early metaphase chromosomes from untreated root tips of mature plants showing varying chromosome lengths of 1-12 μm . Chromosomes were fixed and isolated with the drop/cryo method. Chromosomes between 2-12 μm are acrocentric or metacentric; smallest chromosomes appear spherical with no obvious primary constriction (arrow). SE images at higher magnification show that chromosomes of all sizes can be three-dimensionally well-preserved, with well-defined chromomeres, characteristic primary constrictions, but undistinguishable sister chromatids (C-E), although in some cases an invagination at the longitudinal axis of symmetry could be discerned (D, dotted line).

metaphase spreads that were largely free of nucleoplasm. *L. sylvatica* chromosomes are holocentric, and do not show distinguishable chromatids (Figure 2 G).

Chromosomes of two animal species were tested, *G. gallus* (chicken) and *H. sapiens* (human) (Figure 2 H, I). In both cases, chromosomes spread by the drop/cryo method appeared largely nucleoplasm-free in phase contrast with LM. In SEM, chromosomes were recognizable in „relief“ at low magnification (Figures 5 A, 5B; 6A). At higher magnifications however, SEM images showed residue nucleoplasm which partially or completely concealed the chromosomes and prevented high resolution analysis of chromosome ultrastructure, with exception of chromosomes on the periphery of the metaphase spreads that appear to have „slipped“ out from the nucleoplasmic layer (Figure 5 B). On chicken specimens, the nucleoplasm appears to have receded from individual chromosomes, presumably due to marginal shrinkage during critical point drying. This allows recognition of the chromosomes, but not adequate examination of ultrastructural details (Figure 6 B). Nucleoplasm did not prevent semi-quantitative DNA staining with DAPI for LM (Figure 7 A, B), nor did it preclude specific protein immunodetection (topoisomerase II, phosphorylated histone H3 at serine 10, Figure 7 A, B). In these animal metaphase spreads studied, as with *A. thaliana* (see above), DNA-specific stains (DAPI and Pt-blue, respectively) labeled chromosomes but not residue nucleoplasm.

Isolation of human and chicken chromosomes

It is standard practice in some cytological protocols with human chromosomes to treat chromosomes to a mild enzymatic digestion to improve DNA accessibility, *e.g.* for *in situ* hybridization and Giemsa staining. To determine whether chromosomes of animal species, human in particular, could be freed of nucleoplasm, different enzymatic treatments were applied (Table 7). Criteria for choice of enzymes was, in the case of pepsin and trypsin their routine implementation in *in situ* hybridization (LEITCH *et al.*, 1994) and Giemsa staining. Pepsin, a carboxy protease with its activity optimum at pH < 2.3, was the most effective in removing nucleoplasm, although not in a routinely reproducible manner (Figure 5E, 5 F, 6C, 6 D). Cathepsin and rennin were chosen because they are of the same protease family as pepsin, but with different pH optima and different proteolytic specificity. Cathepsin was inferior to pepsin in digesting nucleoplasm (images not shown), and rennin

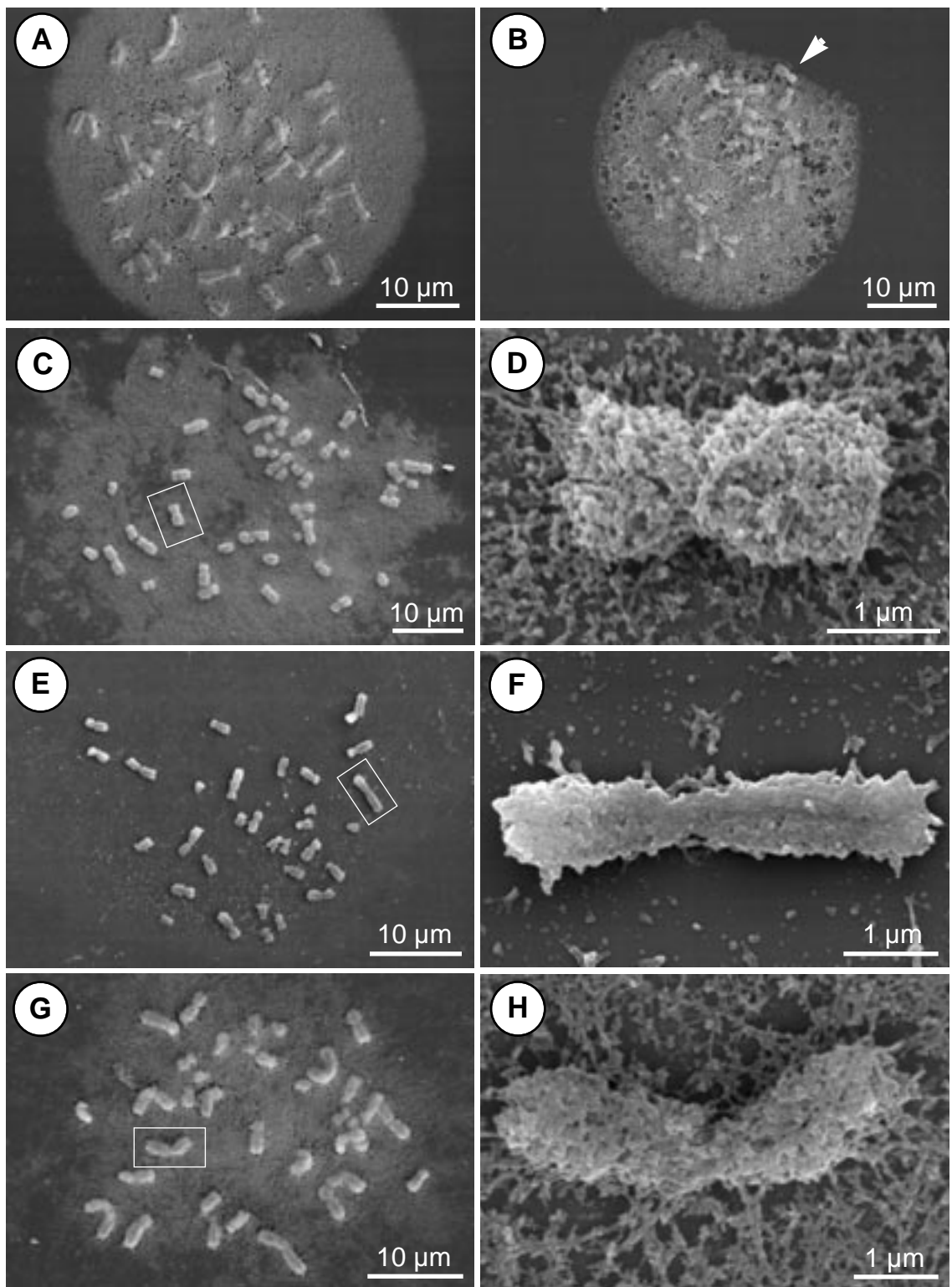
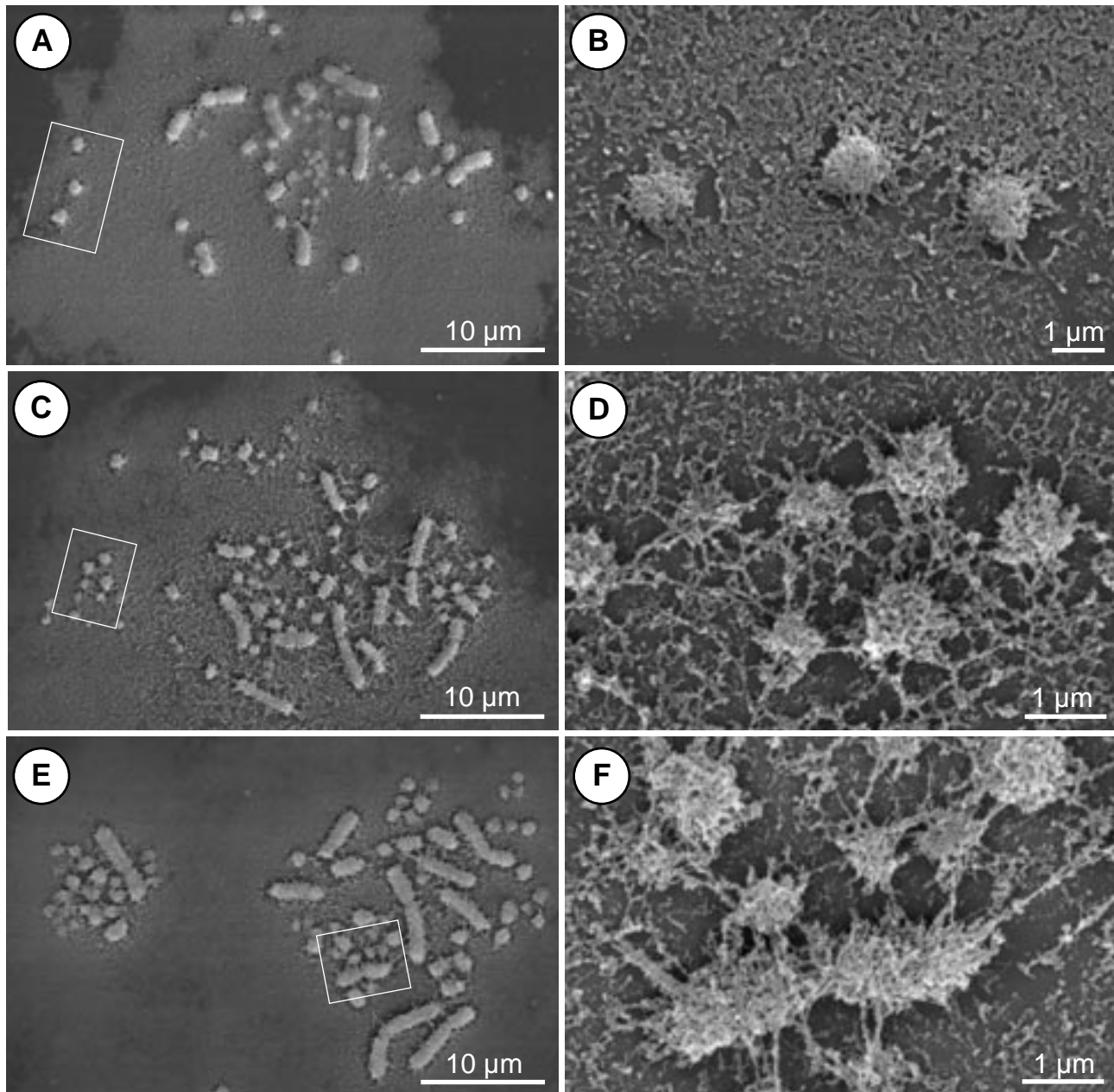
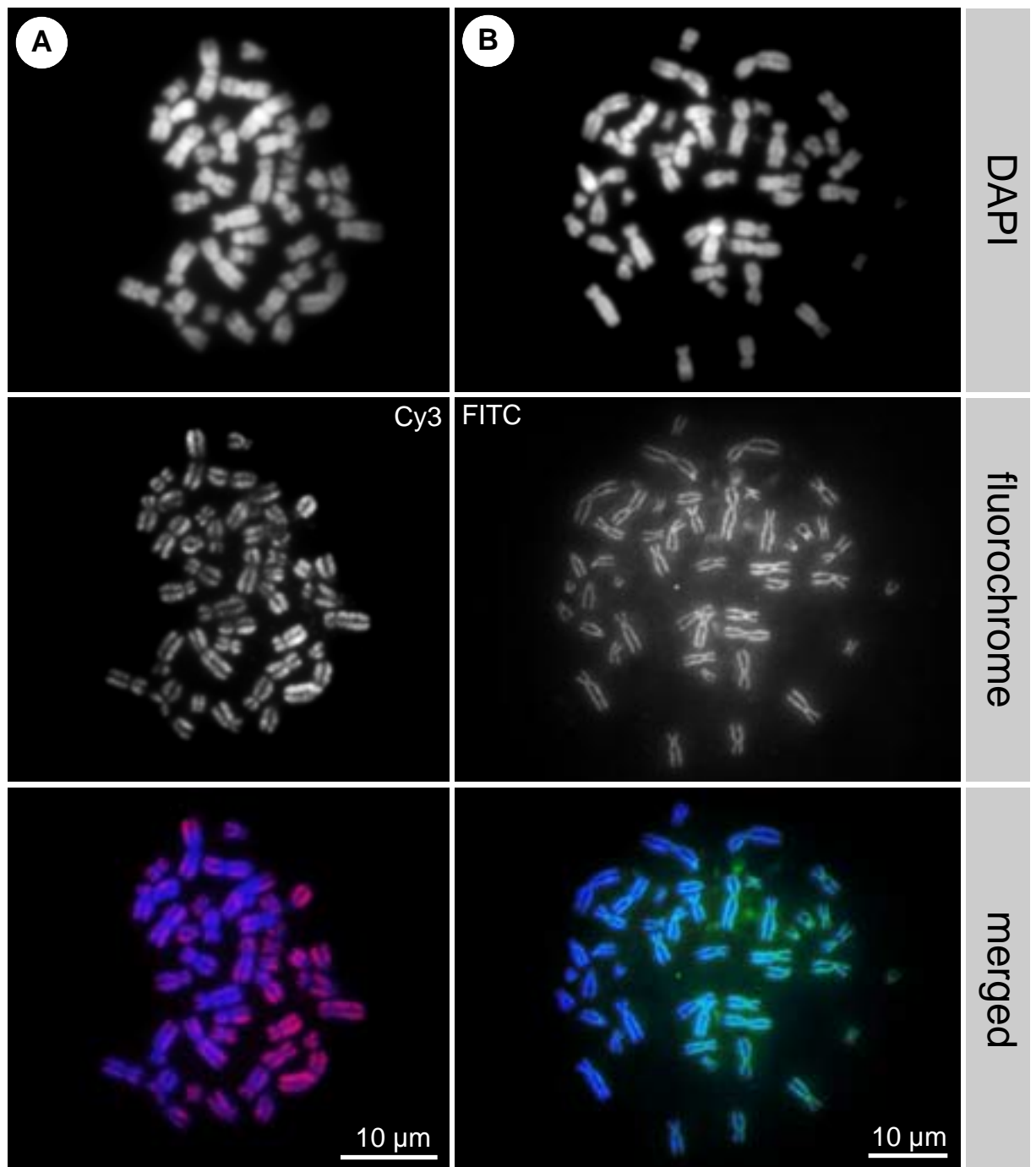


Figure 5

SE micrographs of human chromosomes prepared with the drop/cryo method. Chromosomes of undigested metaphase spreads typically are recognizable in relief, but not discretely in structural detail, through the nucleoplasmic layer (A, B), with exception of an unconcealed “periphery” chromosome (B, arrow). Untreated metaphase spreads rarely appeared unconcealed by the nucleoplasmic layer at low magnification (C), but structural details are not adequately discernable from the nucleoplasmic residue when examined with higher magnification (D, detail of framed region in C). Treatment with 0.01% pepsin resulted in nucleoplasmic digestion (E), but in a rather smooth chromosome surface (F, detail of framed area in E) suggesting chromatin digestion. Treatment with 0.1% trypsin also allows easy recognition of individual chromosomes at low magnification (G), but inadequate digestion of nucleoplasmic residue for discernment of structural detail (H, detail of framed area in G).

**Figure 6**

SE micrographs of *Gallus gallus* (chicken) chromosomes. Metaphase spreads without enzymatic treatment show a nucleoplasmic layer which allows recognition of chromosomes at low magnification (A), but at higher magnification does not allow adequate differentiation of the chromosomes from residual nucleoplasm (B, detail of framed area in A). Treatment with pepsin and rennin also allows recognition of individual chromosomes (C, E), but does not digest nucleoplasm adequately for discernment of structural details of chromosomes (D, detail of framed area in C; F, framed area in E). After digestion with both rennin and pepsin, a web-like interconnecting residue remains between, and presumably on, the chromosomes.

**Figure 7**

Fluorescent LM images of human mitotic metaphase chromosomes indirectly immunolabeled for H3P (**A**) and topoisomerase II (TPII, **B**) and counterstained with DAPI. The nucleoplasmic layer does not prohibit LM analysis for specific DNA and protein staining. The images of DAPI counterstain (**A**, **B** first row) show individual chromosomes, but no indication of a nucleoplasmic layer; Images showing fluorescent signals for the respective proteins (second row, **A** H3P; **B**, TPII) also label specifically on the chromosomes, not in nucleoplasm. Both proteins can be detected along the entire length of the chromosome, with a striking lack of signal between the sister chromatids, in contrast to DAPI images, as best illustrated in the color merged images (**A**, **B**, third row) giving the impression of discrete labeling of sister chromatids.

was comparable to pepsin (Table 7, Figure 6 E, F). Trypsin, which is routinely used in Giemsa staining, was ineffective in removing nucleoplasm (Figure 5 G, H). Although nucleoplasm could not be totally removed, chromosomes were in general exposed and recognizable at moderate magnifications (see criterion above) but revealed loose chromatin structure, indicating that chromatin was also subject to digestion. Reproducibility could not be improved. Since the enzymatic treatment did not dramatically improve chromosome isolation, the criteria for further high resolution investigation were not fulfilled, and the investigation of animal chromosomes were discontinued in this study.

Table 7 Enzymes applied for digestion of nucleoplasmic layer

| Enzyme | Concentrations applied | Effect on digestion of nucleoplasm |
|-----------|------------------------|------------------------------------|
| trypsin | 0.10% | ± |
| pepsin | 0.01% | ± |
| | 0.001% | ± |
| cathepsin | 0.001% | – |
| rennin | 0.01% | ± |
| | 0.001% | ± |

± some effect; – no effect

Phosphorylated histone H3 signal distribution on barley chromosomes as detected by LM

Tests for optimization of the immunogold labeling procedure were performed on mitotic barley chromosomes labeled indirectly for phosphorylated histone H3 serine 10 (H3P). H3P is an epigenetic modification universally detected during mitosis in eukaryotes and is well characterized for plants and animals. In mitotic animal cells H3P is distributed from prophase through metaphase evenly along chromosome arms, but in plant chromosomes is distributed in the pericentric region (WEI *et al.*, 1999; GARCIA-ORAD *et al.*, 2001; MANZANERO *et al.*, 2000, 2002). Chromosomes isolated with either drop/cryo or suspension methods were investigated to determine whether specific fluorescent labeling of H3P is applicable for both 3:1 and formaldehyde fixations.

For chromosomes isolated with the drop/cryo method, localization of H3P with the primary antibody anti-H3P in rabbit and secondary anti-rabbit IgG -Cy3 show one, or in some cases two, intensely labeled region(s) on both chromosome arms at the centromere with a length in

the range of 2-3 μm (Figure 8 A). However, the Cy3 image alone reveals that the signal is not exclusive to the pericentric region (Figure 8A, second row). Although maximum signal intensity is in the pericentric region, the signal is distributed with decreasing intensity toward the telomeres. Chromosomes isolated with the “suspension” preparation showed a strong signal of similar intensity and distribution to that of the drop/cryo chromosomes (Figure 8 B).

H3P signal distribution on chromosomes of other plant species

Since H3P distribution in barley and other plant species (HOUBEN & SCHUBERT, 2003) is associated with the centromere, additional plant species were chosen to investigate metaphase chromosomes of different size and centromeric orientations. H3P immunolabeling for fluorescent light microscopy was performed on *Oziroë biflora*, *Aribidopsis thaliana*, and *Luzula sylvatica* (Figure 9 A-C). *O. biflora* has both small and large chromosomes (1-12 μm) of metacentric and acrocentric orientation; the smallest chromosomes are of uncertain centromeric orientation. *A. thaliana* has very small chromosomes (1-3 μm) of metacentric and submetacentric orientation (SINGH, 2002) which is not visible on metaphase chromosomes in LM or SE. *L. sylvatica* has moderately sized holocentric chromosomes (6-8 μm). Routine chromosome preparation of unsynchronized and non-arrested *L. luzuloides* and *L. sylvatica* has been initiated in our lab. The *L. sylvatica* is the more procreative, and therefore the species on which experiments have been performed to date.

O. biflora displayed a strong fluorescent pericentric H3P signal on large and small chromosomes (Figure 9 A). For *A. thaliana* and *L. sylvatica*, fluorescent signals appeared to be distributed over entire chromosomes (Figure 9 B, C), supporting recent reports for this labeling behavior in *L. luzuloides* (GERNAND *et al.*, 2003). Smaller chromosomes in *A. thaliana* display weaker signals than those in its larger chromosomes; one strong signal of uncertain origin does not correspond to a DAPI signal (Figure 9 B, arrow). For *L. sylvatica*, signals are distributed over entire chromosomes, but show varying signal intensity along the chromosome arms, indicating that there may be areas of concentrated H3 phosphorylation (Figure 9 C).

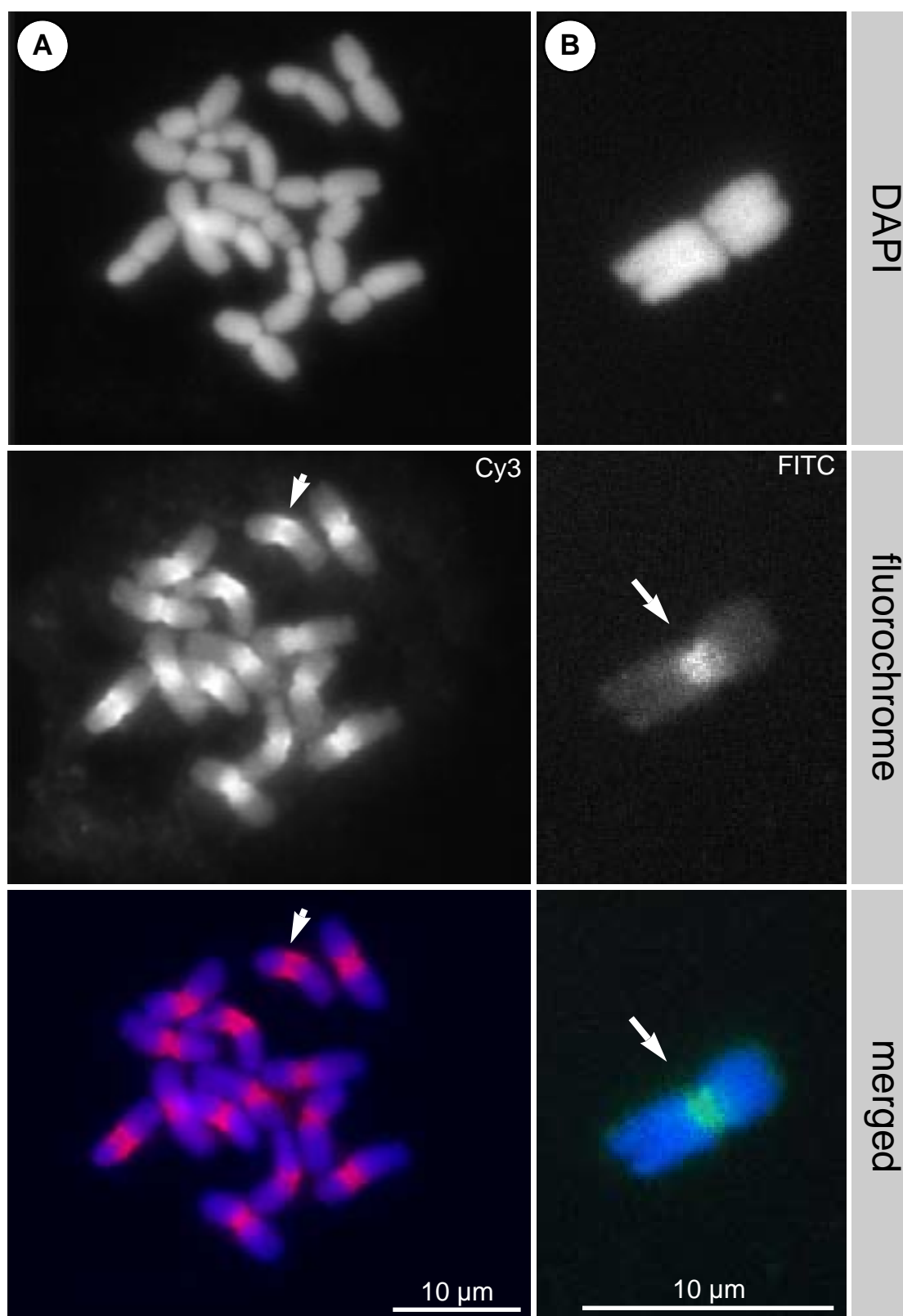


Figure 8

Fluorescent LM for drop/cryo (**A**) and suspension (**B**) *Hordeum vulgare* (barley) chromosomes indirectly labeled for H3P. The drop/cryo preparation was detected with anti-rabbit Cy3; suspension preparations with anti-rabbit FNG. With the drop/cryo method, entire chromosome complements in metaphase spreads may be isolated; the suspension method allows isolation of individual chromosomes outside of their nuclear context. Images from DAPI counterstain show outline of entire chromosomes, and reflect their DNA content (**A**, **B** first row). Fluorochrome (and merged) images detecting labeled H3P show a strong signal in the pericentric and centromeric region of the chromosomes for both fixation protocols (arrows, **A**, **B** second and third rows).

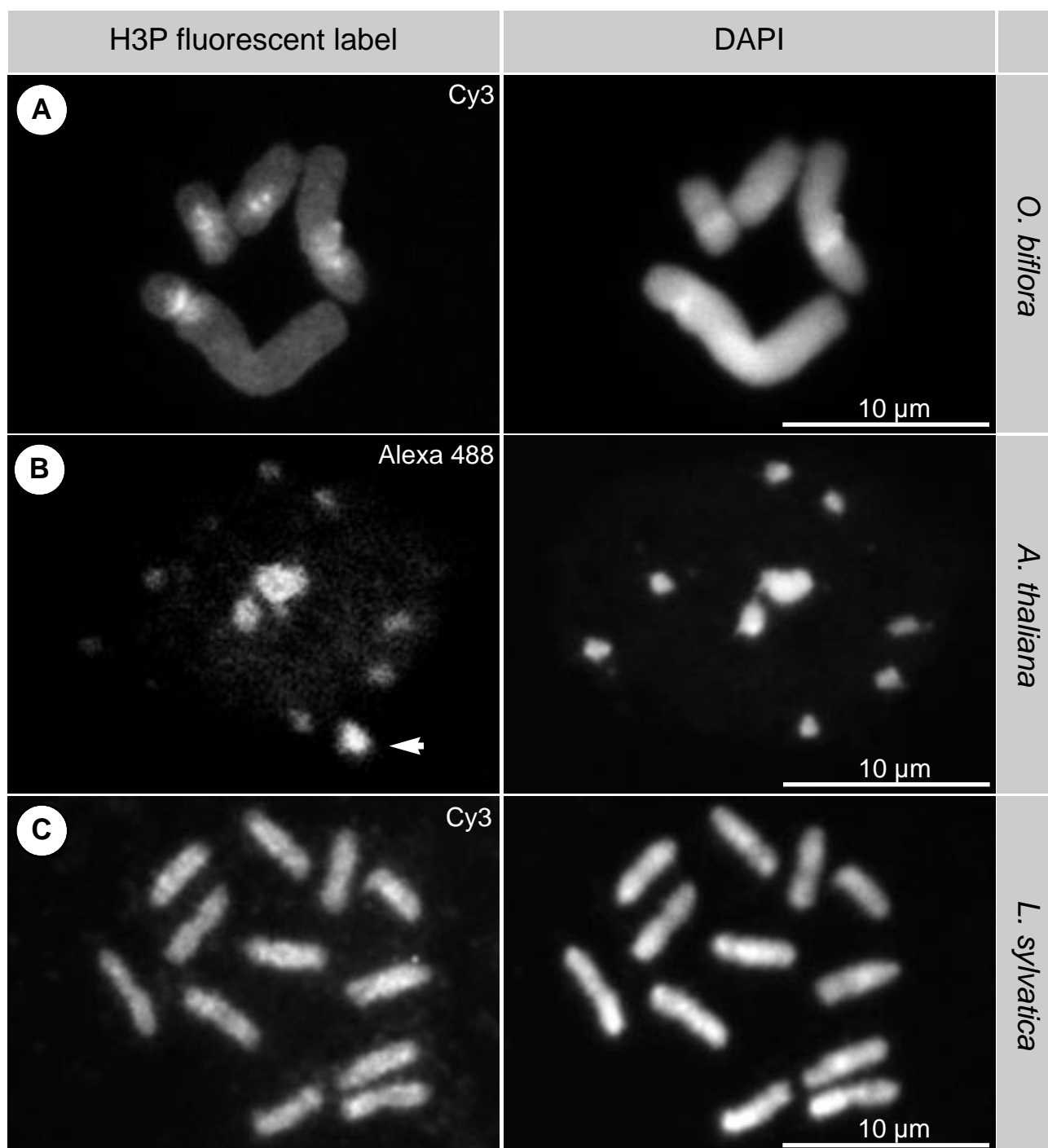


Figure 9

Fluorescent LM images of chromosomes from three different plant species, prepared with the drop/cryo method, indirectly labeled for phosphorylated histone H3 and fluorescent anti-rabbit antibodies, and counterstained with DAPI. The Cy3 image of H3P-labeled *Oziorö biflora* chromosomes shows strong signal areas bordering the centromeric constriction (A). In corresponding DAPI image, bands with higher signal intensity are located across the centromeric constriction. The Alexa image of H3P-labeled *Arabidopsis thaliana* shows the two largest chromosomes with strongest signal intensity (B); the smaller chromosomes show weaker signals than those in the corresponding DAPI image. One strong signal in the Alexa image (B, arrow) does not correspond to a DAPI signal. Cy3 image of H3P-labeled *Luzula sylvatica* chromosomes shows signal distribution along the entire chromosome, with intermediate punctual regions of higher signal intensity (C). The corresponding DAPI signals are rather unhomogenous, show no obvious constrictions, and occupy the same area as the Cy3 signals.

Optimization of immunolabeling procedure for SEM investigation

Shrinkage due to critical point drying

The process of critical point drying (CPD) is crucial to structural preservation for SEM investigations, as it prevents gradual collapse during specimen drying, maintaining its three-dimensional structure to a large degree. Chromosomes that are air-dried are flat and display an artificial surface layer that conceals chromosome structure (ALLEN *et al.*, 1988; MARTIN *et al.*, 1994; SUMNER, 1996; WANNER *et al.*, 2004). CPD-mediated shrinkage and shifting of chromosomes, even after fixation, has been observed in LM and measured in volume by atomic force microscopy (AFM) (SCHAPER *et al.*, 2000; SHICHIRI *et al.*, 2003; WANNER *et al.*, 2004). The effect of CPD on binding affinity of antibodies, signal distribution and overall fluorescence was investigated on barley chromosomes in LM. Barley chromosomes were indirectly immunolabeled for H3P with a secondary antibody conjugated with Cy3 and routinely prepared for LM (anti-fading agent and coverslip applied). Fluorescent signals on chromosomes in LM were recorded, the coverslip and anti-fading agent removed, and the specimens were dehydrated in acetone and critical point dried according to routine procedure. Images of the same chromosomes were taken after critical point drying (anti-fading and coverslip omitted). Comparison of length and breadth of fluorescent (DAPI) signals before and after CPD shows a decrease in area of approximately 15% (Figure 10A, B). The Cy3 signal differs slightly in appearance before and after CPD; whereas before CPD the signals were bright patches in the pericentric region, after CPD the signals are strong, but have a "spot-like" character, and appear distributed along the whole chromosome arm (Figure 10 A, B). Medial signal gaps visible on chromosomes before CPD are no longer visible after CPD. This indicates that shrinkage occurs rather homogeneously over the whole chromosome, not radiating outward from the centromere, which would create or widen a signal gap.

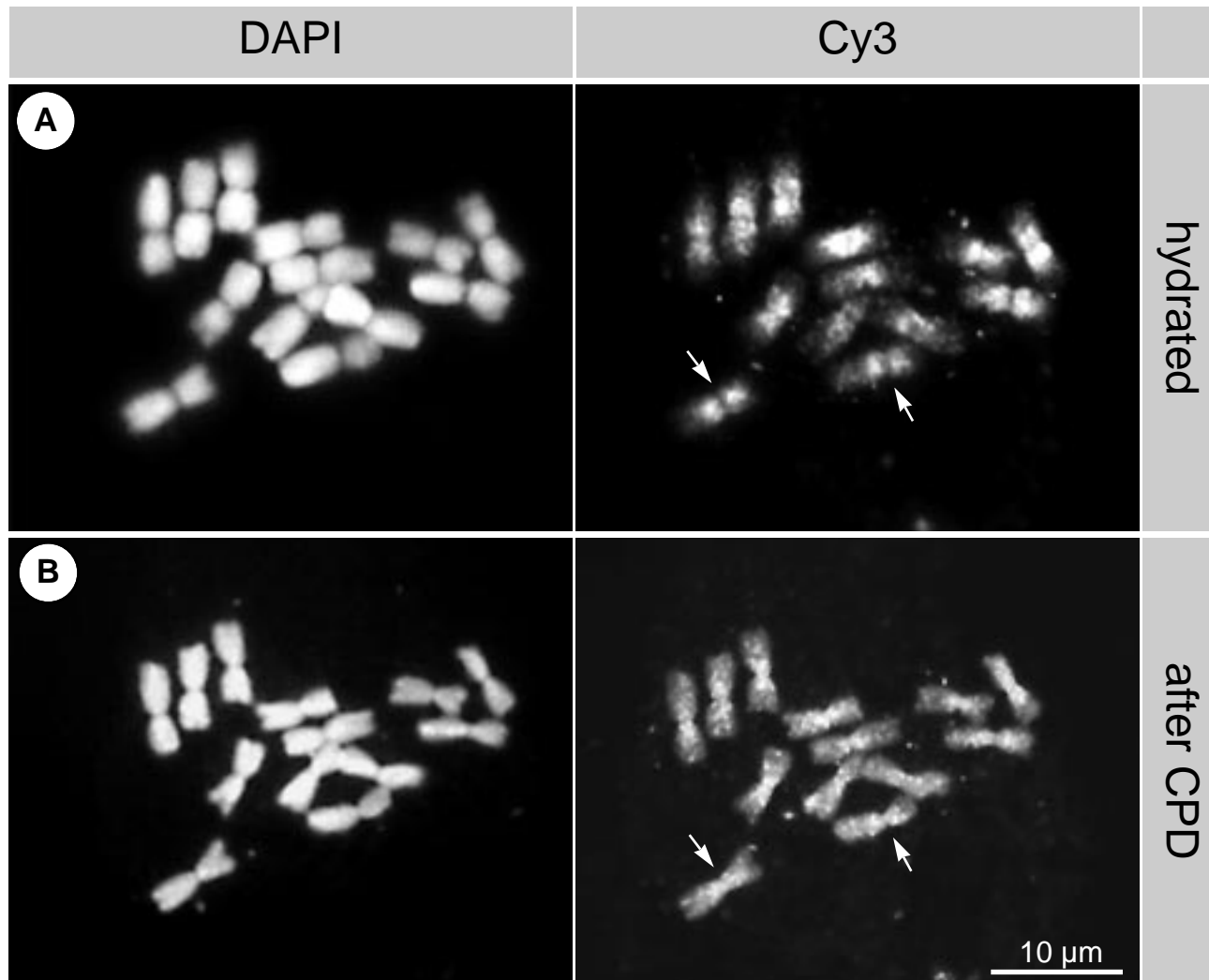


Figure 10

Fluorescent signals from a barley metaphase chromosome spread, indirectly immunolabeled for H3P, before (**A**) and after (**B**) critical point drying (CPD). Comparing lengths and widths of DAPI signals from chromosomes before (**A**) and after (**B**) critical point drying, a shortening and narrowing of chromosomes can be determined which amounts to an average shrinkage of 15% in length. The Cy3 image from hydrated chromosomes (**A**, second column) shows H3P signals as bright patches in the pericentric region and diffuse weak signals toward the distal chromosome arms; a signal gap at the centromere is visible on some chromosomes (arrows, **A**, image on right). After CPD, the Cy3 signal still appears strong, but has a “spot-like” appearance, with stronger signals in the pericentric and centromeric area (**B**, image on right). After CPD, signal gaps are not visible at the centromeres (arrows, **B**).

Immunogoldlabeling with different gold markers

Experiments aimed at optimizing immunogold labeling were performed on barley using H3P to enable numerous routine parallel assays. Three different secondary antibodies were tested individually for detection in SEM: an IgG conjugated with 10 nm gold, Fab' fragments covalently bound with both FITC and 1.4 nm Nanogold[®] (FNG) (POWELL *et al.*, 1998), and Fab' fragments covalently bound only with Nanogold[®] (NG). As the size of Nanogold[®] is at the resolution limit of the SEM, Nanogold[®] labeling systems must be enhanced with gold or silver, a time-dependent process of autometallography resulting in gold and/or silver compound particles of detectable size. Parallel controls with IgG-Cy3 for LM monitored specific performance of the primary antibody.

With IgG-10 nm gold, virtually no "gold signals" (recognized as bright spots in the BSE image) could be detected in the SEM (Table 8). Chromosomes labeled with H3P-IgG 10 nm gold with a tertiary antibody, (anti-goat)-IgG-Cy3, applied to detect the presence of the anti-rabbit IgG to which the colloidal gold is conjugated, showed a distinct pericentric signal in LM, but in SEM no recognizable signal pattern in BSE image at lower magnification, and negligible signals at adequate magnification for resolution of individual 10 nm signals (10 000 fold) (Figure 11 A-E). With Fab'-FluoroNanogold[®], a pericentric signal distribution could be observed in LM but not in SEM (Table 8, Figure 12). With Fab'-Nanogold[®] a distinct pericentric signal region, of comparable intensity to that observed in LM, could be detected in SEM (Table 8), which encouraged further detailed studies optimizing this application.

Table 8 Comparison of different gold markers used for immunolabeling in SEM

| Gold marker | Detection in LM | Detection in SEM |
|---|-----------------|------------------|
| Colloidal gold (10 nm) (anti-rabbit IgG) | – | – |
| Fluoronanogold [™] (FNG)* (Fab' fragment) | +++ | – |
| Nanogold [®] (NG)* (Fab' fragment) | | |
| • 6 min Ag-enhancement | – | ++ |
| • 10 min Ag-enhancement | + | +++ |

*enhancement necessary for detection in EM

Signal intensity from none (–) to weak (+) to strong (+++)

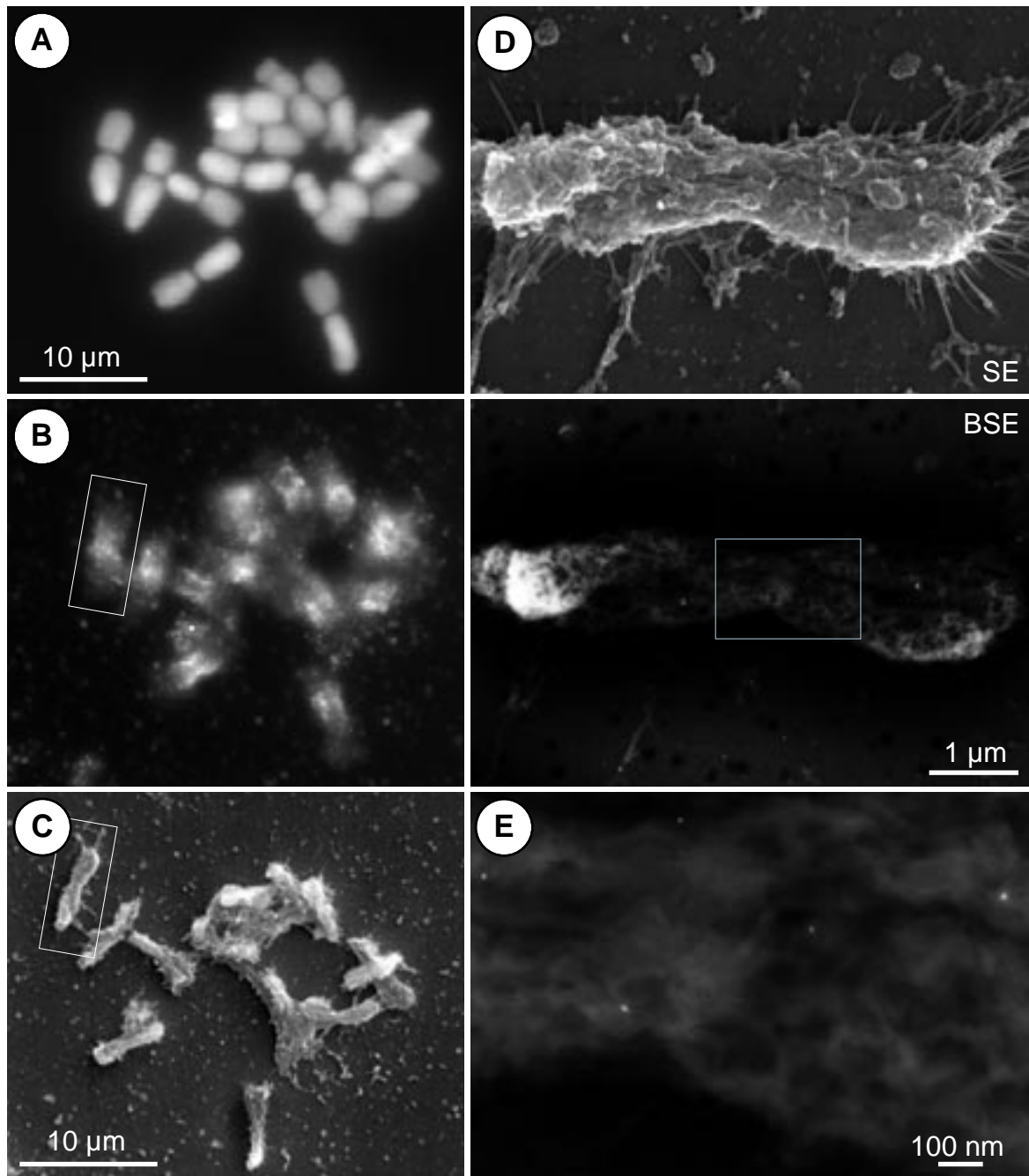


Figure 11

LM and SEM images of a barley metaphase chromosome spread labeled for H3P with anti-rabbit 10 nm gold (in goat) and with a tertiary anti-goat Cy3 antibody. DAPI image (A) shows DNA distribution; Cy3 image (B) shows the distribution of goat-IgG (secondary antibody conjugated with 10 nm gold). Amongst considerable background, a strong pericentric signal is detected, proving that the secondary antibody was bound. The corresponding SE image at low magnification provides a structural survey of this metaphase spread (C). With the SE image at moderate magnification, chromosome surface structure can be visualized (D, upper image, detail of chromosome framed in B and C), whereas the corresponding BSE image shows that only very few signals originating from conjugated 10 nm gold particles can be detected (D, lower image). A detail of the pericentric area shows only few widely dispersed signals from gold particles, even at high magnification (E, framed area from D, BSE image). The “gold” signal distribution as detected in the BSE mode in SEM does not correspond whatsoever to the fluorescent signal distribution in LM.

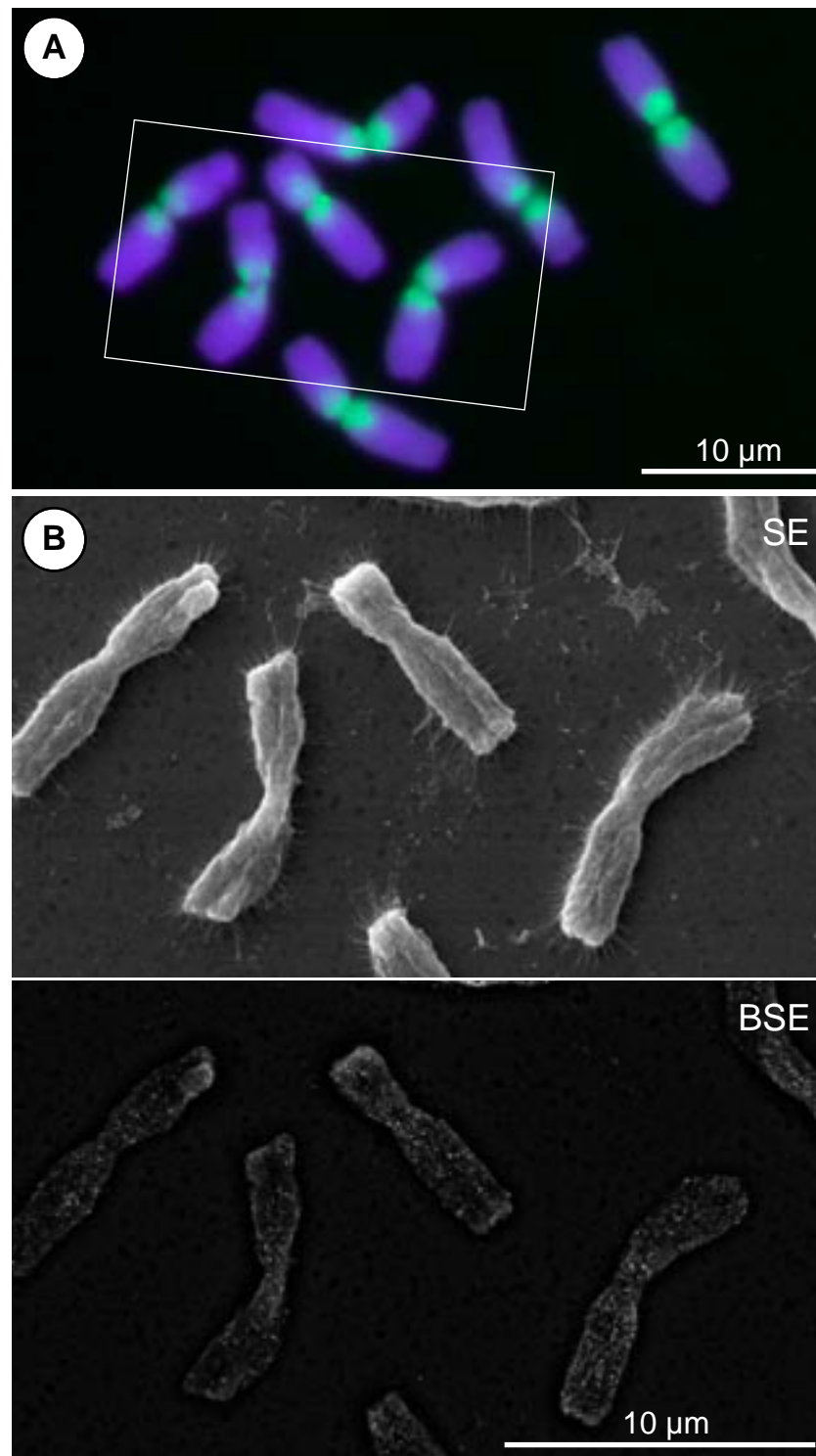


Figure 12

LM and SEM images of the same barley metaphase chromosomes immunolabeled for H3P with FNG and Au-enhanced for 6 min. Superimposed FITC and DAPI images show strong typical LM signals on all chromosomes in the pericentric region (A, green areas). SE image detail of framed region in A shows rather smooth chromosome surface structure after removal of anti-fading agent and critical point drying (B). At this magnification chromosomes show a longitudinal axis of symmetry, indicating distinguishable sister chromatids, but no chromomeres or parallel fibers are visible. Simultaneous BSE image of the same region shows the even distribution of Nanogold® signals along the entire chromosome, differing greatly from the signal distribution in LM image.

Optimizing enhancement time

Using Nanogold Fab' fragments as secondary antibodies, the influence of enhancement time on the signal intensity in SEM was investigated, with the intention of finding an optimal enhancement time and kind – gold (^{79}Au) or silver(^{47}Ag) – for routine application. Barley chromosomes labeled for H3P and Nanogold® Fab' fragments and enhanced with gold, a light-insensitive process, for 6 and 10 min (Table 9; Figure 13) or with silver, a light-sensitive process that must be performed under darkroom conditions (Table 10, Figure 14). With both kinds of enhancement, diameter of the signals from gold particles increased with time, as determined by measuring diameter of signal spots on the BSE image (with a “line measure” tool in Digital Micrograph software). Neither enhancement method resulted in uniform signal size. Given the same enhancement time, Ag-enhancement resulted in smaller signal diameters on average and greater number of signals than Au-enhancement (compare Tables 9 and 10). For this reason, the signal distribution pattern of Ag-enhanced specimens appears more distinct, which was considered advantageous for the purposes of this study. Using Ag-enhancement, the minimal enhancement time required for signal detection in SEM at a moderate magnification of 5 000-10 000 fold was 5 min (Figure 14). With increasing 1 min increments, the number of detectable signals increased. Where signals could be detected as individual spots, it could be determined that the diameter of signals increased with increasing enhancement time for both gold and silver (Tables 9 and 10). After 7 min, individual signals became less distinguishable, apparently overlapping or aggregating to “bright” patches rather than individual signal spots. Between 9-10 min enhancement, the signal could be detected with phase contrast and DIC in LM prior to SEM investigation. Signal number could only be estimated due to overlap (Figure 14). For the purpose of this study, 6 min enhancement time was chosen as the optimum for further investigation, and was used in further experiments unless otherwise indicated.

Energy dispersive X-ray (EDX) analysis confirmed that detected signals originated from enhanced particles of the respective enhancement metal (Figure 15 A, B). The underlying 1.4 nm Nanogold® particle was not resolved in the spectral analysis of silver-enhanced specimens (Figure 15 A) and of un-enhanced specimens (data not shown), presumably due to X-ray absorbance of the specimen.

Table 9 Comparison of signal number, signal diameter and relative specificity after Gold-Enhancement

| Enhancement time | Number of signals | Diameter of signals (nm) | % Background to total number of signals per chromosome |
|------------------|-----------------------------|--------------------------|--|
| 6 min | 102 (n=34, range 41-308) | 55 | 37% |
| 10 min | 283 (n=1) | 63 | 43% |

Table 10 Comparison of signal number, signal diameter and relative specificity after Silver-Enhancement

| Enhancement time | Number of signals | Diameter of signals (nm) | % Background to total number of signals per chromosome |
|------------------|---------------------------------|--------------------------|--|
| 6 min | 359 (n=27, range 50-852) | 20 | 48% |
| 10 min | 3040 (n=5, range 2200-3600*) | 35 | 16% |

*partially estimated due to signal overlap

Influence protocol steps on labeling efficiency

Effects of further parameters of the immunolabeling protocol on labeling efficiency were investigated. It was necessary to establish a “lean” protocol, omitting any dispensable (otherwise routine) steps for the sake of structural preservation, but also optimizing labeling efficiency and specificity. Wash and incubation solutions, blocking solutions, unspecific antibody labeling and the enhancement procedure were taken into consideration. With few excep-

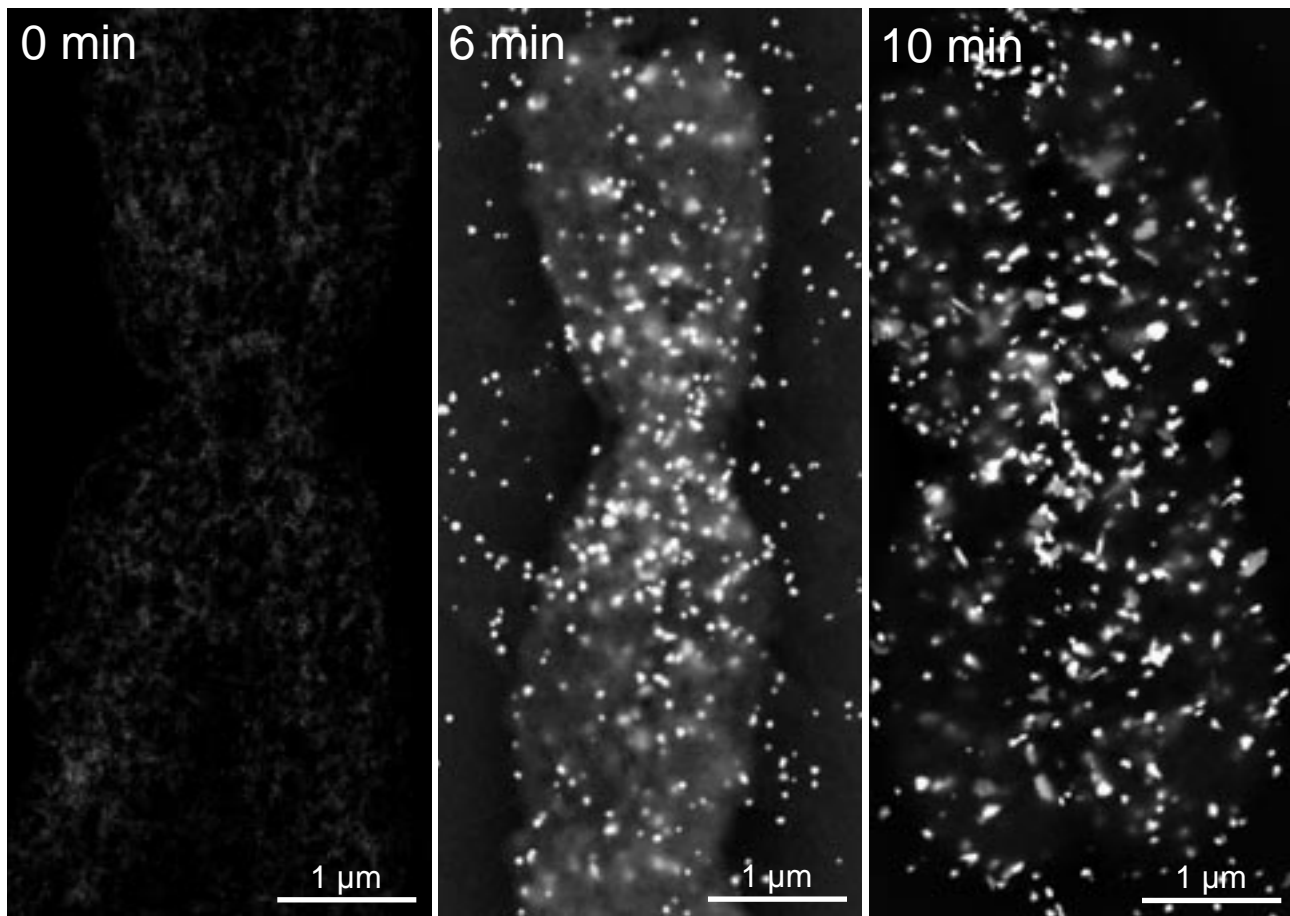


Figure 13

BSE micrographs of barley chromosomes immunolabeled for H3P with NG and Au-enhanced showing signal distribution and size with respect to duration of Au-enhancement. No NG signals were detected on specimens that were not enhanced. 6 min enhancement resulted in an average signal size of approx. 55 nm; 10 min enhancement resulted in an average signal size of 63 nm. Signals are not uniform in size, especially in the case of 10 min Au-enhancement.

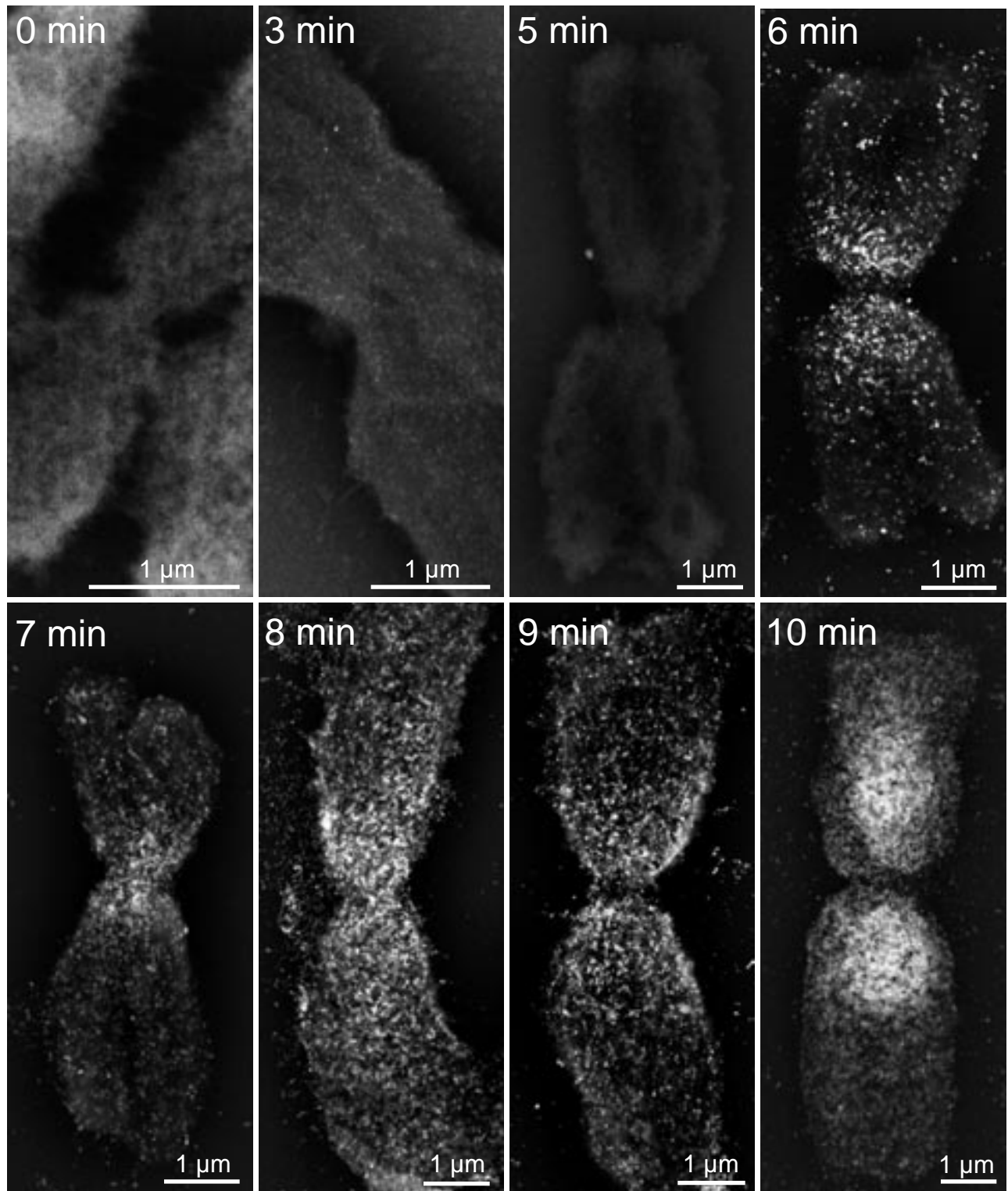


Figure 14

BSE micrographs of barley chromosomes labeled for H3P and NG showing signal intensity with respect to duration of Ag-enhancement. At the magnification shown, enhanced signals were first visible after 5 min enhancement. With 6 to 8 min enhancement signals could be discerned and counted as individual "spots". After 8 min signals were generally seen as bright regions of aggregate signals due to enhancement overlap. For the purposes of this study, a routine enhancement time of 6 min was chosen.

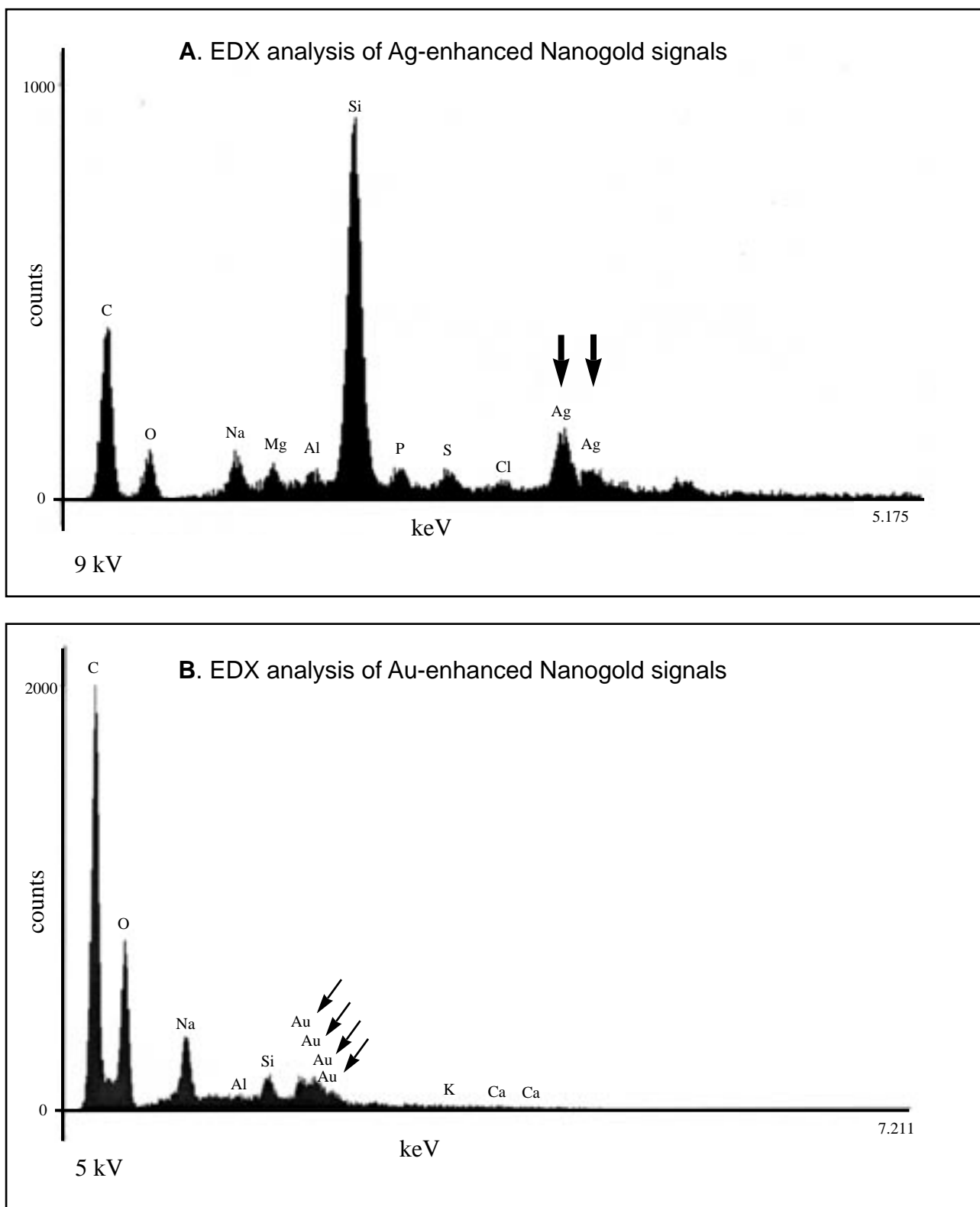


Figure 15

Energy dispersive X-ray analysis (EDX) spectra demonstrating (A) detection of Ag on Ag-enhanced signals and (B) Au on Au-enhanced signals. The 1.4 nm gold particle could not be detected on Ag-enhanced preparations, presumably due to X-ray absorbance of specimen. For gold detection an optimum accelerating voltage was 5 kV was determined; duration of recording was 8 min. Au ($M_{a1}+M_{\beta}+L_{a1}$). Ag ($L_{a1}+L_{\beta1}$) at an optimum accelerating voltage of 9 kV.

tons, each factor was tested for titttions, each factor was tested for both Au-enhancement and Ag-enhancement. Signal number was determined by counting total signal “spots” per chromosome from an enlarged BSE image (DIN A4 computer printout).

Wash solutions PBS, with and without detergent (Tween 20), and *aqua dest* were compared. Immunolabeling experiments using Tris and SSC buffers for washing and incubation resulted in negligible signals (compared to use of PBS buffer), and these buffers were not included in further experiments. To test unspecific enhancement (signals resulting solely from unspecific metallonucleation during the enhancement procedure), chromosome specimens were washed in *aqua dest*, PBS/Tween, or PBS/Tween/Block solution and then silver or gold enhanced without application of primary or secondary antibodies. After Au-enhancement, there was no unspecific signal detected on chromosomes washed with *aqua dest* or PBS/Tween, whereas silver-enhanced chromosomes of the same wash solutions resulted in a small amount of unspecific labeling (Table 11 A). Washing with *aqua dest* resulted in a larger number of unspecific signals than PBS/Tween (Table 11 A). For both gold and silver enhancement, washing in PBS/Tween and PBS/Block resulted in very few unspecific signals.

Table 11 Signal numbers resulting from different immuno(Nano)gold labeling protocol steps

| Enhancement 6 min | A. Signals prior to immunolabeling | | | B. Signals after immunolabeling | | | | |
|----------------------------------|------------------------------------|------------------------|------------------------|---------------------------------|-----------------------|------------------------------|-------------------|-----------------------------|
| | washed in H ₂ O | washed in PBS/Tween | washed in PBS/Block | Prim. Anti- body | Sec. Anti- body | Post- fixation omitted | Post- fixation | Post- fixation +Block |
| Ag- enhanced 6 min | 11 (n=4) | 1 (n=3) | 16 (n=3) | H3P | NG | 852 (n=2) | 496 (n=2) | 660 (n=6) |
| | | | | -- | NG | | 400 (n=1) | 344 (n=5) |
| | | | | H3P | -- | 12 (n=3) | 58 (n=3) | — |
| | | | | -- | -- | 64 (n=2) | none | — |
| Au- Enhanced 6 min | none | none | not detectable* | H3P | NG | 308 (n=3) | 205 (n=3) | 220 (n=8) |
| | | | | -- | NG | 145 (n=3) | | 137 (n=2) |
| | | | | H3P | -- | 112 (n=3) | 12 (n=2) | — |
| | | | | -- | -- | | 52 (n=3) | |

Grey units are not included in comparison.

*Signals could be detected at higher magnification, but not at magnification used (5000 x 4) for serial comparison of other protocol steps

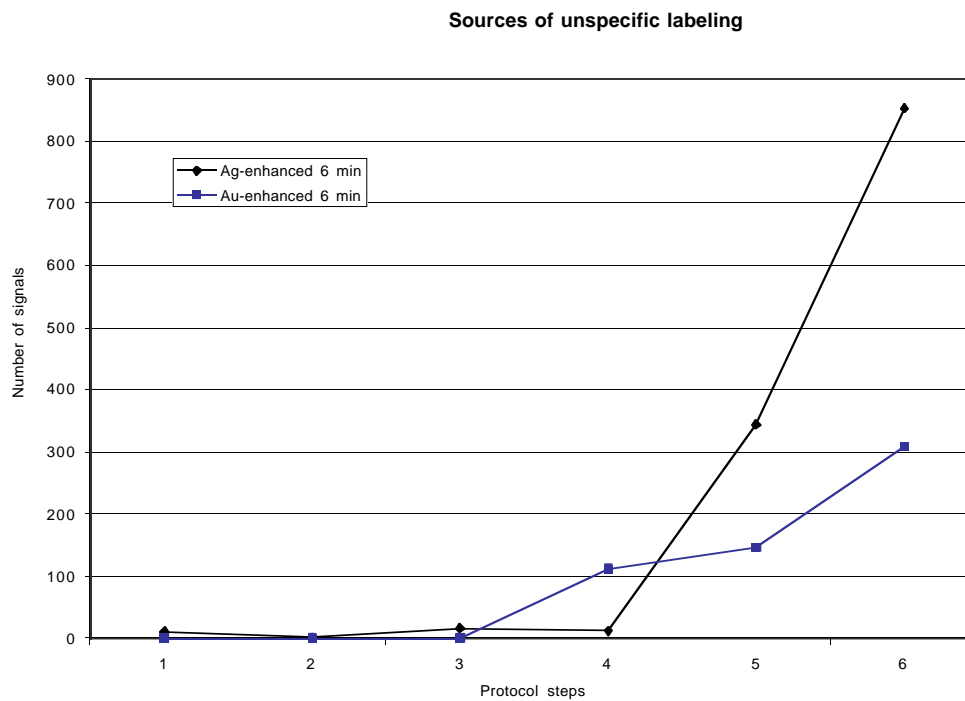
-- antibody omitted

— chromosome specimens not quantifiable

Unspecific and specific labeling were investigated by 1) comparing number of signals resulting from application of primary and secondary antibodies with those on preparations for which either primary or secondary antibody were omitted, and 2) comparing number of signals resulting from application or omission of block solution during antibody incubation and 3) comparing number of signals after post-immunolabeling fixation with 2% formaldehyde. As with pre-immunolabeling investigations, assays were tested for both Au-enhancement and Ag-enhancement.

Despite standardized protocols and procedures, signal numbers varied considerably between individual applications, rendering it difficult to make clear conclusions about the different protocol steps using actual signal numbers examined (Tables 9, 10). The ratio of unspecific signal numbers from control preparations (with the primary antibody omitted) to total number of signals per chromosome (primary antibody included) was, however, relatively consistent from experiment to experiment and could be used as a basis of comparison. With increasing enhancement time this ratio decreases, and can be represented as percentage background to total signal number (Table 9, 10). In general, there was considerable unspecific labeling in specimens with primary or secondary antibody omitted; in no case was the number of “unspecific” signals as low as those prior to immunolabeling (compare Table 11 A with 11 B).

In all cases studied application of only the primary antibody resulted in less unspecific labeling than the secondary antibody (Table 11 B), indicating that the secondary antibody is primarily responsible for unspecific labeling. A distinction between Au-enhancement and Ag-enhancement with respect to unspecific labeling after incubation with either primary or secondary antibodies can also be determined (Table 12). Au-enhancement shows a slightly higher level of unspecific labeling with application of only primary antibody; Ag-enhancement results in a substantially higher number of unspecific signals with only the secondary antibody. After incubation with both primary and secondary antibody, Ag-enhancement results in higher overall signal number (Table 12).

Table 12 Schematic representation of signal numbers after successive immunolabeling protocol steps for Ag-enhancement and Au-enhancement

Protocol steps/parameters:

- 1 = wash with H₂O
- 2 = wash with PBS/Tween
- 3 = wash with PBS/Block
- 4 = incubation with primary antibody
- 5 = incubation with secondary antibody
- 6 = incubation with primary and secondary antibody

Influence of post-fixation on chromosome ultrastructure

For routine drop/cryo preparation, chromosomes are fixed in a 2.5% glutaraldehyde solution after they are “dropped” on slides. Preliminary experiments (and experiments for ISH) showed that labeling efficiency is lower with glutaraldehyde-fixed chromosomes than with formaldehyde-fixed or unfixed chromosomes (unpublished data). To counteract this, a slight modification of the drop/cryo technique was made by omitting the 2.5% glutaraldehyde fixation in order to promote diffusion of the antibodies throughout the chromatin without potentially hindering protein interconnections. This protocol modification was made, however, under the condition that post-labeling fixation, a common procedure for immunolabeling, with either 2% formaldehyde or 2.5% glutaraldehyde is performed. Post-fixation, however, also influences signal number and unspecific labeling. Chromosomes for which post-fixation was omitted had the highest total signal number. Post-fixed chromosomes had lower total signal num-

ber, but considerable unspecific labeling. Blocking free aldehydes with BSA blocking solution (according to manufacturers recommendation) in an additional wash step increased total signal number and decreased unspecific labeling with respect to (solely) post-fixed chromosomes, but had lower overall signal number than those where post-fixation was completely omitted (Table 9).

Since un(post)-fixed specimens allow highest signal number and specific labeling, the influence of post-fixation (or its omission) in combination with Ag-enhancement and Au-enhancement on chromosome ultrastructure was investigated. The criteria for well preserved chromosome ultrastructure were the same as previously described (Figure 16 A). In general, immunolabeled chromosomes were flatter than standard drop/cryo chromosomes, and a “soft-lobed” chromomere structure is not preserved (Figure 16 B-E). Parallel fibrils are still observed on Ag-enhanced chromosomes (Figure 16 B, C). The surface structure of Au-enhanced specimens was characterized by rather smooth “folds” or “ripples” (Figure 16 D, E) Post-fixation influenced the adhesion of chromosomes to glass slide, which increased the total number of chromosomes available for investigation, and prevented flattening of Au-enhanced specimens chromosomes. As this is prerequisite to further high resolution analysis, 3D analysis in particular, post-fixation with 2.5% glutaraldehyde was maintained as an indispensable step in the immunogold labeling procedure for SEM.

Effect of fixation technique on labeling efficiency

The standard drop/cryo fixation for SEM chromosome investigation requires the fixation of cell suspensions in 3:1 (v/v, ethanol: acetic acid) and application of 45% v/v acetic acid after dropping cell suspension onto glass slides to facilitate spreading of full chromosome complements. An alternative fixation, the suspension method, which is routinely applied in other labs for LM studies, does not require acetic acid, but entails fixation of root tips with 2% formaldehyde prior to preparation and sonification of meristematic tissue (SCHUBERT *et al.*, 1993). Individual chromosomes are then isolated in a filtered suspension of dissociated cell contents and are not isolated in metaphase spreads. Experiments showed that “suspension” chromosomes are more or less three dimensional. Structural preservation varies greatly, presumably due to mild fixation. Chromomeres and parallel fibrils could be recognized, although the chromosome arms tend to be stretched, especially at the centromere (Figure 17). This preparation method could be established in our lab, but proved to be marginally appropriate for routine analysis in SEM. Limited yield of chromosomes, which dictates time-consuming searching, and, more importantly for this study, inconsistent

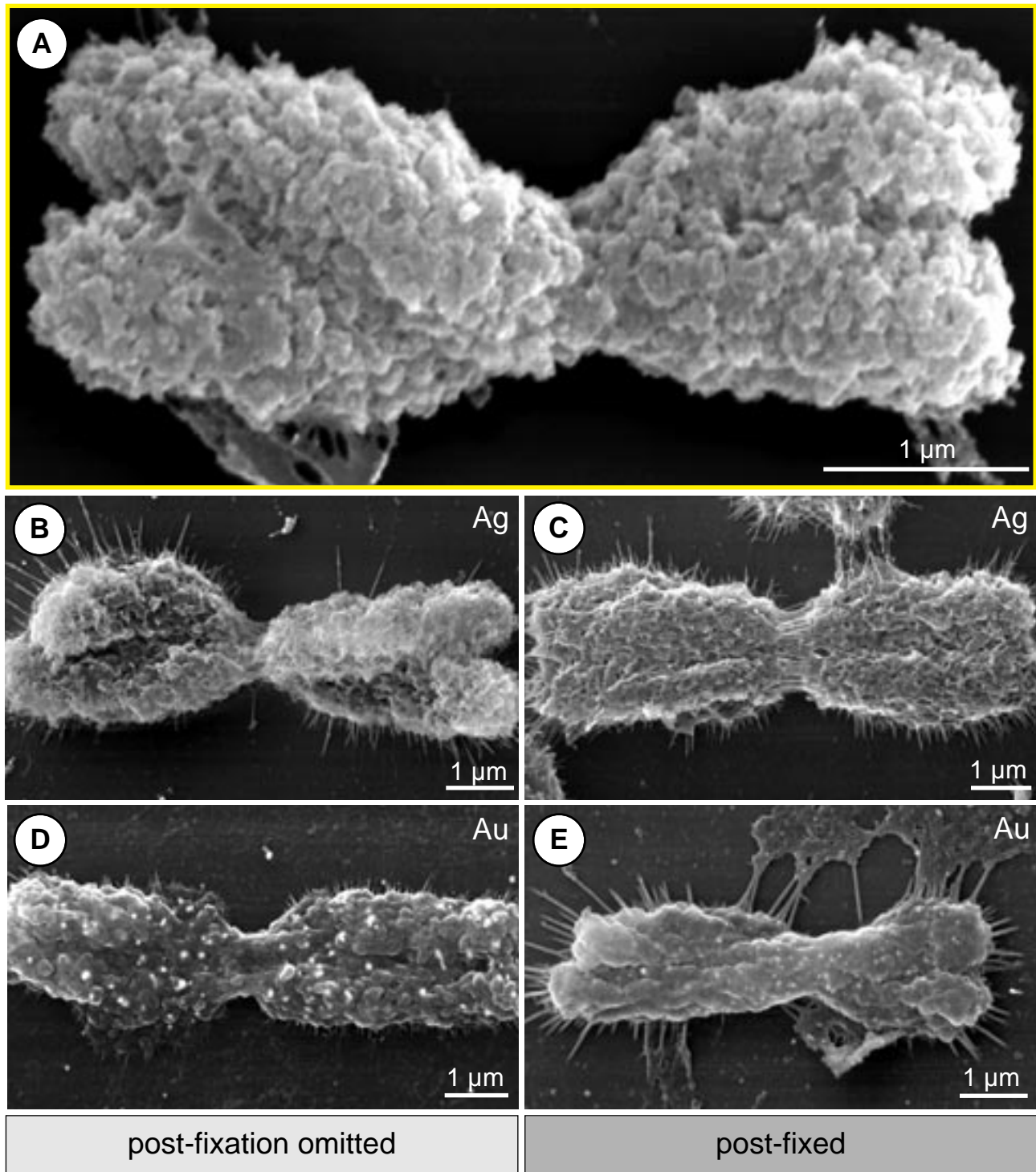


Figure 16

SEM SE images from immuno(Nano)gold labeled barley chromosomes, illustrating the effects of 2% formaldehyde post-fixation in combination with Ag-enhancement or Au-enhancement on the structural preservation, as compared to a standard barley chromosome prepared with the drop/cryo method that was not immunogold labeled (A). In general, chromosomes are flatter and maintain less pronounced chromomeres compared to the “standard” drop/cryo chromosome (B-E, compare with A). Ag-enhanced chromosomes (B, C) remain structurally better preserved than Au-enhanced chromosomes (D, E), regardless of inclusion or omission of post-fixation. Post-fixation seems to affect adherence of chromosomes to glass slide (D), prevents flattening in Au-enhanced chromosomes (compare D, E).

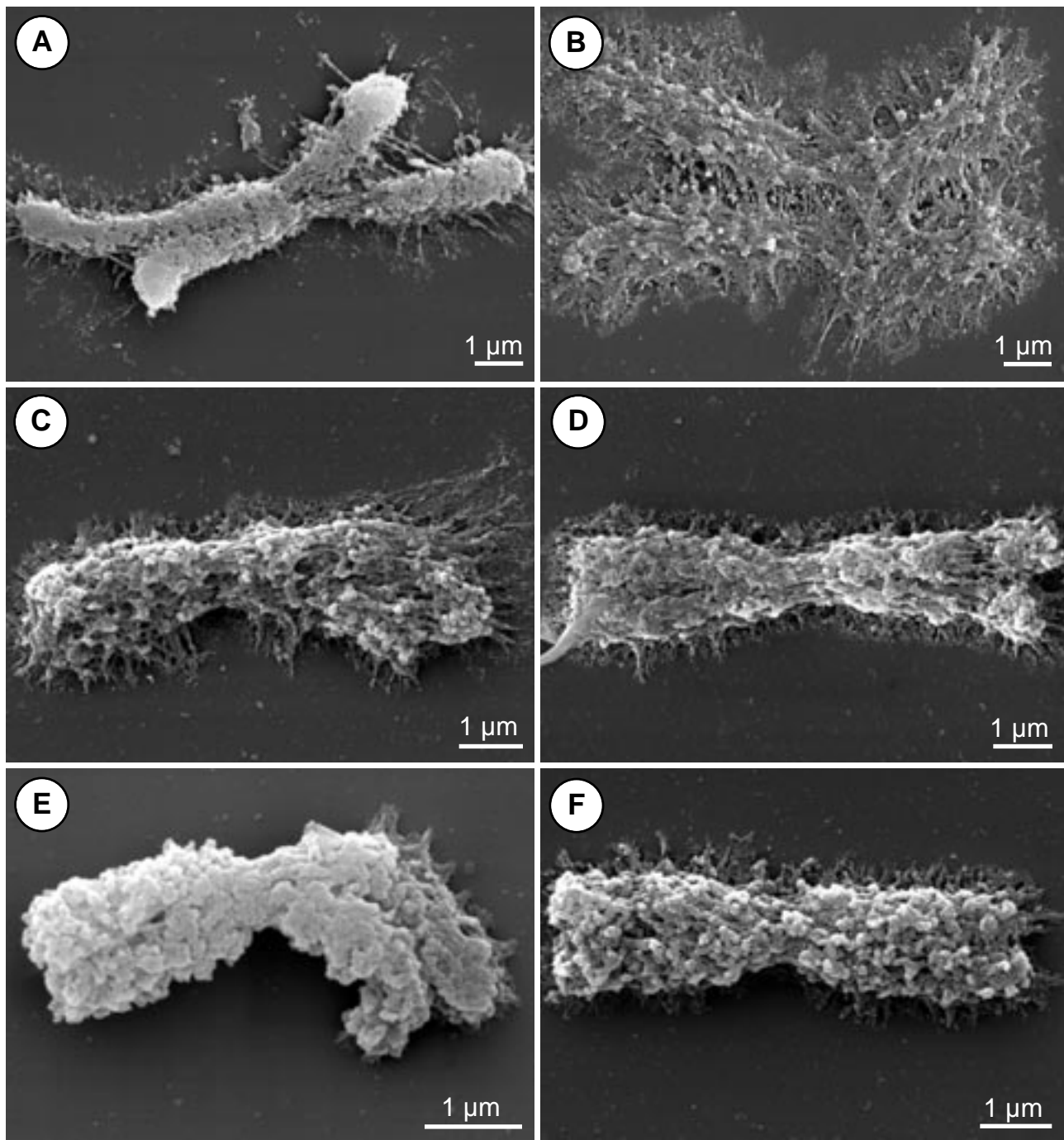


Figure 17

SEM micrographs of mitotic barley metaphase chromosomes isolated by the suspension method showing examples of their widely varying states of structural preservation. (A) Chromosome with distorted, asymmetrical position on the glass slide; sister chromatids are of different length, and the chromatid arms are widely separated. (B) Chromosome is dramatically flattened, and sister chromatids are almost completely disjoined. Knobby structures could be derived from chromomeres, and parallel features are recognizable in the otherwise highly deviant chromosome structure. (C) Chromosome is partially flattened at a distal arm. (D) Chromatids appear stretched in a symmetrical manner, and the chromomere structure appears loosened. (E and F) Chromosome structure is well preserved, with distinguishable sister chromatids, recognizable chromomeres, constriction at the centromere and underlying parallel fibrils just obvious at the centromere. Chromatin appears generally compact in (E), but chromomeres are visible. In (F) chromomeres are somewhat less compact. Accelerating voltage = 8 kV.

structural preservation, precluded large series for immunolabeling SEM analysis. Nonetheless, chromosomes fixed with the suspension preparation were included as crucial parallel controls for antibody recognition of epitopes in immunolabeling experiments.

Quantifying signal distribution

By counting the number of signals in defined transverse sections of BSE micrographs, and plotting the signal number versus the relative length of chromosome, signal distribution could be graphically represented in profile (Fig 18 A). Likewise, a “background” profile, reflecting unspecific labeling from the secondary antibody and enhancement, could be quantified by counting signals per segment on chromosomes from which the primary antibody was omitted (Figure 18 B). By averaging data from numerous chromosome, larger scale tendencies could be graphically represented (Figure 19 A). Investigations were able to show that labeling efficiency was the same or stronger for “suspension” chromosomes than on “drop/cryo” chromosomes (Figure 19 B, C). In general, the labeled pericentric regions of chromosomes isolated with the suspension method showed a greater number of signals compared to those isolated with the drop/cryo method, but fewer signals along the chromosome arms. The signal distribution is similar for both fixations (Figure 19 A). Variations only occurred with respect to signal number, represented as the amplitude of the curve, and position of peaks due to varied structural preservation of the “drop/cryo” and “suspension” chromosomes studied (19 A-C). This shows that immunogold labeling of phosphorylated histone H3 is not precluded by fixation with acetic acid, although it results in slightly lower labeling efficiency (signal number). Fixation with 3:1 (v/v ethanol:acetic acid) has the advantage of superior preservation of chromosome ultrastructure and its application for large numbers of chromosomes in routine.

SEM detection of H3P distribution in *Hordeum vulgare* (barley)

Using the parameters determined in optimizing experiments, the signal distribution of H3P detected with NG on barley chromosomes was characterized for SEM. At low magnifications in SEM (approx. 500 fold), signals can be recognized with the BSE detector only if they form strongly labeled regions as “bright” areas. Individual signals of 30 nm diameter, the average for the routinely applied Ag-enhancement time of 6 min, could not be recognized at this magnification. For specimens with strong labeling intensity or longer enhancement times, the

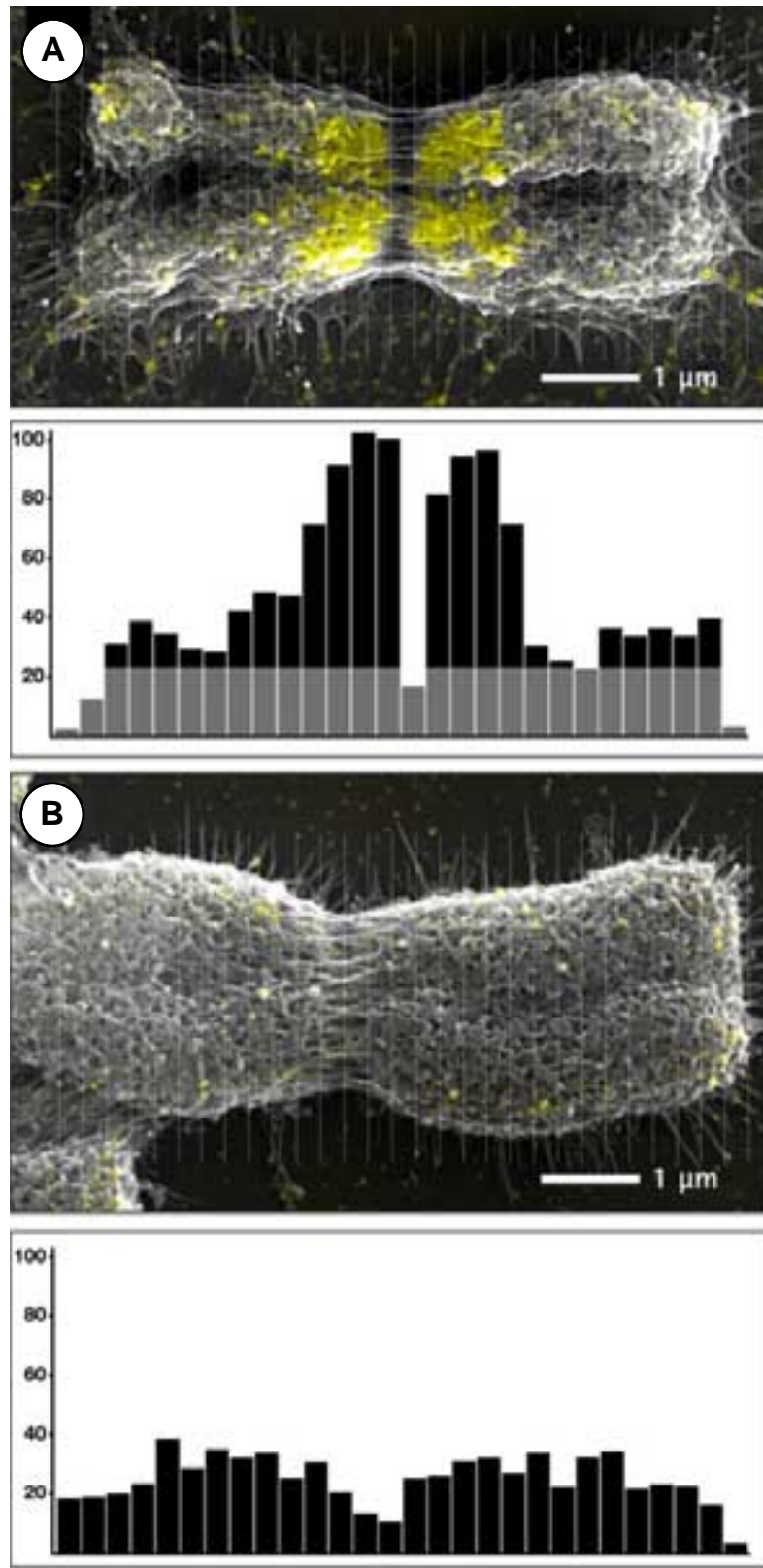


Figure 18

Quantification of signal distribution on a barley metaphase chromosome labeled for H3P with Nanogold® and Ag-enhanced for 6 min. Superimposed simultaneously recorded SE and BSE micrographs allow colocalization of signals (yellow) to structural elements of the chromosome (A). The corresponding diagram shows signal number (y-axis) and distribution per chromosome segment (x-axis) as two maxima (black) on a “base level” of background signals (grey). Background was determined by counting signals on a “control” chromosome (primary antibody omitted) per chromosome segment (B). (From SCHROEDER-REITER *et al.*, 2003)

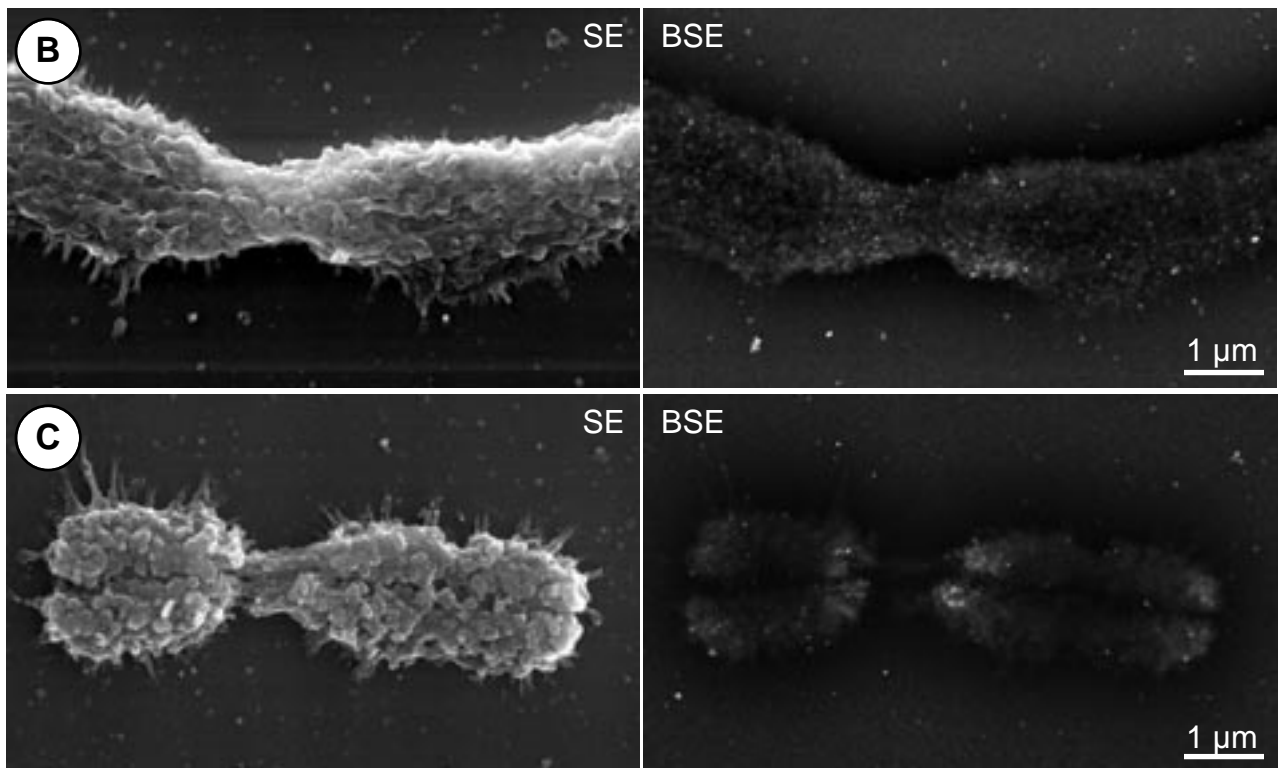
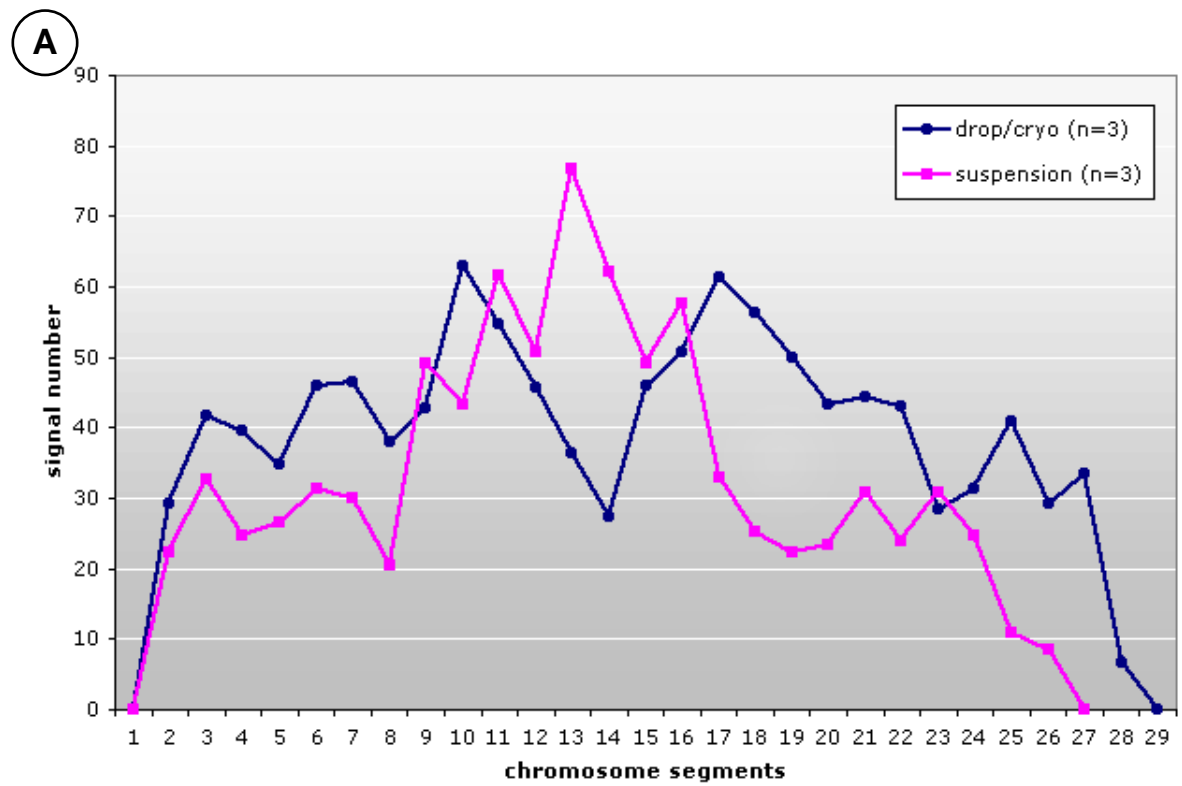


Figure 19

Signal distribution profile for H3P on barley chromosomes prepared with different protocols: drop/cryo and suspension preparation (A). SE and BSE micrographs illustrate chromosome surface structure and signal distribution for drop/cryo chromosomes (B) and chromosomes isolated with the suspension preparation (C).

BSE image of H3P labeled with NG correlates well to LM images with fluorescent labeling (Figure 20 A), while the simultaneous SE image provides additional information about surface details of the chromosomes (Figure 20 B, C). Distinctly three dimensional sister chromatids, compact “bunched” chromosome surface, and discrete constrictions at the centromere (Figure 20 B, C).

Whereas signals appear as “bright” areas in BSE images at low magnifications, they appear more distinctly at moderate magnifications (5 000-fold) as irregularly shaped areas of conglomerate signals or individual signal spots. Simultaneous SE images enable localization of the signals/signal areas to defined chromosome structural elements (Figure 20 B, C). Individual signals can be detected along the whole chromosome arms and at the telomeres. The majority of the signals is found on the chromomeres in the pericentric region. A signal gap at the centromere is visible on all chromosomes in the BSE image, and corresponds to exposed parallel fibrils. No gap can be recognized on the Cy3 image in LM, suggesting that the size of the signal gap is below the resolution limit of LM (Figure 20 A).

SEM detection of H3P distribution in *Luzula sylvatica*

SEM analysis of the H3P distribution pattern was also performed for *L. sylvatica*. (*A. thaliana* could not be isolated from residual nucleoplasm for high resolution analysis; see Figure 9). Immunogold labeling experiments with *L. sylvatica* included barley specimens as a positive control ensuring reactivity of primary and secondary antibodies. SE images show that metaphase spreads were not completely free of nucleoplasm, which typically appeared to radiate from individual chromosomes and to interconnect neighboring chromosomes, but which did not conceal chromosome surface structure (Figure 21 A, B). Higher magnification confirmed the lack of constrictions on *L. sylvatica* chromosomes (Figure 21 C, D). Chromomeres could be recognized on metaphase chromosomes of different degrees of condensation (as judged by length) (Figure 21 C, D). Parallel fibrils and interconnecting structures were rarely seen for *L. sylvatica* chromosomes at an extreme state of compaction ($< 5 \mu\text{m}$) (Figure 21 C). Simultaneous BSE images of specimens labeled with Nanogold and Ag-enhanced for 7 min (a precautionary increase in enhancement time to ensure detection even in the case of poor binding efficiency) show few signals, on average 9 per chromosome, with no indication of an accumulation of signals on a particular area of the chromosomes (Figure 21 C, D). Signals also were detected in the nucleoplasmic residue. Because of the low number of signals, BSE data can neither support nor dispute the claim of signal distribution along entire

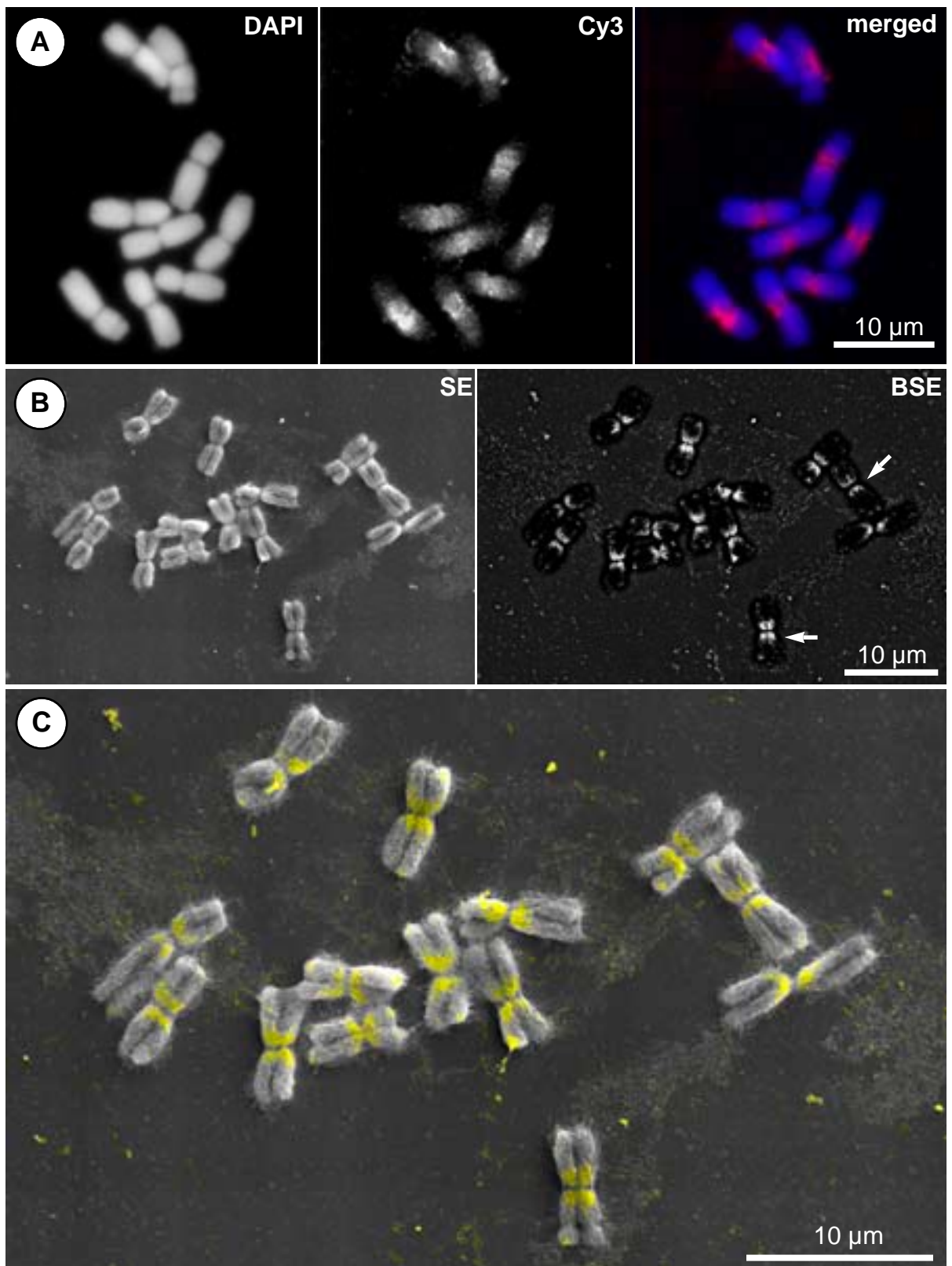


Figure 20

LM and SEM images of two different barley metaphase spreads, in which chromosomes are indirectly immunolabeled for H3P with anti-rabbit Cy3 for LM images and with anti-rabbit Nanogold® Ag-enhanced for 6 min for SEM images. The DAPI counterstain displays an outline of whole chromosomes, and the Cy3 image shows a strong signal for H3P spanning the pericentric and centromeric regions (A). A weak signal toward the distal chromosome arms can be seen in the Cy3 image, but not in the merged image (A, compare center and far right images). SEM images recorded at 9 kV display basic chromosome features (B, SE image) and strong signals in the pericentric regions with signal gap at the centromere on all chromosomes (B, arrows in BSE image). Already at low magnification, superposition of BSE (yellow) and SE images allows colocalization of signal regions and chromosome structural features (C). (From SCHROEDER-REITER *et al.*, 2003)

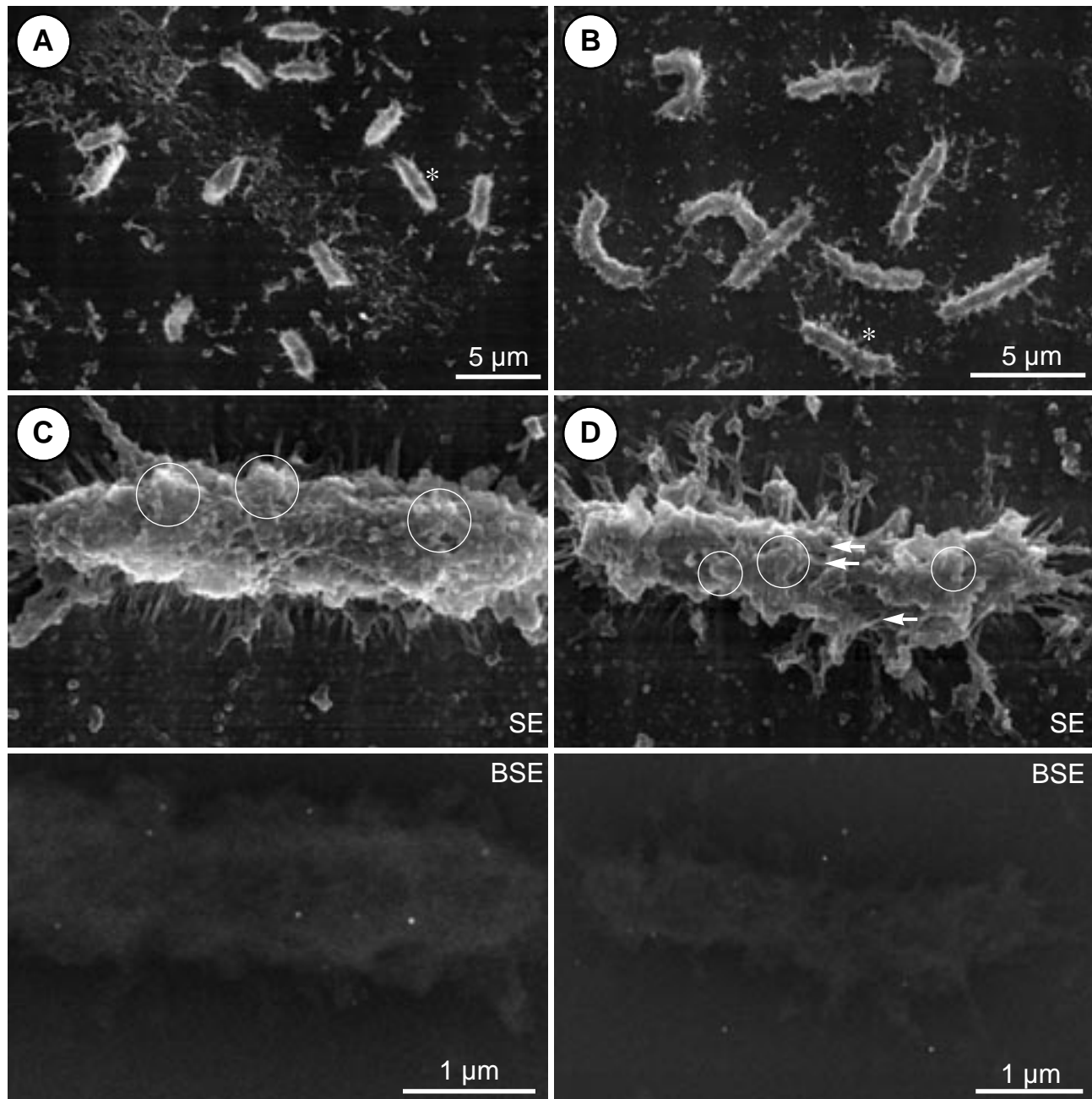


Figure 21

SEM micrographs of *Luzula sylvatica* chromosomes after indirect immunolabeling with H3P, Nanogold® and 7 min Ag-enhancement. At low magnification neither highly condensed (**A**) nor less condensed (**B**) chromosomes have visible constrictions, as is characteristic for holocentric chromosomes. Asterices mark the chromosomes for which details are shown. Higher magnification SE image of chromosome from **A** reveals chromomeres, but not parallel fibers (**C**, circles). In the SE image of the chromosome marked in **B**, chromomeres and fibrils are visible (**D**, circles and arrows, respectively). Simultaneous BSE images of both chromosomes show very few sparsely distributed gold signals from H3P labeling (**C**, **D**).

chromosomes. The positive control with barley chromosomes also showed very few, albeit specific, signals, suggesting suboptimal reactivity of the Nanogold antibody and/or Ag-enhancement.

Correlative LM and SEM microscopy with Alexa Fluor® 488-Nanogold®

An attractive prospect in correlative microscopy is examining one and the same specimen with LM and SEM in order to successively and narrowly define the location and (ultra)structure of labeled epitopes. With this, analysis could profit from the combined advantages of signal amplification and whole-cell context in LM and increased magnification and resolution of cellular substructures in SEM. Fluoronanogold (FNG) offered the possibility of such correlative investigations, but did not show good correlation of LM and SEM images (see Figure 12). Further experiments, and comparison with data from immunogold labeling with (non-fluorescent) Nanogold®, indicated that the presence of FITC in FNG fostered unspecific Ag-enhancement. The recently available Alexa Fluor®488-Nanogold® (ANG), a Nanogold® antibody bound with the fluorochrome Alexa Fluor® 488, provided an alternative for this correlative approach.

Using ANG, the same signals could be detected first with LM, and then, after further preparation, with SEM (Figure 22 A, B). LM images show strong specific signals in the pericentric region of the barley chromosomes (compare Figure 22A with Figure 8 A). SE images showing topographical structural information indicate that chromosomes are three-dimensionally preserved, and that the centromeric constriction and sister chromatids are recognizable (Figure 22 B). In general, as deduced from higher resolution SE images of all chromosomes investigated, parallel fibrils, but not chromomeres are preserved, which is similar to structural preservation on NG specimens (Figure 22 a, b, c). BSE detection of the Ag-enhanced ANG signals shows a striking difference in signal intensity to the Alexa Fluor®488 signals from the LM images; fluorescent signals on all chromosomes in the metaphase spread appear much stronger than the BSE signals, which are not even visible at a magnification equivalent to that of the LM images (Figure 22 A, B). At higher magnification, however, signals can be resolved; the specific labeling pattern is clearly visible in the BSE image (Figure 22 a, b, c). Consistent with data from immunolabeled specimens using non-

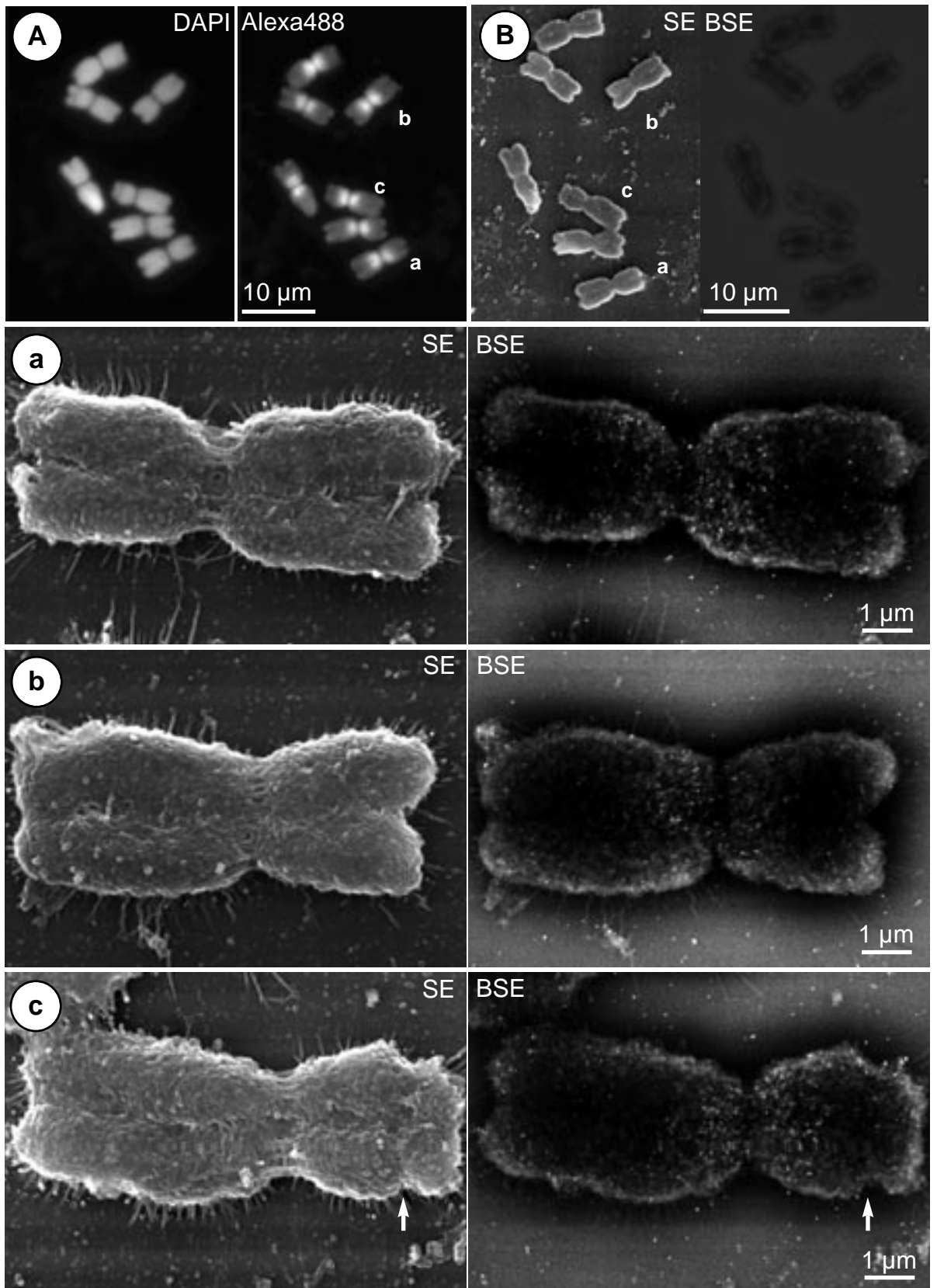


Figure 22

Direct correlation of LM and SEM images of barley metaphase chromosomes immunolabeled for H3P with ANG and Ag-enhanced for 6 min. LM images of DAPI counterstain and specific fluorescent labeling of H3P with AlexaFluor®488 show that strong signals are detected in the pericentric region, and that a signal gap can be detected on both DAPI and AlexaFluor®488 images (A). SEM analysis of the same chromosomes provide a general survey of chromosome structural preservation with SE image at low magnification, but no BSE signals from Ag-enhanced Nanogold particles (B). At higher magnification, however, signals can be resolved in the pericentric region. (a-c, righthand images). Signals are found neither on exposed parallel fibers at the centromere nor surrounding secondary constrictions (c, arrow). Corresponding SE images show parallel fibers at the centromere, barely distinguishable sister chromatids, but not typical chromomere structures (a-c, lefthand images).

fluorescent Nanogold®, signals are visible as individual spots or, in some case, “bright” areas resulting from overlap of Ag-enhanced gold particles. Signals are sparse on the distal chromosome arms, and there is an obvious signal accumulation in the pericentric and at the centromeric region. Signals are found neither in areas colocalizing with exposed parallel fibrils at the centromeric constriction nor surrounding secondary constrictions (Figure 22 a, b, c).

Effects of Nanogold® and fixation technique on H3P signal number and distribution

In response to the obvious difference in signal intensity between fluorescent and gold signals, and to investigate whether there is a difference in binding efficiency between the two Nanogold® products, a quantitative comparison of signal number between NG and ANG was performed. In addition, in the same study, experimental parallels of chromosomes fixed by the drop/cryo and by the suspension method were compared. The goal was to determine the most efficient combination of fixation and labeling system in terms of signal number and specificity (with respect to unspecific background labeling).

Signal distribution profiles were calculated; the background signal numbers were averaged, and represented as horizontal lines (Figure 23 A). Different combinations of chromosome fixation (drop/cryo and suspension methods) and secondary Nanogold® antibodies (NG or ANG) were investigated. Signal distribution profiles for all four combinations were superimposed for survey comparison of the data (Figure 23 A). BSE images show examples of the signal distribution on chromosomes with respective fixation and Nanogold® antibody combinations (Figure 30, B-E). For chromosomes fixed with the “suspension” protocol and labeled with ANG, the signals were so strong that it was necessary to extrapolate signal number in the pericentric region due to very strong signal overlap (Figure 23B). The signal distribution profiles exhibit two medial maxima; for ANG slight peaks at the extremities of the chromosome arms are evident (Figure 23 A). The distribution profiles differ in “amplitude”, but the lateral distribution is similar in all cases. Minor lateral profile deviations are due to variations in chromosomal length and linearity (position on slide). In terms of the secondary antibody, ANG had highest signal count, but also a correspondingly high background level compared to NG (Figure 23). Signal number and background differed for respective fixations: suspension fixation resulted in higher signal numbers for both ANG and NG than did 3:1 fixation; background for ANG assays was higher for suspension fixation than for 3:1 fixation (Figure 23 A), but for NG assays was negligible for both kinds of fixation

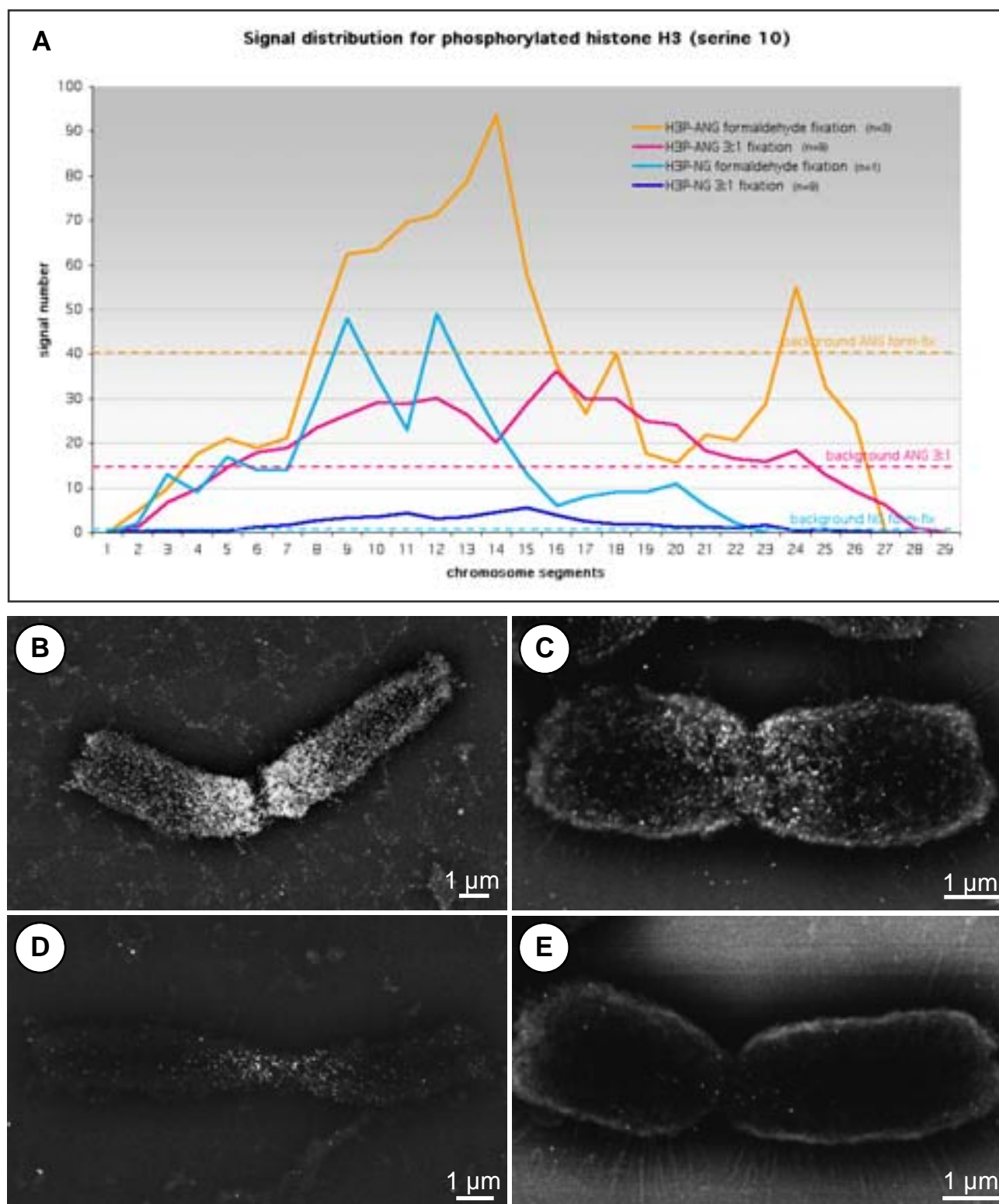
(Figure 23 A). SE data shows, however, that the isolated suspension chromosomes are flattened, stretched, and in general deviate from the criteria of structural preservation (Figure 24 A, C). Although signal number, *i.e.* binding efficiency is lower for chromosomes fixed with 3:1 fixative, the structural preservation is preferable to that of suspension chromosomes for SEM analysis (Figure 24 B, C). The performance of the secondary antibodies can also be generalized: in terms of signal number (binding efficiency), despite increased background level, implementation of ANG is advantageous; in terms of binding specificity (reduced background), NG is the more appropriate.

Immunogold labeling of other histone modifications

The immunogold labeling method with Nanogold® was applied for investigation of other histone modifications: dimethylated histone H3 at lysine position 4 [H3M (K4)], postulated to label euchromatin, and at lysine position 9 [H3M (K9)], postulated to label heterochromatin in eukaryotes (NAKAYAMA *et al.*, 2001; SOPPE *et al.*, 2002; HOUBEN *et al.*, 2003; LEHNERTZ *et al.*, 2003; PETERS *et al.*, 2003). LM studies have described H3M (K4) in barley as located in a broad “band” on the distal chromosome arms and H3M (K9) as distributed evenly over the entire chromosome (HOUBEN *et al.*, 2003). Using the protocol developed for H3P in this study, the signal distribution of these two histone modifications were investigated with LM and SEM in barley, with particular interest in a correlation of cytologically defined euchromatin and heterochromatin to chromosome structural features.

LM data show that signals are weak in general for both modifications. For H3M (K4) signals are detected on the telomeres; on the AlexaFluor®488 image two signals can be resolved on each telomere, appearing to decorate the telomeres of each sister chromatid (Figure 25 A).

The signal distribution pattern for H3M (K9) is indistinct. Although the fluorescent signal appeared evenly distributed along the chromosome in fluorescent and merged images, there was no significant difference in signal intensity to control specimens, from which the primary antibody was omitted (Figure 25 B, C). ANG binds unspecifically to the centromeric region in absence of the primary antibody, and the fluorescence on the chromosome arms appears more homogenous than that on the H3M (K9) specimen, but a clear difference between the signal

**Figure 23**

Signal distribution profile of H3P on barley chromosomes fixed with different protocols: suspension preparation fixed with formaldehyde (“form-fix”, yellow and light blue lines) and 3:1 (“3:1-fix”, magenta and dark blue lines) combined with either NG or ANG secondary antibodies (A). Dotted horizontal lines of corresponding color indicate the average number of signals on specimens with the primary antibody omitted. Background levels for NG (both form-fix and 3:1-fix) were negligible (A). BSE images show corresponding examples of labeled barley chromosomes: (B) form-fix with Alexa-NG; (C) 3:1-fix with Alexa-NG; (D) form-fix with NG; (E) 3:1-fix with NG. Higher signal number on chromosomes labeled with ANG in B and C is evident. Low background levels, therefore higher binding specificity, for chromosomes labeled with NG are evident in D and E.

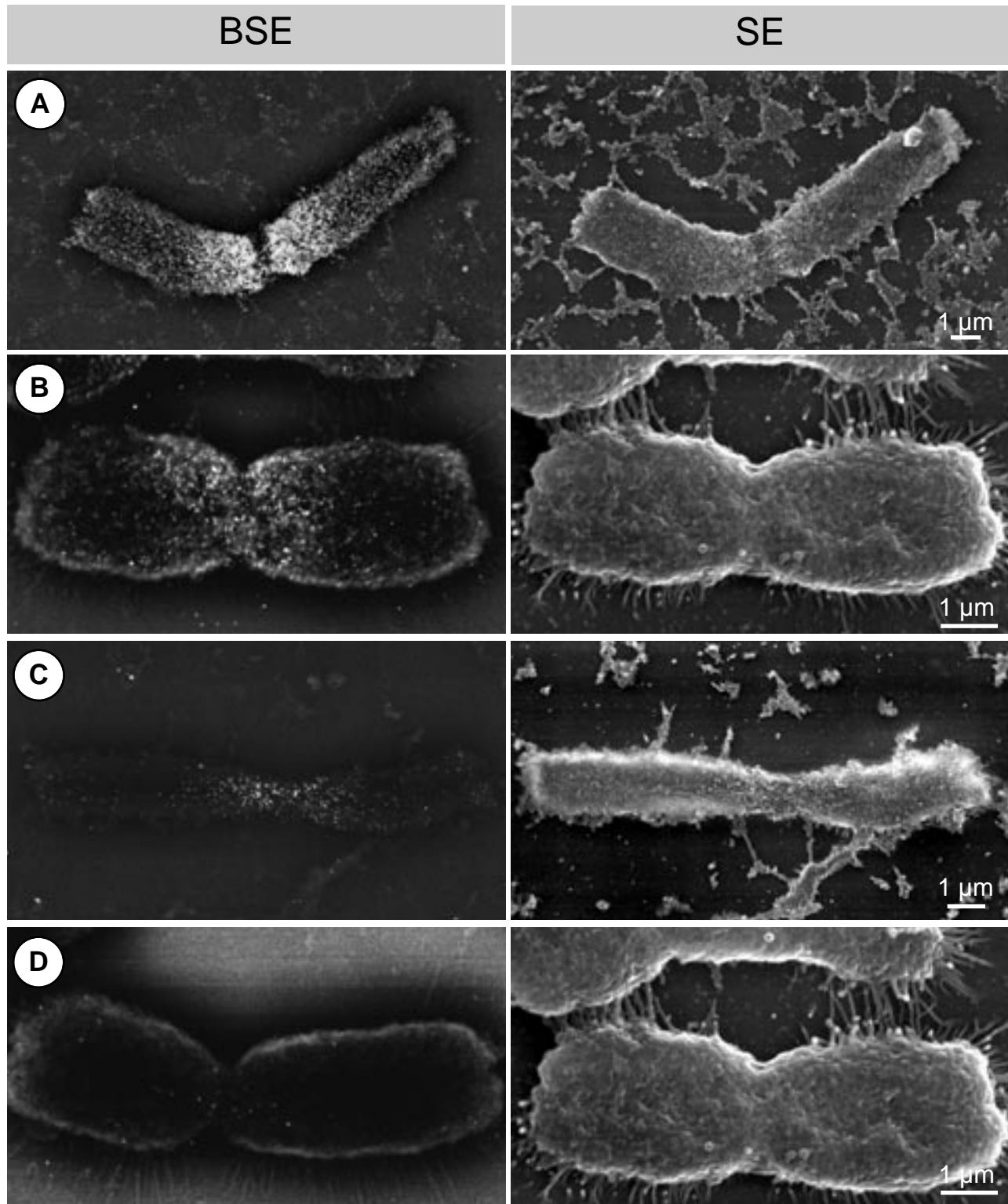
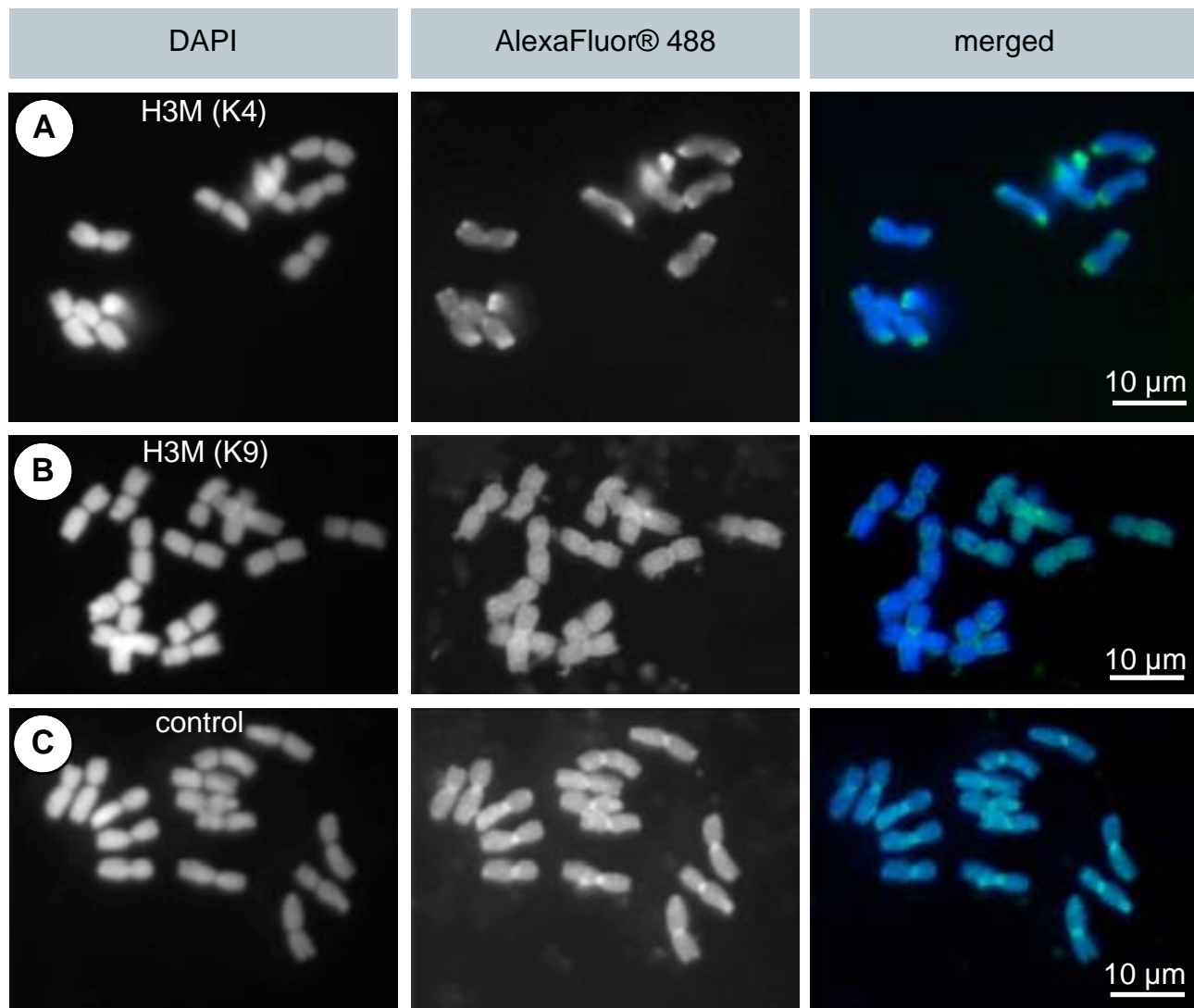


Figure 24

SEM simultaneous BSE and SE images of the same chromosomes shown in Figure 23. SE images (right column) provide chromosome surface structural data for the different applications of fixation protocol and Nanogold® products; BSE images (left column) shows corresponding signal distribution. Chromosomes in **A** and **C** were fixed with formaldehyde and isolated as suspension preparations (“form-fix”). Chromosomes in **B** and **D** were fixed with 3:1 and prepared by the drop/cryo method (“3:1-fix”). Flattened and stretched form-fix chromosomes show strong signals, the signal number for ANG being higher than that for NG. Chromosome surface is not homogenous, and does not fill the criteria for adequate structural preservation. 3:1-fixed chromosomes are three-dimensionally preserved, with exception of chromomeres and distinguishable sister chromatids, and display greater signal number when labeled with ANG than with NG.

**Figure 25**

LM images of barley metaphase chromosomes immunolabeled for H3M (K4)(**A**), H3M (K9) (**B**) and with primary antibody omitted (**C**) with ANG. Fluorescent signals for H3M (K4) indicate an increase in brightness at the telomeres (**A**). H3M (K9) labeling shows weak fluorescence distributed along the entire chromosome arm (**B**). In absence of the primary antibody, ANG has an affinity to the centromere, but also weak fluorescence on the chromosome arms (**C**). Fluorescence for H3M(K9)labeling does not differ significantly from the control specimen for which the primary antibody was omitted.

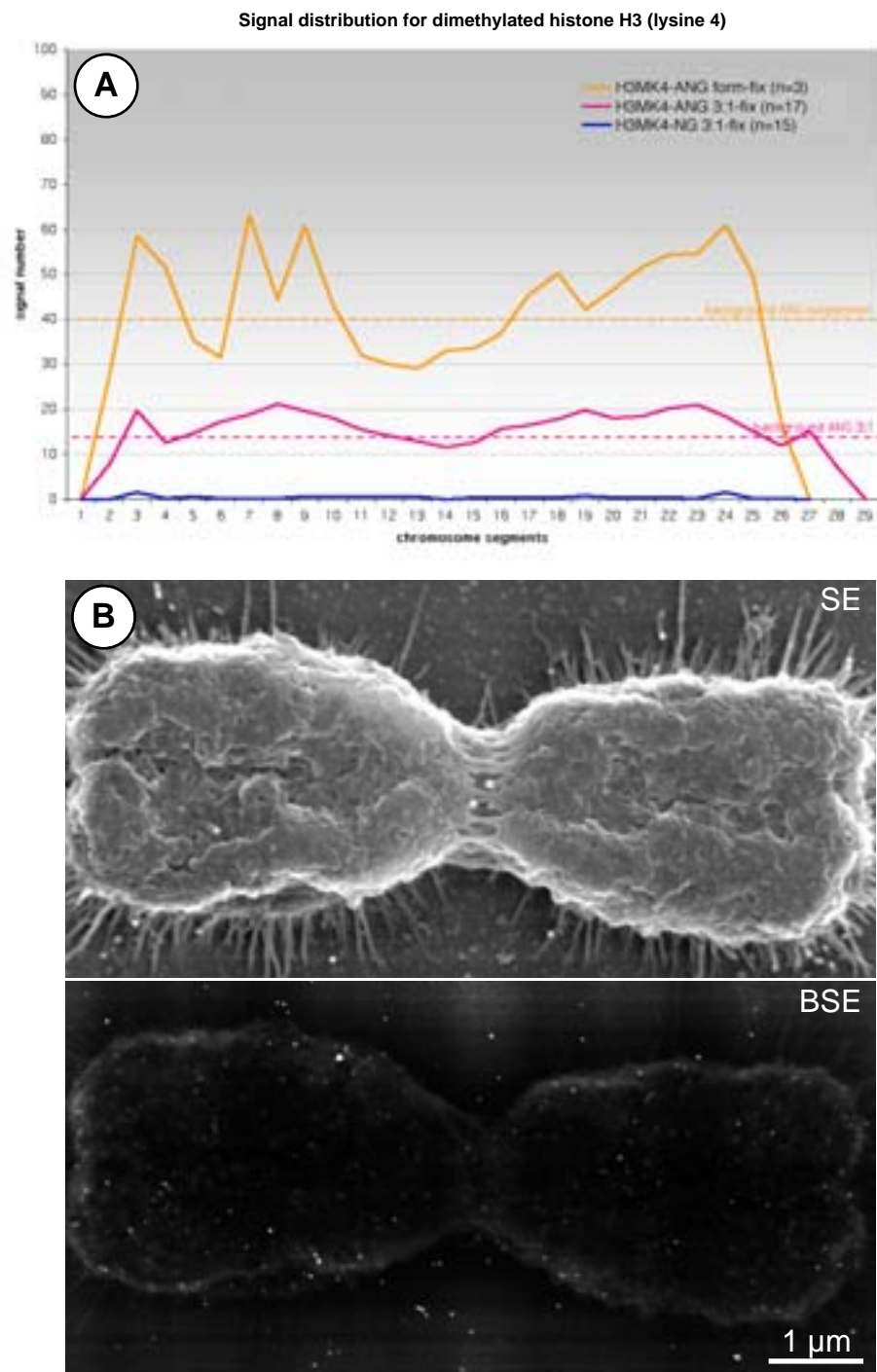
distribution on the chromosome arms cannot be seen. This is indicative of unspecific labeling rather than an even signal distribution.

For SEM investigation, a series of comparative immunogold labeling experiments were performed to determine an optimal combination of fixation and secondary antibody for both H3M (K4) and H3M (K9), as previously shown for H3P. Signals were quantified on individual chromosomes; signal distribution profiles for each application were compiled and superimposed to facilitate comparison. Unspecific labeling was calculated by averaging signal number per chromosome segment from specimens from which primary antibody was omitted.

In SEM, H3M (K4) signals could be detected along the entire chromosome, but a labeling pattern could only be recognized after compilation of data from several chromosomes to a distribution profile (Figure 26 A). Signal number was low in general, indicating poor binding efficiency. Signals could be counted as individual “spots” in all cases (Figure 26 B). The distribution profiles show slight maxima at the distal chromosome arms, with one minimum at the centromere corresponding approximately to the average background level (Figure 26 A). This lateral distribution pattern can be seen with varying “amplitude” for each antibody-fixation combinations. The highest binding efficiency, but also highest unspecific labeling was for chromosomes labeled with ANG. Only chromosomes fixed with 3:1 (drop/cryo method) show adequate three-dimensional structural preservation, albeit without preserved chromomeres and distinct sister chromatids (Figure 26 B).

SEM data for H3M (K9) is consistent with observations from LM (Figure 27 A, B). The BSE image shows very few individual signals with no obvious region of preference (Figure 27 B). Comparison of “specific” signal number with average background on the signal distribution profile reveals that what appears to be a weak but even signal distribution actually reflects unspecific labeling from the secondary antibodies and/or Ag-enhancement for both fixations (Figure 27 A).

Since this result contradicts published data (HOUBEN *et al.*, 2003), further steps were taken to test the affinity of the H3M (K9) antibody for barley chromatin. SDS-PAGE Western blot and silver staining assays could show that the anti-H3M (K9) antibody detects a protein of approximately 17 kDa, the size of histone H3, in precipitates of unfixed, 3:1- fixed, and formaldehyde-fixed barley cell suspensions *in vitro*, and in all corresponding supernatants, with exception of the unfixed cell suspension (Figure 28 A). This affinity is not reflected *in situ* in the present study. Subsequent silver staining of the PAA gel shows a representation of the proteins present in the different fractions (Figure 28 B). The qualitative protein content, as

**Figure 26**

Immunogold signal distribution of H3M(K4) on barley chromosomes. A signal distribution profile summarizes data on H3M(K4) signal distribution on barley chromosomes fixed with different protocols: suspension preparation fixed with formaldehyde (“form-fix”, yellow line) and 3:1 (“3:1-fix”, magenta and blue lines) combined with either NG or ANG secondary antibodies. For all applications, a slight increase of signal number on the distal chromosome arms is indicated (A). No data is available from this assay for the form-fix /NG combination. Dotted horizontal lines of corresponding color indicate the average number of signals per segment on specimens with the primary antibody omitted. Background levels for NG (both form-fix and 3:1-fix) were negligible. Form-fix chromosomes labeled with ANG had the highest signal number, but also the highest background level. Simultaneous SE and BSE images of a 3:1-fix chromosome labeled with AlexaNG prove that the chromosome is three-dimensionally adequately preserved, albeit with less pronounced chromomeres and marginally distinguishable sister chromatids (B, upper image), and that the signal distribution appears rather homogenous along the chromosome arms (B, lower image).

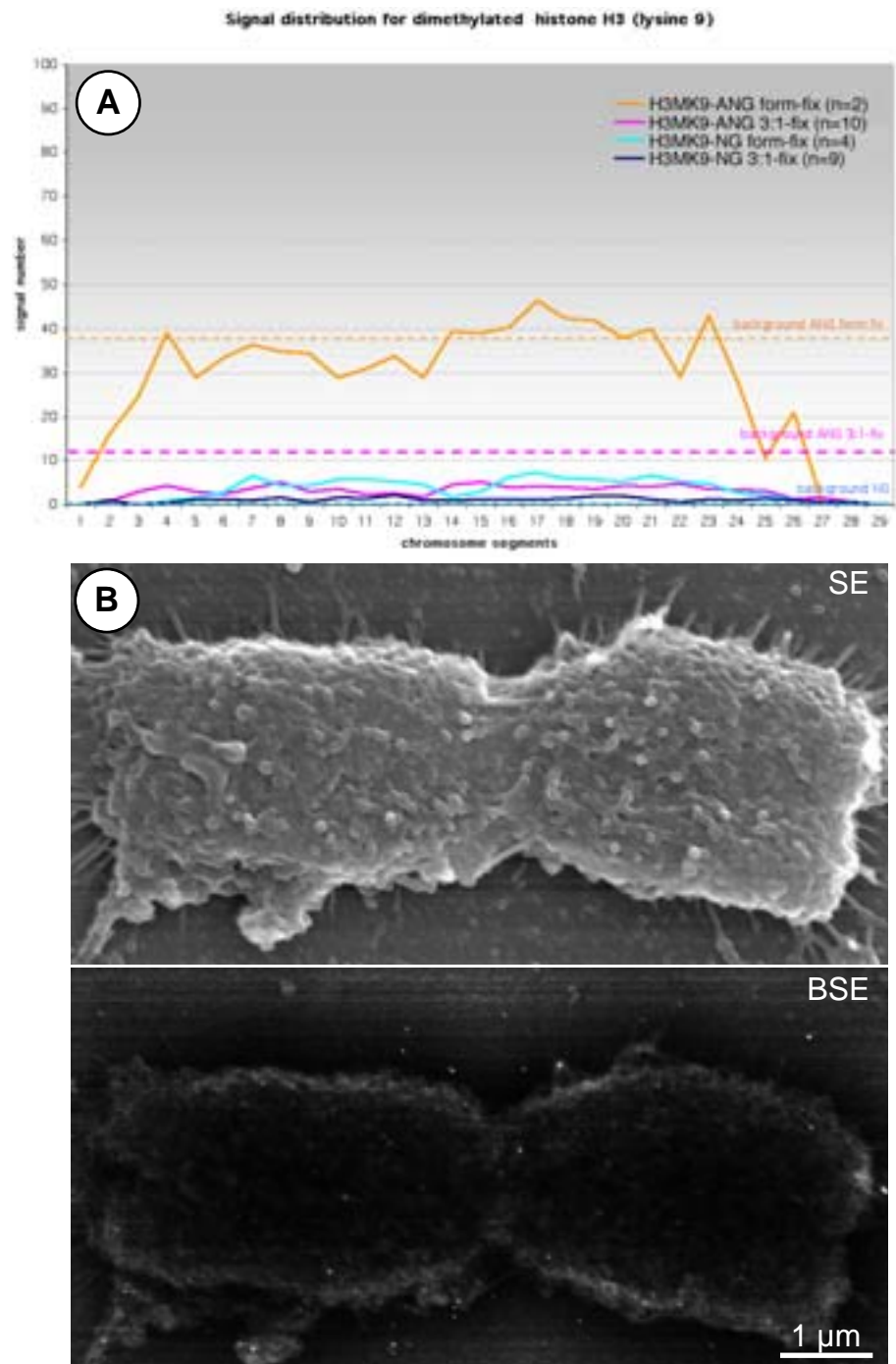


Figure 27

Immunogold signal distribution of H3M(K9) on barley chromosomes. A signal distribution profile summarizes data on H3M(K4) signal distribution on barley chromosomes fixed with different protocols: suspension preparation fixed with formaldehyde (“form-fix”, yellow and light blue lines) and 3:1 (“3:1-fix”, magenta and dark blue lines) combined with either NG or ANG secondary antibodies (**A**). Dotted horizontal lines of corresponding color indicate the average number of signals on specimens with the primary antibody omitted. Distribution curves show that no significant labeling is evident; signal number is approximately the same (or below) background level. Labeling with ANG and formaldehyde fixation results in the highest signal number, represented here by the amplitude of the signal distribution curve, but also the highest background level. Simultaneous SE and BSE images of a 3:1-fixed chromosome labeled with ANG prove that the chromosome is three-dimensionally adequately preserved, albeit with less pronounced chromomeres and barely distinguishable sister chromatids (**B**, upper image), and that signal number is extremely low (**B**, lower image).

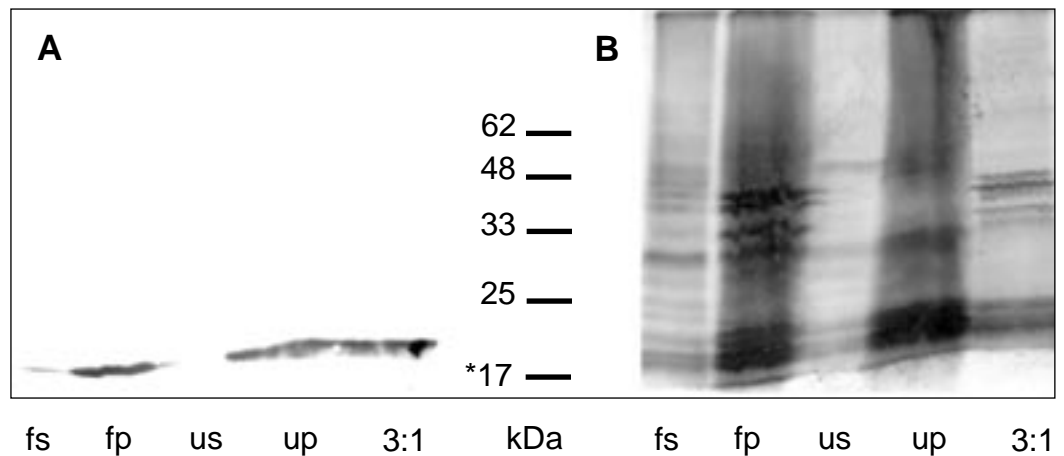


Figure 28

SDS-PAGE analysis of barley cell suspensions fixed with different protocols. Western blot shows bands labeled with the H3M(K9) antibody (**A**); the respective silver staining of the polyacrylamide (PAA) gel represents protein content of the different suspension fractions (**B**). fs=supernatant from formaldehyde-fixed cell suspensions, fp=precipitate from formaldehyde-fixed cell suspensions, us=supernatant from unfixed cell suspensions, up=precipitate from unfixed cell suspensions, 3:1=cell suspension after 3:1 fixation (only precipitate fraction because the soluble contents of the cell suspensions are intentionally washed away during the fixation procedure). The Western blot shows that in all fractions, with exception of the supernatant of unfixed cell suspensions, a protein of approximately 17 kDa, the size of a histone H3 protein, could be detected with the antibody against H3M(K9) used in this study (**A**). Silver staining of the PAA gel used for Western blot shows that the same darkly staining bands can be found in fp and 3:1 lanes (**B**).

determined by number and position of stained protein bands, is the same in fractions fixed with formaldehyde and 3:1 fixative.

3D SEM analysis

Depth perception with back-scattered electron BSE signals

By nature, BSEs conserve enough energy to exit a specimen from a certain range of depths that are loosely defined by the atomic composition of the specimen. As a consequence, the BSE images of immunogold labeled chromosomes represent signals detected from different depths in the chromatin. Signal resolution was compared on BSE images recorded with accelerating voltages from 10-30 kV, influencing penetration depths and diameters of the primary electron beam and exit depths of BSEs (Figure 29). Accelerating voltages below 10 kV produced very weak signals, and were therefore not included in the comparison. To limit experimental variables, Au-enhanced rather than Ag-enhanced preparations were used, providing conditions for which the physical properties of only one heavy metal must be taken into consideration. At 10 kV some signals were bright and had a distinct shape, but other areas were diffuse, albeit with higher contrast to dark “signal negative” areas (Figure 29). Because focus adjustment was aided by the simultaneous SE recording that by nature originates from the chromosome surface, the focused signals at 10 kV can be assumed to be at the surface, and the diffuse signals from varying depths. With increasing accelerating voltage, BSE signals from gold particles could be detected from increasing depths within the chromatin, as evident by tracing signals monitored at different accelerating voltages on identical chromosome regions (Figure 29). Signals from the chromosome interior can be detected only after sufficient energy for exiting BSEs is provided, causing signals to “appear” or become more focused (Figure 29). Tracing surface and subsurface signals on images recorded at 10-30 kV also shows that maximum brightness is displayed at an accelerating voltage of 20 kV, but that resolution continues to increase up to 30 kV (Figure 29). BSE interaction in the volume surrounding the beam entry path increases with increasing beam energy, causing a fraction of the BSEs to be absorbed in the specimen or transformed to inelastic electrons with insufficient energy for detection. BSE interaction volume also varies with specimen composition. For this reason, optimal accelerating voltages for immunogold

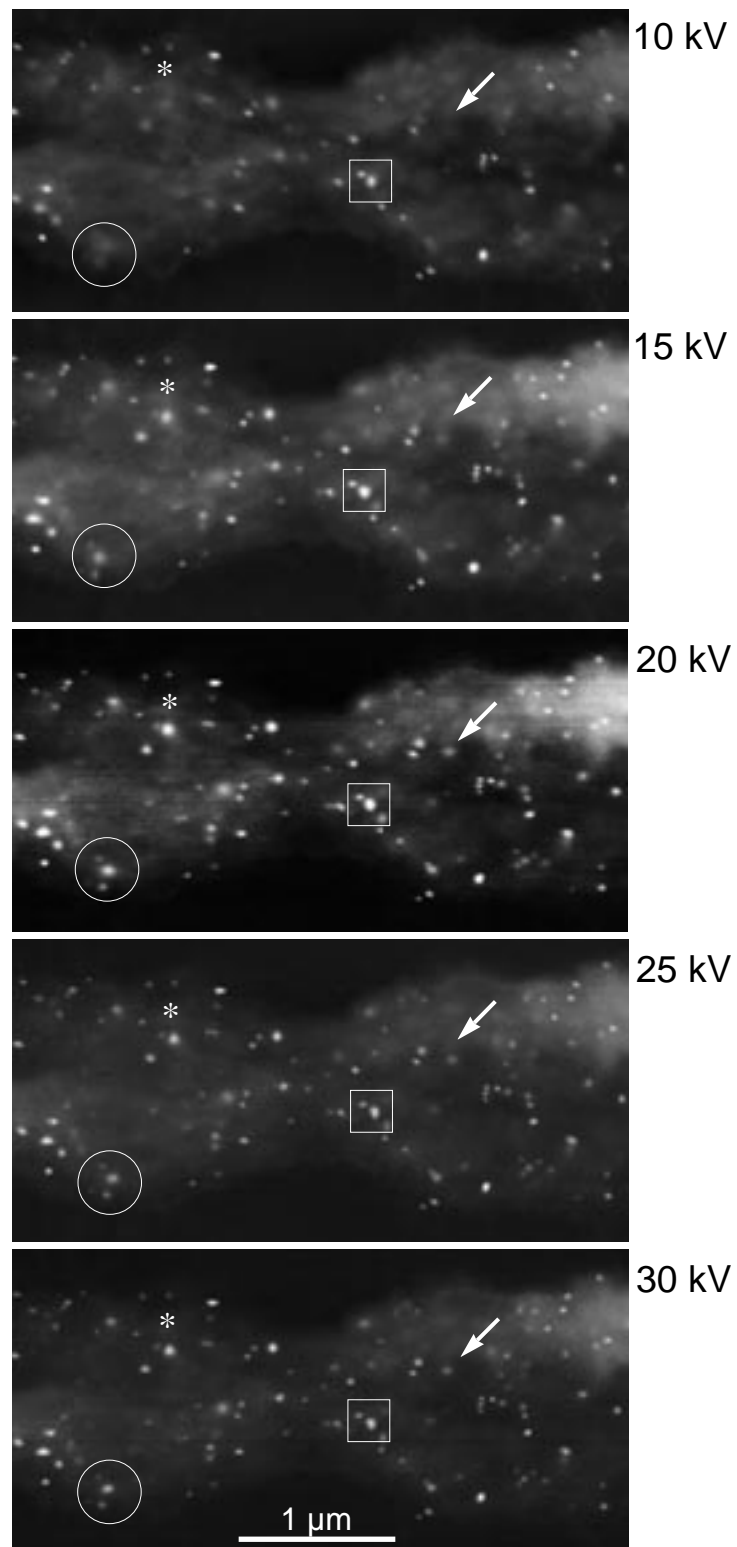


Figure 29

SEM BSE images of a gold-enhanced H3P-NG-labeled barley chromosome taken at different accelerating voltages (kV). With increasing acceleration voltage, signals originating from gold particles from increasing depths within the chromosome can be detected. Areas that show no or only diffuse signals (circle, asterix, arrow) at 10 kV show increasingly stronger signal brightness up to 20 kV, and increasing signal resolution up to 30 kV due to higher interaction volume of BSEs. Signals visible in at all accelerating voltages (e.g. square framed area) originate close to or at the chromosome surface.

labeled chromosome specimens depend on enhancement metal and enhanced particle sizes. For the present study, optimal accelerating voltages varied between 12-20 kV. On the BSE recordings shown, signal spots ranged in diameter, “brightness” and focus, depending on their depths and the diameter of the gold-enhanced particle from which the signal originates. Because chromosome specimens are composed of a mixture of elements of a wide range of atomic number (*e.g.* ^{12}C , ^{79}Au), theoretical exit depth for BSEs originating from enhanced gold particles ranges from 160 nm (theoretical value for solid ^{79}Au) to 1.7 μm (theoretical value for solid ^{12}C), which is sufficient to penetrate the average thickness of a well-preserved critical point dried barley chromosome (600 nm, as reported in SCHAPER *et al.*, 2000).

Two dimensional BSE images represent a projection of information from different depths. Because the signals are not uniform in size, it is difficult to judge its depth orientation by signal diameter alone from these projections. Three dimensional stereo pair images not only prove that signals are detected from different depths, but also assist in establishing depth orientation of neighboring signals to each other (Figure 30). Even signals of non-uniform size can be visually oriented in depth; it can be determined which signals lay in front of or behind each other. In addition, using the general formula (1) for approximation of depths for discrete signals,

$$(1) \quad Z = \frac{P}{2M (\sin^a/2)}$$

where Z is the depth approximation, P is the parallax (the difference between images in distance from the reference point to the point in question), M is the magnification of the image, and a is the angle at which the specimen was tipped (GOLDSTEIN *et al.*, 1992),

signal depths could be calculated ranging between 50 and 400 nm.

Regions detected as strong signal patches in projection images, can be resolved in stereo images as individual signals from different depths, proving that these patches originate not only from signal aggregation due to enhancement, but also from “overlap” of signals from different depths (Figure 30). This overlap limited the precise measurement of the parallax and approximation of the signal depths according to formula (1). Using the diameter of the

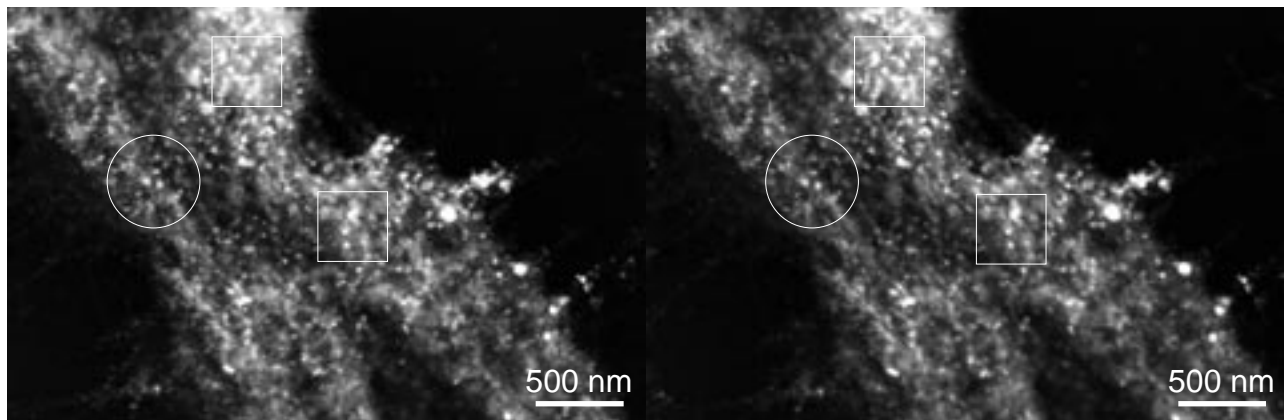


Figure 30

BSE stereo pair of the pericentric region of a barley chromosome labeled for H3P with NG and Ag-enhanced. 3D imaging proves that signals come from different depths. This can be recognized even for signals of non-uniform size (circle). Individual signals can be distinguished in bright areas of signal overlap (squares). (See Appendix for instructions to stereo viewing.)

individual signals as a visual scale, depths of signals in overlap regions could be visually estimated in the range of 30-100 nm.

Optimizing parameters with an alternative specimen

To explore the practical possibilities of more precise depth measurement of BSE signals in SEM, an alternative specimen that was close in composition to immunogold labeled chromosomes was pursued. The bacterium *Enterobacter faecalis*, labeled for a cell surface aggregate protein with 10 nm gold IgG and embedded in epoxy resin, was investigated (GALLI *et al.*, 1989; WANNER *et al.*, 1989). This specimen met the following criteria convenient for depth measurement and comparison to chromosome results: 1) it is carbon-based, 2) regular in size, 3) strongly labeled with gold colloid particles of uniform size, and 4) detectable at moderate SEM magnifications. Sections were of a defined thickness (1- 6 μm), contained preserved bacteria of a defined size range (600 nm), and were labeled with a gold particle of uniform size (10 nm). Sections were examined in SEM at different instrumental parameters: varying spot size with condenser lens current (instrumental unit increments; changing the beam convergence angle and the diameter of the focal point), working distance (mm; the distance between focal point on specimen and objective lens aperture) and accelerating voltage (kV, voltage between anode and cathode). Each parameter theoretically influences signal intensity (number of electrons detected), detection depth, resolution and depth of focus. Initial magnifications applied were 5 000-10 000 fold, comparable to those used for chromosome investigations. Stereoscopic BSE images provide perspective on the location of the bacterial cells and signals in relation to each other.

Since the specimens were slices of (bacteria-containing) resin, the SE images showed the surface of the resin section, but no bacterial surface details (images not shown). The BSE images, on the other hand, showed ghost-like structures composed of strong signal "speckles" from the immunogold labeled bacterial surface outlining a weak diffuse signal from the osmium tetroxide contrasting bacterial cell contents (Figure 31 A). Since the bacteria were embedded as a suspension, distribution of the bacteria in the resin sections is random. Some locations on the specimen included longitudinal and transverse cross-sections of *E. faecalis* as well as tangential areas of the labeled surface aggregate protein (Figure 31 A-C), which were convenient for investigating different signal depths. Specimen resolution due to strong fixation and uniformity of signal size allowed high resolution even at higher magnifications (20 000-25 000-fold) (Figure 31 B, C). Gold signals from the labeled surface protein were clearly distin-

guishable and were visible as individual “spots” of uniform size (Figure 31 A-C). In the sectioned areas a weak diffuse signal could be detected in general at high magnification, in some locations suggesting signals from the other side of the bacterial cell, but no signal details could be discerned (Figure 31 B).

Stereo pair BSE images show that bacterial cells are clearly not located on one plane, as judged in the case of sectioned bacteria by the position and shape of the cut surface and amount of visible immunogold signal from the surface aggregate protein. The orientation of the bacterial cells could be approximated by measuring diameter of the area between surface signals, whereby a diameter of 600 nm was considered the center of the bacterial cell. By monitoring bacterial cross-sections, the effects of varying SEM parameters on resolution of signal depths could be investigated (Figure 32).

Increasing working distance from 14 mm, at which investigations in this study were routinely performed, drastically deteriorated the resolution of the BSE image, preventing demonstration of any effect working distance may have on depth of focus. Decreasing working distance, however, to 11 mm increased resolution of gold signals in combination with other parameters (to follow). Varying only spot size with condenser lens current had slight effect on the resolution of individual gold signals at moderate magnifications (5 000 -10 000 fold) applied. However, in combination with the high accelerating voltage (30 kV), an optimal instrumental setting could be determined. In general, for initial signal detection, a moderate condenser setting was employed to allow generous spot size and maximum number of exiting electrons and maximum signal intensity. Fine adjustment could be made on an appropriate area on the specimen to optimize resolution and instrumental signal to noise ratio, in most cases by decreasing spot size and, in some cases, enlarging the objective aperture. Even with optimal adjustment, signals from the opposite side of bacterial cells could not be resolved.

The effects of accelerating voltage on the depth detection of signals were the most obvious. Within the range of 15-30 kV it could clearly be demonstrated that signals, *i.e.* labeled structures, undetected or weakly detected at lower accelerating voltages, could be detected with increasing resolution and intensity with increasing accelerating voltage (Figure 32). This progression was only observed for signals detected through the epoxy resin, not for signals originating from successively deeper bacterial structures; the epoxy resin, not labeled bacteria,

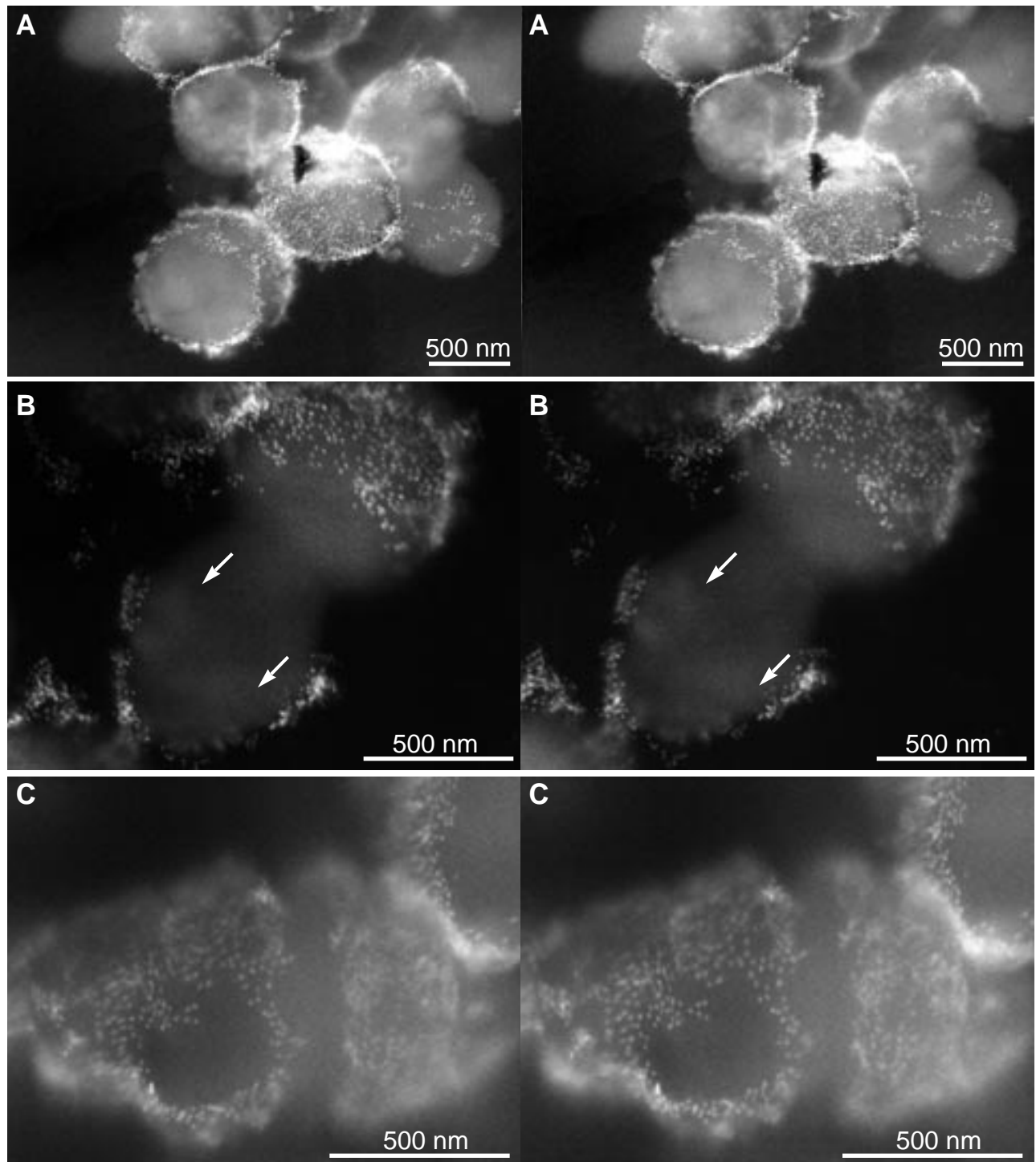


Figure 31

BSE stereo pairs of *Enterobacter faecalis* labeled for a surface aggregate protein and embedded in epoxy resin. **A** and **B** from 5 μm section, and **C** from 2 μm sections. **(A)** Bacteria are not located on one plane and appear in the BSE images as ghost-like structures composed of diffuse signal from interior of bacteria, and relatively uniform signal spots from labeled aggregate surface protein. At this magnification, even with high acceleration voltage (30 kV), signals opposite to surface cannot be detected through bacteria cells. **(B)** Dividing bacteria cross-sectioned diagonally along a considerable length and showing the labeled surface on one end. Arrows show positions at which very weak signals are barely visible. **C** At higher magnification (25 000-fold) signals from uniform 10 nm gold colloidal particles on bacterial surface can be clearly resolved. (See Appendix for instructions to stereo viewing.)

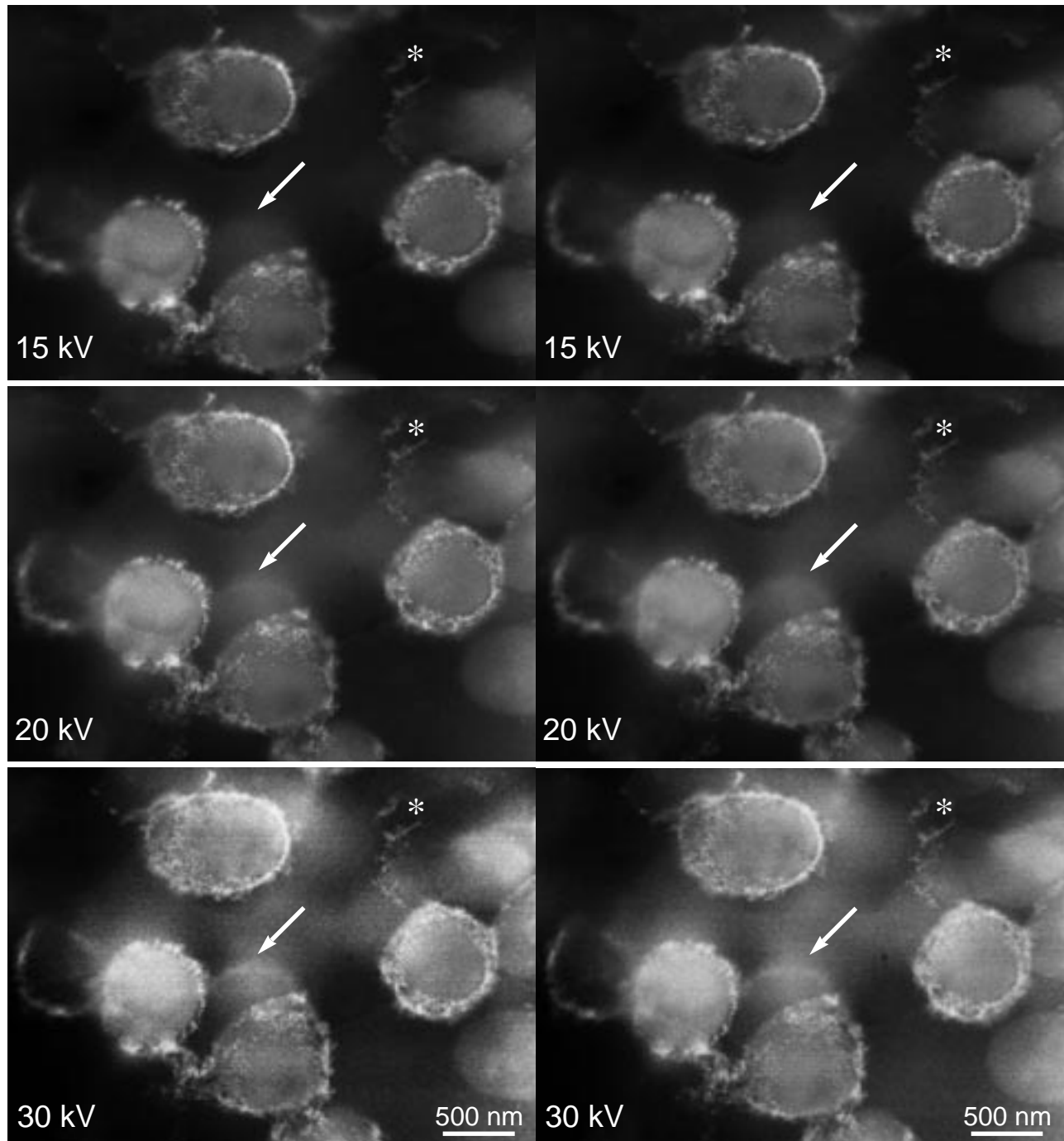


Figure 32 BSE stereo pairs of pre-embedded 10 nm immunogold labeled *Enterobacter faecalis* in a 5 μm epoxy resin section. Images were recorded at accelerating voltages of 15, 20 and 30 kV. Stereoscopic imaging shows that bacteria are not located in the same plane. With increasing accelerating voltage, structures from deeper in the resin section can be detected (asterix, arrow). Resolution is at an optimum at 20 kV, as judged by the recognizable signal spots (asterices), which are concealed by additional diffuse signal at 30 kV. Since increasing the acceleration voltage increases the number and interaction volume of BSEs, a diffuse “background” signal, not only from osmium contrasting, but also from surrounding epoxy milieu and glass slide signals, can be detected. (See Appendix for instructions to stereo view-ing.)

became increasingly “transparent” with increasing accelerating voltage. At 20 kV and 30 kV signals “appear” from a structure that is approximately 300 nm “behind” the sectioned bacterium (assuming the bacterium was medially sectioned as estimated by the diameter of the cross-section, see above). Even with high accelerating voltage (30 kV) and highest condenser setting (smallest spot size), immunogold signals from the opposite side of an individual bacteria could not be detected through the cell contents (Figure 32), presumably due to post-fixation with osmium. For this reason, the depth detection limit for BSEs originating from 10 nm gold particles for this specimen cannot be narrowed down farther than 300-600 nm. Specimen damage was monitored in terms of signal resolution depletion and drift, both of which increased with increasing energy (accelerating voltage) and beam exposure time.

High resolution localization of signals to chromosome structure with SEM

Applying information accumulated from experiments on immunolabeling procedure, signal distribution of H3P on barley, and 3D stereoscopic analysis, a closer look was taken at H3P-labeled barley chromosomes with SEM to attempt to localize H3P signals to specific chromosome structures with high resolution.

As has already been shown, with SEM a signal gap could be resolved at the centromere, which corresponds to exposed parallel fibrils (see Figure 20). By examining labeled chromosomes with high resolution, it was possible to differentiate signal distribution patterns for progressing stages of condensation in metaphase. Up to and including late prophase, at which mitotic stage chromomeres are loosely formed and the constriction and parallel fibrils at the centromere are not yet visible, H3P is homogenously distributed along the entire centromeric region (Figure 33 A). Early metaphase, which can be recognized by length of chromosomes and the appearance of primary constrictions and parallel fibrils, shows increasing signal accumulation toward and across the centromere (Figure 33 B). In late metaphase, signals are accumulated on the chromomeres of the pericentric region bordering the signal gap, measuring approximately 200 nm, which corresponds to the parallel fibrils exposed at the centromere (Figure 33 C).

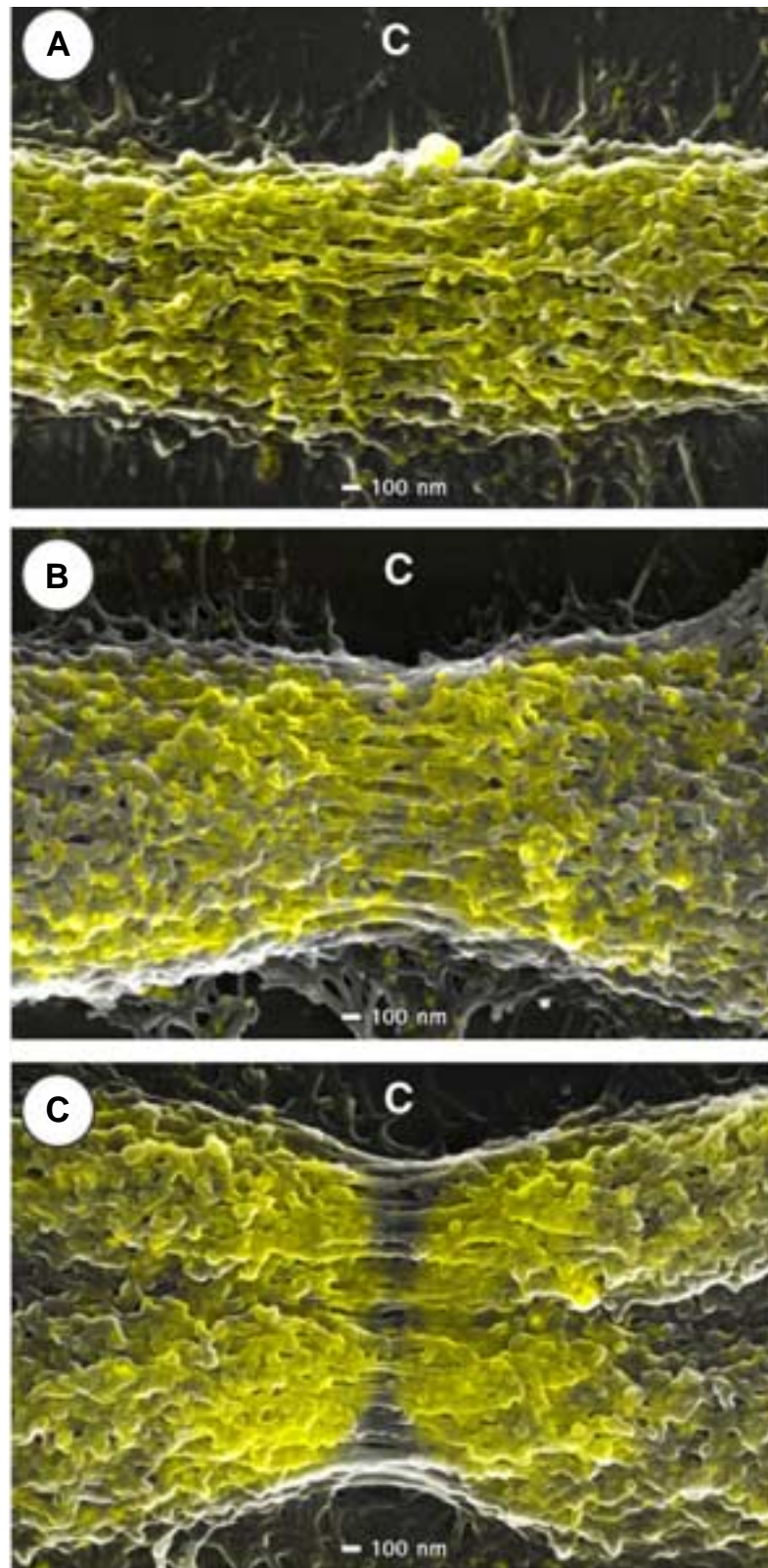


Figure 33

High resolution SEM micrographs of superimposed SE and BSE (yellow) images of the centromeric region (centromere labeled “C” in each micrograph) of barley metaphase chromosomes illustrating the changes of H3P signal distribution and co-localization to chromosome structures from late prophase to late metaphase during mitosis. In prophase and early metaphase, there is an even signal distribution over the centromere which is characterized by parallel matrix fibrils (A and B). In metaphase, the parallel matrix fibrils at the centromere are exposed in a narrow region which is coincident with the signal gap (C). (From SCHROEDER-REITER *et al.*, 2003)

High resolution 3D images of signal distribution

This high resolution signal distribution of H3P can also be imaged in 3D (Figure 34 A, B). 3D SE images of chromosomes provide dimension for surface structures, and show that parallel fibrils are not only locate at the centromere surface, but also from the centromere interior (Figure 34 A, B). 3D imaging of BSE signals proves that signals are located at different depths (Figure 34 A, B). Signals that appear as bright areas can be resolved as individual signals coming from different depths (Figure 34 A, circle). An innovative application of 3D imaging by superimposition of (color) BSE and SE stereo images to a color anaglyph allows 3D visualization of signals and structural information on one image (Figure 35). 3D color imaging of the centromeric and bordering pericentric region of a chromosome labeled for H3P clearly shows that only very few BSE signals can be localized at parallel fibrils even at different depths. A strong signal region bordering can be recognized *behind* the parallel fibrils, proving that labeling is not only on upper chromosome surfaces, but also from accessible depths (Figure 35). This is the most obvious at the interface of centromeric and pericentric region, where both signal regions, and individual signal spots can be observed. Individual signals can be collocated to 30 nm fibrous structures on interior of the centromere and on the chromomeres.

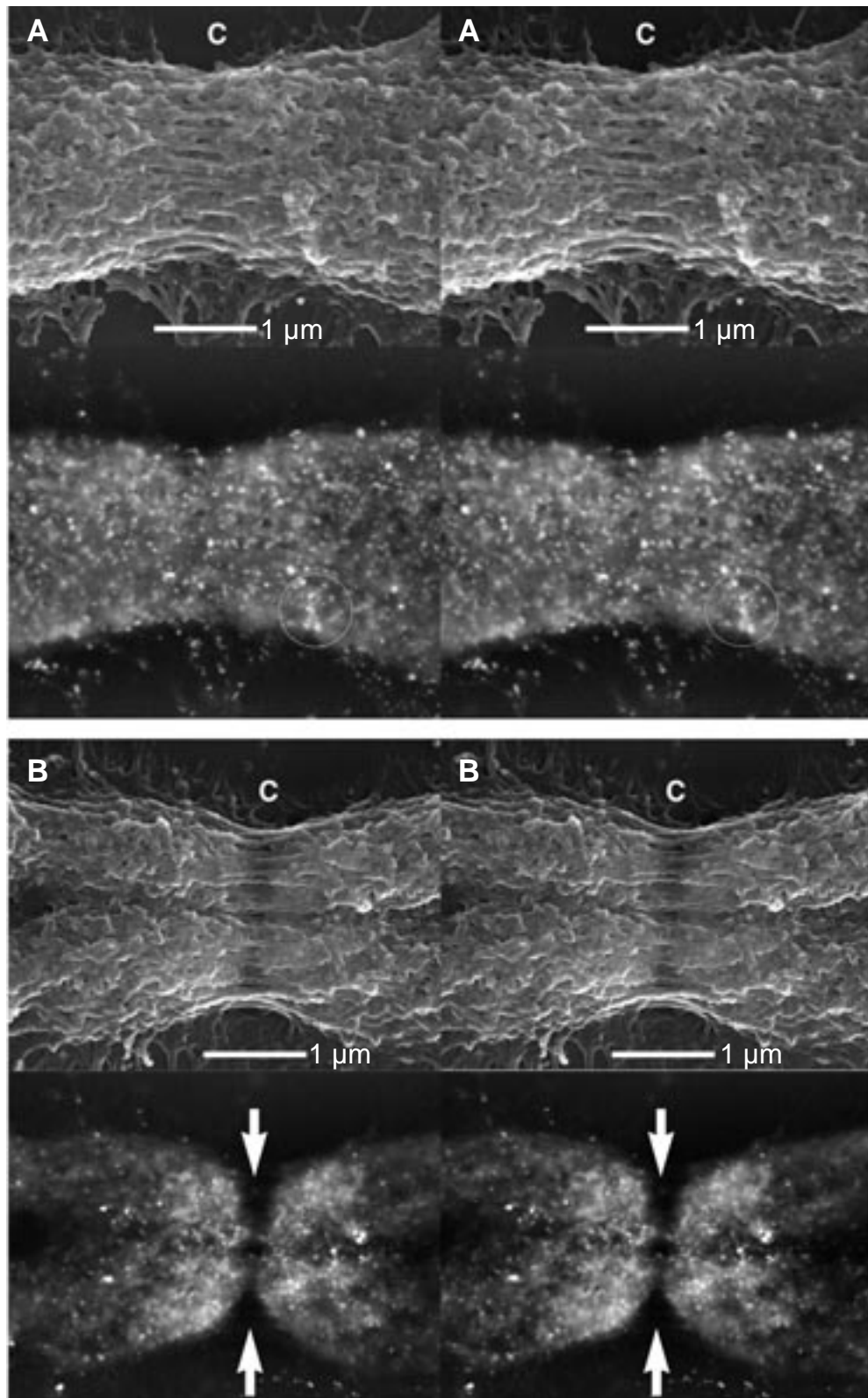


Figure 34

High resolution SE and BSE stereo micrographs of early (**A**) and late (**B**) mitotic metaphase barley chromosomes labeled for H3P with Nanogold® and Ag-enhanced for 6 min from Figure 33. High resolution allows convergence of surface information from SE stereo pairs and three-dimensional depth information from BSE stereo pairs. Signals can be observed from different planes within the chromosomes, facilitating recognition of individual signal spots, especially in regions of high signal density (**A**, circle). Although parallel matrix fibrils at the centromere (**C**) are exposed in both stages of metaphase, the signal gap is exclusive to late metaphase (**B**, arrows). (From SCHROEDER-REITER *et al.*, 2003) (See Appendix for instructions to stereo viewing.)

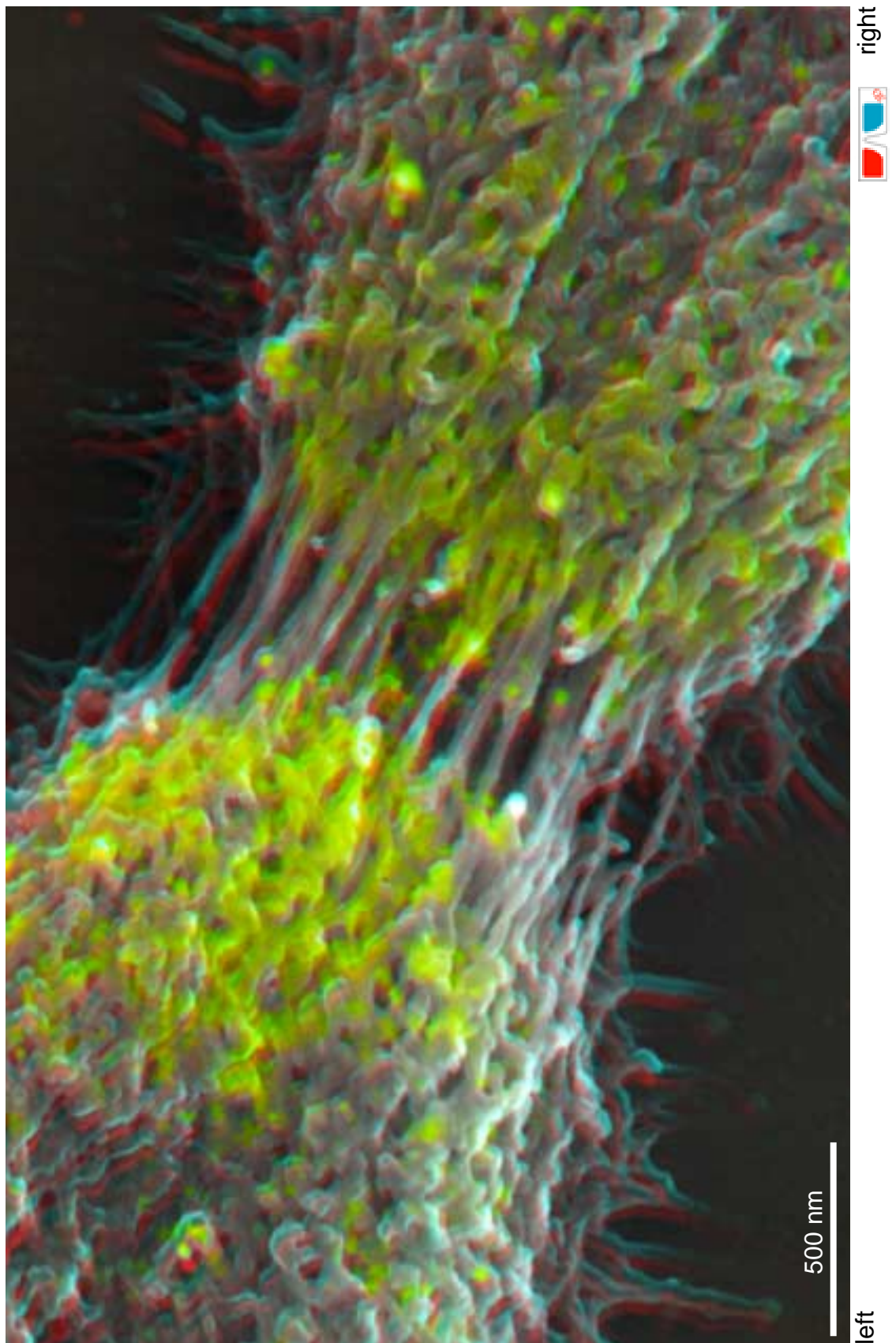


Figure 35

Anaglyph of superimposed SE and BSE micrographs, showing the centromeric region of a barley metaphase chromosomes labeled for H3P with NG and Ag-enhanced (to be turned horizontally and viewed with red/blue stereo glasses, included in back cover). Signals (yellow) are detected from different depths from within the chromatin, especially on the chromomeres bordering the 30 nm parallel fibrils at the centromere. The signal “gap” corresponds to the parallel fibrils. Individual signals can be colocalized to 30 nm fibers in chromomeres and parallel fibrils (With permission from G. Wanner)

Discussion

Universal applicability of drop/cryo chromosome isolation technique

Although there are many techniques currently available, three dimensional structure of chromosomes can be investigated to date with the highest resolution with SEM. Numerous studies implement the drop/cryo technique for high resolution SEM analysis of rye and barley chromosomes (WANNER *et al.*, 1991; MARTIN *et al.*, 1994; WANNER & FORMANEK, 1995, 2000; ZOLLER *et al.*, 2004a, b); equivalent studies for other plant families or for other eukaryotes include few studies for *Tradescantia reflexa*, *Drosophila melanogaster*, and mammalian chromosomes (ALLEN *et al.*, 1986, 1988; SUMNER, 1991; INAGA *et al.*, 2000; WENGENROTH *et al.*, 2001). Models for higher order chromatin structure assume a certain universality in eukaryotes (MANUELIDIS & CHEN, 1990; STACK & ANDERSON, 2001; WANNER & FORMANEK, 2000). Considering differences in nuclear content and in morphology of chromosomes, comparing overall three dimensional chromosome structure of different organisms is not trivial. High resolution structural analysis in SEM provides a means toward this end, but requires good structural preservation in addition to isolation of chromosomes. Testing the applicability of the drop/cryo isolation method to other species both defined the scope of this study and contributed data concerning the universality of chromosome features.

Not all features used as criteria for good structural preservation based on barley chromosomes can be recognized on other chromosomes studied. Constrictions at the centromere, parallel fibrils, and distinguishable sister chromatids cannot be considered generally recognizable features. Although centromere sequences are well-characterized as species-specific heterochromatic repetitive sequences that are essential for chromosome segregation (SUMNER, 2003), it remains unclear why there are constrictions at centromeres, and how centromeres function where constrictions are not obvious, *i.e.* on very small chromosomes. It possible that small chromosomes do indeed have constrictions at the centromere that are not recognizable due to the orientation of chromosomes on the glass slides after “dropping”. In addition, is feasible that chromatin of small chromosomes must economize and take on multiple “functions”, which manifests itself in less specialized structural features. Implementation of Nanogold® labeling for centromere-specific ISH probes in SEM would contribute to solving this question. Parallel fibrils can also not be universally recognized in this study at metaphase, depending on the degree of condensation. They have been observed in SEM in human (WENGENROTH *et al.*, 2001) and in plant chromosomes in less condensed mitotic and meiotic states, not only in the centromeric region, but also along the

chromosome arms, providing evidence that parallel fibrils represent a commonly found structural feature (MARTIN *et al.*, 1996; WANNER & FORMANEK, 2000; ZOLLER *et al.*, 2004a, b). Distinguishability of sister chromatids was not observed for small chromosomes, but was also not exclusive to large chromosomes. It cannot even be generalized for related species: rye has been previously reported to differ from barley in this respect at mitotic metaphase (ZOLLER *et al.*, 2004a). This presents a challenge to universal higher order chromosome models, which must accommodate a condensation modus that allows for easy separation of sister chromatids, even when they appear unified at mitotic metaphase. “Unwinding” of higher order helical coils seems unlikely during mitosis which displays a critical economy of time (takes up only a fraction of the cell cycle) and space (the chromatin is highly compacted by a factor of 40 000). Linearly condensed higher order chromatin, postulated in the Dynamic Matrix Model, allows for different degrees of lateral merging of sister chromatids up to metaphase and for easy separation at anaphase (Figure 36; WANNER & FORMANEK, 2000).

A common surface structure, however, is striking for all chromosomes investigated. Chromosomes show a compact surface that appears only marginally symmetrical, with exception of the degree of condensation that appears identical on both chromatids without exception. In all condensation stages of mitotic chromosomes investigated, no helical winding is evident at the resolution for SEM investigation, an observation that supports recent publications on mitotic and meiotic chromosome structure in rye (ZOLLER *et al.*, 2004a, b). The compact topography seen in mitotic chromosomes with SEM is difficult to precisely define, as chromosomes appear as “soft-lobed” solid entities, but are implicitly a higher order conglomerate of chromatin fibers. Recently, the compact structure has been described as numerous highly condensed chromomeres, which satisfies explicit SEM observations and the implicit definition of a chromosome as a unit of compact chromatin (WANNER & FORMANEK, 2000). This shared quality of chromosome surface structure on all chromosomes studies allows for one tenet of the Dynamic Matrix Model, that the underlying mechanism for this chromosome feature, a linear accumulation and compaction of chromomeres along matrix fibers, is also universal (WANNER & FORMANEK, 2000; Figure 36).

Applicability of the drop/cryo method for chromosome isolation varies for the species studied. For human and chicken, the problem of isolation lies not in three dimensional preservation of chromosomes, but in removal of the nucleoplasmic layer. Due to fixation, even protease digestion could not entirely remove nucleoplasmic residue. In general,

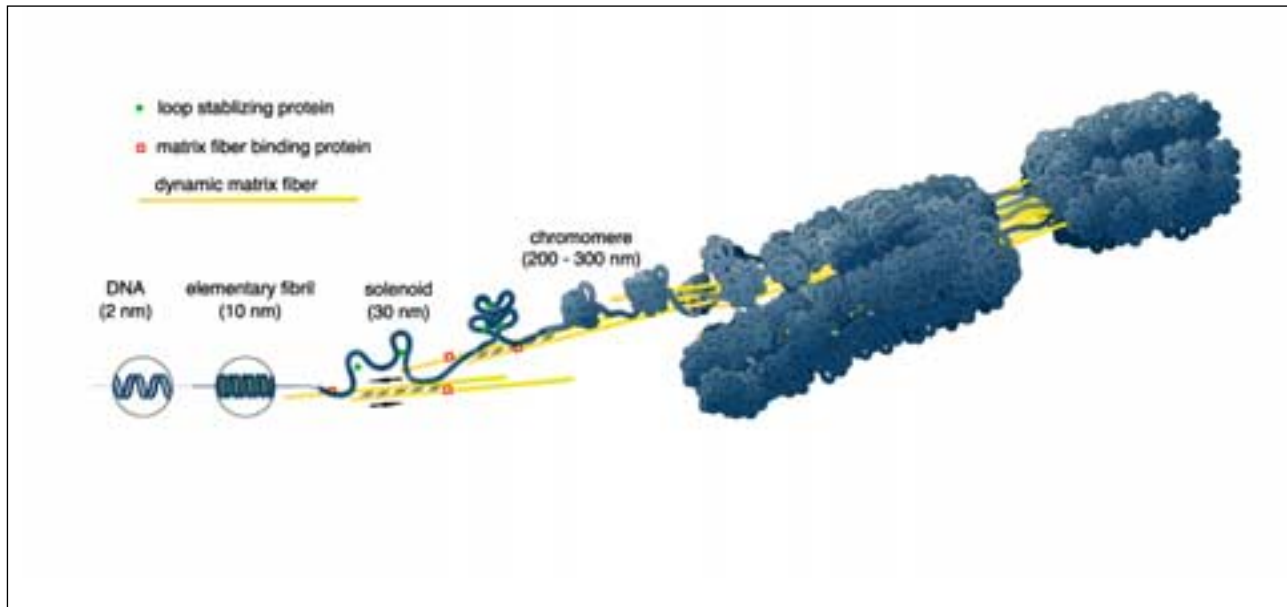


Figure 36

Schematic drawing illustrating different levels of chromatin condensation according to the Dynamic Matrix Model (according to Wanner and Formanek, 2000). DNA (2nm) assembles with histone proteins, forming nucleosomes and the elementary fibril (10 nm) which winds up to a solenoid (30 nm). Solenoids attach to polymerizing matrix fibers by matrix fiber binding proteins. Dynamic matrix fibers associate and move in an anti-parallel fashion (arrows). As condensation progresses, attached solenoid loops are "bunched" into chromomeres (200-300 nm) which are stabilized by loop stabilizing proteins. During condensation chromosomes become shorter and thicker as more chromomeres are formed. This creates a tension perpendicular to the axial direction which forces the chromatids apart. (From WANNER *et al.*, 2004).

however, protease digestion is not ideal in assays attempting to investigate well-preserved chromatin structure and protein participants in chromosome remodeling. For some plant species investigated, nucleoplasm was also persistent, in addition to incomplete metaphase spreading that hindered chromosome accessibility and, in most cases, prevented recognition of structural features.

There are undoubtedly multiple reasons for the various degrees of success for isolating chromosomes of different organisms. Some obvious reasons can be divided into two categories: 1) varying cell composition, in particular of the nucleoplasm, and 2) size of the chromosomes. The packaging of the DNA macromolecule into chromatin and chromosomes, as well as the process of high fidelity transfer of genetic material to progeny by mitosis, is believed to be universal for eukaryotes. The mechanisms involved, however, are different. It cannot be assumed that nuclear content is identical, even for related species. It is not, then, surprising that chromosome isolation techniques should require different modifications for different species. As an example, in mitosis, animal nuclei exhibit bipolar centrioles in their microtubule organizing center (MTC), which are completely absent in plant MTCs. There are structural differences between plants and animals in mechanisms of cytokinesis (APPELS *et al.*, 1998). At initiation of cytokinesis plant cells develop a phragmoplast, assumed to be a microtubule divider providing orientation for excretory organelles involved in the development of the cell wall, whereas animal cells divide by means of progressive medial furrowing of the cell membrane. Laminar proteins line the nuclear membrane of animal cells, but only little data is known to date characterizing “laminar-like” proteins for plants (IRONS *et al.*, 2003; BLUMENTHAL *et al.*, 2004). There are distinctions in functional proteins involved in chromatin remodeling, such as heterochromatin protein (HP), species-specific kinetochores, and structural proteins (SMC) (HECK, 1997; TEN HOOPEN *et al.*, 2002; GAUDIN *et al.*, 2001). These examples illustrate that protein composition differs between even related species, let alone such distant eukaryotic relatives as humans, chickens and barley. Qualitative comparisons of nuclear content of different organisms could demonstrate this difference. Although a variety of cytological techniques, including *in situ* hybridization and staining methods, has proven universally applicable, the drop/cryo technique proves to be only marginally applicable to human and chicken cells, requiring substantial modification for future routine implementation in high resolution SEM analysis.

The drop/cryo method proves generally applicable to the plant species studied with chromosomes 5 μm or larger, with minor modifications of maceration time. Observations over the course of a decade indicate that isolation from nucleoplasm and spreading of metaphase

chromosomes prepared with the drop/cryo method is more complete for larger chromosomes (personal communication G. Wanner; HOUBEN *et al.*, 2000). The results from plants with exclusively small chromosomes, *G. max* and *A. thaliana*, support this observation. For these species, structural details could only be recognized on chromosomes that were somehow lost to their complement, making them extremely difficult to localize, and rendering isolation results highly irreproducible. Although these species, particularly *A. thaliana*, are of global significance in terms of functional genetics and understanding small-scale chromosome architecture, their size in itself makes them unlikely candidates for routine comparative LM and SEM studies of mitotic chromosomes. The fact that the most reproducible isolation and highest resolution of small chromosomes was with *O. biflora* supports earlier observations that the presence of larger chromosomes with smaller ones facilitates spreading and recognition of small chromosomes (HOUBEN *et al.*, 2000). *O. biflora* is therefore a promising specimen for further studies in chromosome architecture with respect to size. *L. sylvatica*, which was also isolated with the drop/cryo method, has proven to be a high yield chromosome specimen, especially considering that preparations are not synchronized and are not arrested. This allows for convenient isolation of a wide range of mitotic stages, and renders it improbable that chromosome compaction is promoted by interference with microtubule spindle assembly (WANNER *et al.*, 2004).

Structural preservation

To date, the classical drop/cryo technique still provides the best preservation of chromosome 3D structure for SEM analysis. 3:1 fixation of cell suspensions prior to dropping is more effective in preserving structure than formaldehyde fixation of root tips prior to their sonification. The drop/cryo method includes chromosome fixation with both 3:1 and glutaraldehyde, stabilizing chromatin enough to allow further analysis (staining of DNA with platinum blue/Pt organic compounds; staining of protein as substance class with silver compounds; controlled enzymatic digestion) with preservation of fine structural details (*e.g.* chromomeres, solenoids, matrix fibrils) (WANNER & FORMANEK, 1995; WANNER & FORMANEK, 2000). Typically, unfixed air-dried chromosomes become totally flat (approx. 60-150 nm) (SHICHIRI *et al.*, 2003). This does not hinder LM analysis, and can even be advantageous for fluorescent microscopy as signals are in one focus plane, but does prevent 3D-structural analysis with SEM. Even under ideal conditions and routine fixation, chromosomes are remarkably elastic and subject to structural changes with change in milieu

(CLAUSSEN *et al.*, 2002; WANNER *et al.*, 2004). Although, shrinkage from critical point drying for SEM must also be taken into consideration, it is not to be equated with flattening, as shown by Schaper *et al.* (2000), and does not preclude 3D analysis. However, a good fixation limits marking efficiency for both *in situ* hybridization (ISH) and immunolabeling; gene sequences and antigenic epitopes are ostensibly not easily accessible or even altered. Any type of fixation (3:1, formaldehyde, glutaraldehyde and combinations thereof) may possibly result in a different “presentation” of epitopes or DNA sequences, and has strong implications on the outcome of an experiment. Omitting glutaraldehyde fixation for immunolabeling increases binding efficiency of antibodies, but has consequences for overall structural preservation considering multi-step labeling procedures. Post-immunogold labeling fixation of the chromosomes contributes to the overall structural preservation, with some compromises in chromosome stability. Further negative influences on structural preservation, *i.e.* of enhancement procedure, critical point drying, or the collective procedural steps for correlative LM and SEM analysis with ANG, would be exacerbated by omitting this fixation.

In the case of immunolabeling of H3P with Nanogold® products, fixation with acetic acid for the drop/cryo method has a hindering but not prohibitive effect on labeling efficiency compared to formaldehyde fixation for the suspension method. Application of the drop/cryo method is justified by its superior preservation of chromosome ultrastructure and its application for large numbers of chromosomes in routine. Reducing steps of the fixation/immunolabeling process for the sake of structural preservation was only possible to a small degree. Blocking and washing steps could not be spared, as insurance of maximum possible labeling specificity is critical for high resolution analysis in SEM. Fixation can also influence the specificity of immunoreagents applied, as in the case of FNG compared to ANG. The presence of FITC on the FNG seems to influence binding on drop/cryo specimens, possibly due to electrostatic forces between immunoreactants and fixative residues (personal communication with FNG manufacturer Nanoprobes). ANG, with its different molecular composition, shows improved binding efficiency. NG (without fluorescent marker) is the most advantageous for binding specificity. Although optimal conditions for binding efficiency of H3M (K4) and H3M (K9) antibodies are not yet determined, these generalizations apply for binding specificity of secondary antibodies and structural preservation.

As it stands, there is no single ideal fixation method for immunolabeling in general. By definition, fixation (Lat. *figere*, to fasten) and analysis (Gr. *ana-* + *lysis* to break apart) are a contradiction in terms. Depending on experimental goals, different fixation techniques should

be compared to reveal the best compromise between structural preservation and labeling efficiency.

Immunogold marker size

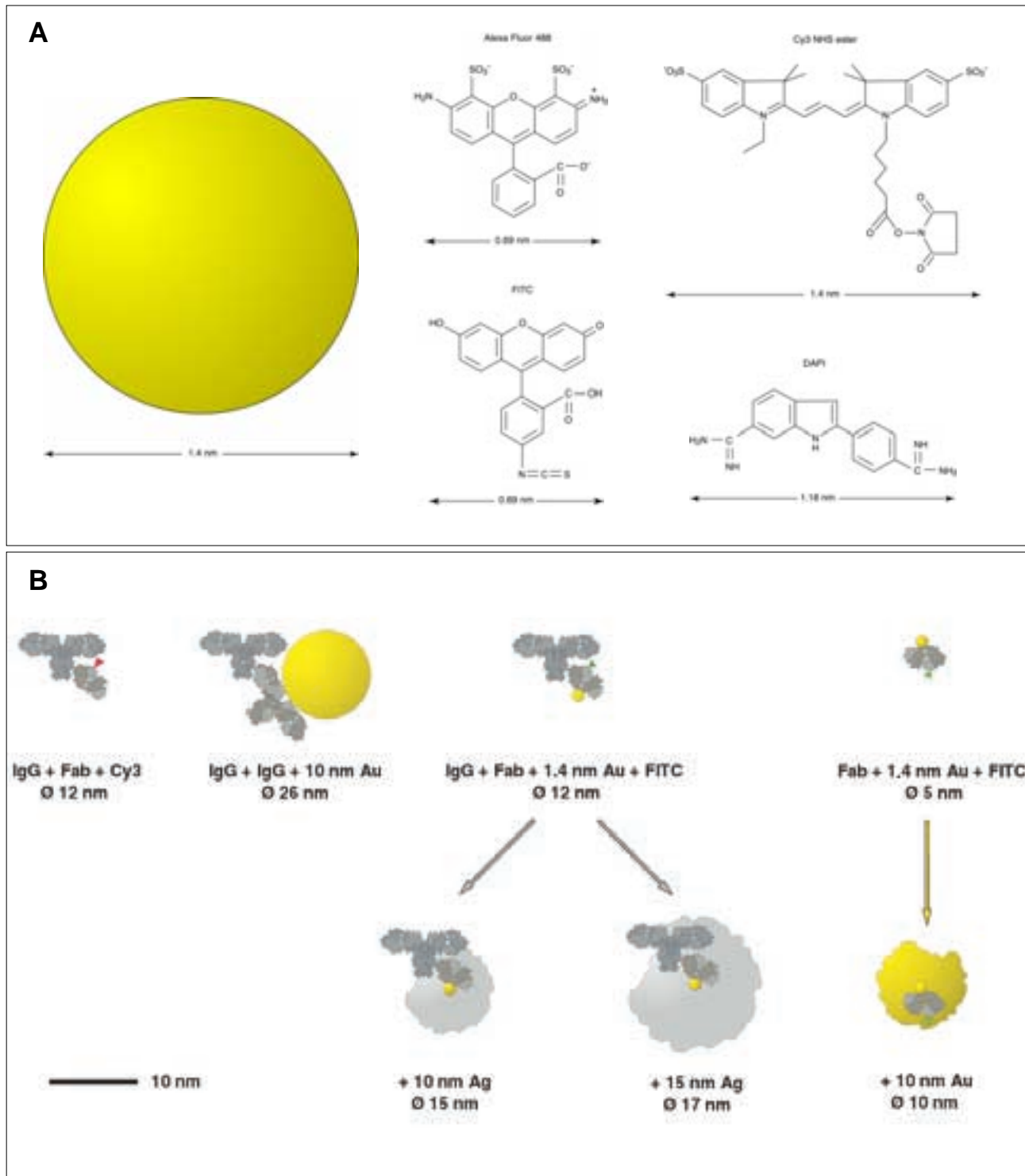
Ideally, high resolution analysis of chromosome ultrastructure in SEM in combination with cytological techniques (ie. DNA and protein staining, immunolabeling for *in situ* hybridization and specific protein detection) requires: (i) best possible preservation of chromosome structure; (ii) ideal markers and (iii) precise labeling.

What is an ideal marker? For routine SEM analysis of chromosomes, a good marker should be a heavy metal, 8-15 nm in diameter, of uniform shape. The most widely used gold marker until the appearance of Nanogold® has been colloidal gold particles (6-15 nm) conjugated to antibodies or immunoreactant proteins (*e.g.* protein A, avidin). Such gold conjugates are routinely applied for TEM studies, but only few studies can be found for SEM (RIS & MALECKI, 1993; HERMANN *et al.*, 1991, 1996; MARTIN *et al.*, 1995). As state of the art, it was shown by Hermann *et al.* (1991) that it is possible to detect 1 nm gold markers conjugated to Fab' fragments on biological specimens with a high resolution "in-lense" field-emission scanning electron microscope (FESEM). This resolution is, however, not easy to achieve with a reasonable amount of effort. For chromosome studies, limiting factors are slide fragments (15 x 15 mm) that are too large for in-lense FESEM, microscope resolution (for 15 kV approx. 2 nm), requiring time-consuming searching and therefore increased beam damage and contamination of chromosomes.

In chromosome research, specific DNA probes via ISH have been detected for barley by means of indirect multi-antibody amplification with 12 nm colloidal gold (MARTIN *et al.*, 1995), but attempts in our lab to reduce the amplification chain of antibodies resulted in negligible signal detection using colloidal gold conjugates. In the past, SEM studies performed in our lab on bacteria have shown strong labeling, albeit for bacterial surface proteins (GALLI *et al.*, 1989; WANNER *et al.*, 1989; RUHLAND *et al.*, 1993; JAURIS-HEIPKE *et al.*, 1999; RÖBLE, 2001). For *Borrelia afzelii*, a direct correlation between size of colloidal gold particle and labeling efficiency (number of signals detected) could be determined (RÖBLE, 2001). In this study, the lack of signals in chromosome experiments using 10 nm gold compared to the strong labeling when using Nanogold® indicates that the size and stability of immunoreactants has indeed been a major problem in SEM chromosome assays. Presumably, this is due to sterical hindrance due to large size of colloidal gold particles compounded by the fact that immunoreactants must also penetrate three-dimensionally well preserved specimens prerequisite for SEM analysis.

An additional problem is the stability of the conjugation of the 10 nm colloidal gold particle to the IgG molecule. Although colloidal gold was not detected in SEM, detection of the anti-rabbit IgG on chromosomes by means of a tertiary fluorescent-labeled antibody proves that the secondary antibody binds specifically, but that the conjugation between antibody and colloidal gold particle is not stable enough to be maintained throughout the preparation for SEM analysis. These large gold particles (6-15 nm) are bound to antibodies by means of reduction of a gold colloid solution, creating a pool of negatively charged gold colloid particles, that in turn bind with positively charged proteins (Nanoprobes product information). The bond between colloidal gold and antibody is essentially of electrostatic nature. For Nanogold® products, the manufacturer claims that the considerably smaller gold particles (1.4 nm) are bound covalently to their respective antibodies by means of a thiol hinge. This stability of the bound gold particle presents a plausible explanation for the improved binding efficiency by implementing Nanogold® over colloidal gold conjugates.

Considering the actual size of the molecules in question, the advantage of Nanogold products is obvious (Figure 37). Nanogold® approaches the size of fluorescent molecules, which considerably reduces the difference in sterical hindrance between gold and fluorescent labeling. Although influence of local electrostatic charges of immunoreactants during binding process cannot be excluded, and the volume difference of a Nanogold® particle is considerably larger than that of “flat” fluorochromes, the diameter of 1.4 nm Nanogold® particle is not significantly larger than the length of a fluorescent molecule (Figure 37 A). For the same reason, there is a clear advantage for implementation of Fab’ fragments, which are one third the size of whole IgG molecules (Figure 37 B). For the indirect labeling system applied in this study using primary and secondary antibodies, the diameter of the entire (unenhanced) labeling complex is approximately 12 nm, a reduction of about 25% from the diameter of two whole IgG molecules (Figure 37 B). The most volume-consuming component in this labeling compound is the primary antibody (Figure 36 B). Aims for future SEM studies should focus on developing direct labeling systems with Fab’ fragments, allowing the least possible sterical hindrance (diameter of 5 nm) (Figure 37) and greatest proximity of the gold particle to the targeted epitope.

**Figure 37**

Comparison of sizes of marker molecules (**A**) and different immuno(gold) antibodies (**B**). (**A**) Nanogold particles with 1.4 nm diameter approach the size of fluorescent molecules. Although there is a volume difference between the spherical Nanogold[®] particle and flat fluorochromes, the diameter of the Nanogold[®] particle is the same length as a Cy3 molecule. (**B**) On a larger scale, sterical hindrance of antibodies to antigens is due mainly to 10 nm gold particles and intact immunoglobulins (IgG), becoming critical with indirect labeling systems using two IgGs. In general, use of small markers which are enhanced after binding are more efficient than unenhanced markers with the ideal size of 10 nm. Using Nanogold[®], the size of gold labeled antibodies approaches that of fluorescently labeled antibodies, therefore equalizing this aspect of immunolabeling efficiency for both LM and SEM. Direct labeling with Nanogold[®] bound to Fab' fragments and subsequent enhancement, preferentially with gold (high atomic number), would ensure the least sterical hindrance and precise signal localization. (**B** previously published in SCHROEDER-REITER *et al.*, 2003).

Metalloenhancement of Nanogold[®]

Because 1.4 nm Nanogold particles are at the resolution limit of SEM, enlargement of the gold particles by metallo-enhancement is necessary for BSE detection, but seems to be critical for overall immunolabeling quality in terms of signal number, specificity and localization. Theoretically, for best BSE signal contrast, and therefore resolution, atomic number of the marker should be as high as possible. For this reason, gold (⁷⁹Au) is preferable to silver (⁴⁷Ag). An additional advantage for gold enhancement is its lower background level. However, in practice silver enhancement results in more favorable labeling than with gold enhancement; silver-enhanced signals are numerous, and their average diameter approaches the desired marker size (see above). Development of a more sensitive gold enhancement procedure, optimizing the chemical and physical parameters of the reagents, could be of great benefit in terms of signal detection contrast. Variation of signal number in experiments with the same enhancement time must be due to unspecific labeling of the antibodies and/or unspecific metallo-nucleation occurring during enhancement. Unspecific metallo-nucleation could be due to unstable reagents or unspecific enhancement of residue halides from buffer, and/or aldehydes from post-fixation (personal communication with Nanoprobes). Variations in fluorescent signal intensity are also observed in LM, supporting the possibility that antibodies bind inconsistently, or even suggesting that immunolabeling is intrinsically inconsistent in binding efficiency. Since at present there is no accurate method to extrapolate the number of bound antibodies from the intensity of fluorescence, a quantitative comparison of binding efficiency in LM and SEM cannot be made

A disadvantage to the enhancement procedure is that it partially obscures the binding site (Figure 37 B). Compound signals, detected as patches in BSE, can form with even few gold markers, making quantification of dense signal regions difficult. More importantly for simultaneous BSE and SE analysis, the precise colocalization of signals to chromosome structure is limited by the size of the enhanced Nanogold[®] particle; signals can be collocated to areas/structures twice the diameter of the signal. Instrumental resolution limit is approximately 2 nm; with ideal specimen stability and fixation, chromosome structures of 10 nm (elementary fibril) can be resolved (WANNER & FORMANEK, 2000). In this study, the structural preservation of the chromosome specimens, and not signal size were limiting in resolving the location of signals. Nevertheless, it could be shown that enhanced signals can be located to structures from chromomeres (200-300 nm) to the solenoid level of chromatin (30 nm). To increase

this resolution, implementation of unenhanced 5-8 nm gold particles would be ideal.

Theoretical considerations for correlative LM and SEM microscopy

When comparing fluorescent signals from LM and BSE signals from SEM images one must keep in mind that they are of a different physical nature and therefore result in images with different overall impressions. Fluorescent signals show a rather continuous signal pattern, and can only be quantified with relative signal intensity. Gold markers detected in the BSE mode of SEM are stable, can be quantified in terms of number of signals (after appropriate enhancement time), but appear to have lower binding efficiency (*i.e.* fewer signals). Both techniques vary in signal to noise ratio, albeit due to different physical phenomena, and, given well-preserved chromosome preparations, can detect signals from different depths or planes of focus. It remains unclear, which signal type represents the highest fidelity to actual epitopes, and whether the apparent differences in signal intensity between LM and SEM are due only to their respective physical differences, or if signals are indeed be lost in further preparation for SEM analysis.

A mathematical exercise proves helpful to estimate how many antibodies would even fit in a given volume of chromatin (assuming free space volume of 30%, SCHAPER *et al.* 2000) (Table 13). The smallest possible marker would be approx. 5-7 nm (Fab' fragment with a fluorochrome/1.4 nm gold marker) for LM/SEM (Figure 37 B). In practice, markers range from 12 nm (primary antibody + Fab' fragment with a fluorochrome/Nanogold®) to 60 nm (primary antibody + Fab' fragment with a fluorochrome/gold or silver enhanced Nanogold®) (Table 13, Figure 37 B). By using small immunoreactants there is enough free space (in well preserved chromosomes) to accommodate markers up to 15 nm in diameter for quantitative labeling of histone H3 (Table 13). Comparing the possible number of histone H3 labels and the number of signals actually counted, it is startling how diminishingly few phosphorylated H3 are detected (Table 13). A recent publication quotes an estimate that only 5% of histones are sterically accessible in nucleosomes (BUSTIN *et al.*, 2004). If this is taken into consideration, the percentage of total H3P detected (last column, Table 13) would be further reduced by a factor of 20. Although highly speculative and provocative, the question poses itself: if sterical hindrance can be excluded, is the labeling efficiency so drastically low, or does this low labeling percentage reflect the degree of phosphorylation for the pericentric area?

Table 13 Estimation of marker accessibility to histone H3 in chromatin

| Marker | Marker \emptyset (nm) | Markers/free space in μm^3 chromatin* | % total H3P potentially labeled [§] | Number of signals/ μm^3 pericentric area | % total H3P detected [¶] |
|--|-------------------------|--|--|---|-----------------------------------|
| Fab' + Cy3 | 5 | $4.5 \cdot 10^6$ | 100% | — | — |
| IgG + Fab' + Cy3/NG | 12 | $3.3 \cdot 10^5$ | 100% | — | — |
| IgG + Fab' + NG + 5 nm gold or silver enhancement | 13 | $2.7 \cdot 10^5$ | 100% | — | — |
| IgG + Fab' + NG + 10 nm gold or silver enhancement | 15 | $1.8 \cdot 10^5$ | 70% | 140 | 0.05% |
| IgG + Fab' + NG + 15 nm gold or silver enhancement | 17 | $1.2 \cdot 10^5$ | 40% | 335 | 0.1% |
| IgG + Fab' + NG + 20 nm gold or silver enhancement | 20 | $7.5 \cdot 10^4$ | 27% | 500 | 0.2% |
| IgG + Fab' + NG + 60 nm gold or silver enhancement | 60 | $3 \cdot 10^3$ | 1% | 75 | 0.03% |

*30% according to Schaper *et al.*, 2001

§assuming 2.7×10^5 H3/ μm^3

¶assuming 2.7×10^5 H3/ μm^3

10^{10} bp/barley genome at metaphase (4n) (Bennet and Smith, 1991)

166 bp/nucleosome

$1000 \cdot 10^7 + 166 = 6 \cdot 10^7$ nucleosomes/barley genome (4n)

14 chromosomes in barley (all similar in size)

$60 \cdot 10^6 + 14 = 4 \cdot 10^6$ nucleosomes/barley chromosome

2 H3/nucleosome = $8 \cdot 10^6$ H3/chromosome

Volume of chromosome $30 \mu\text{m}^3$ (can vary from 10 - $30 \mu\text{m}^3$)

$80 \cdot 10^3 + 30 = 2.7 \cdot 10^5$ H3/ μm^3

Structure and signal detection in three dimension

SE electrons can be detected from a theoretical depth of 1-10 nm of the surface of a specimen, providing topographical information. For structurally well-preserved chromosomes, the SE provides a plastic image allowing insight into regions which are loosened or not compact (*i.e.* parallel fibrils in the centromeric region). The BSE image is created by detecting much higher

energy back-scattered electrons. The primary electron beam has enough energy to penetrate a solid carbon specimen to a depth of 5 μm . SE electrons have only enough energy, given an accelerating voltage of 15-30 kV, to exit the surface of a carbon specimen from a depth of 10 nm; BSE electrons have a theoretical exit depth from carbon of 1.7 μm . AFM studies of chromosomes show that critical point dried drop/cryo chromosomes are a height of 600 nm, so BSEs should be detectable from all depths of a chromosome (SCHAPER *et al.*, 2000). The theoretical beam penetration depth for solid gold is 500 nm, and the BSE exit depth is 160 nm.

Electron energetic properties in immunogold labeled chromosomes are influenced, however, by free space volume (30% by ideal structural preservation of chromosomes, SCHAPER *et al.*, 2000), and by gold or silver particles, and therefore deviate from theoretical values. Exit depth from gold particles is almost certainly greater than 160 nm, as carbon has a less decelerating effect on BSEs than gold. Due to this influence, which varies with chromosome fixation and labeling efficiency, depth boundaries cannot be precisely defined for immunogold labeled chromosomes. In addition, since metallo-enhancement does not result in uniform signal size, it is difficult to judge their depth orientation. Experiments with *Enterobacter faecalis* could show the advantage in signal resolution when gold particles are uniform in size and structures are well fixed. In these specimens, however, depth resolution is limited 300-600 nm presumably due to deceleration of BSEs by osmium. Stereoscopic images of immunogold labeled chromosomes allow relative depth orientation of signals and approximation of the depth of individual signals according to measured parallax, and could be further reduced to 50-400 nm. This resolution is surprisingly low compared to 2D resolution of signals on immunogold labeled chromosomes (10-15 nm) and does not seem to reflect the resolution capability of the electron microscope nor of the specimen. Precise measurement of the parallax depends on resolution of the specimen, size of signal, and exact relocation of specimen after 3° tilting (which is adjusted manually). More sensitive enhancement procedures and /or small direct labeling systems (as discussed previously) would also contribute to the improvement of Z-axis resolution. At present, by combining approaches by stereo viewing (using signal size as a visual scale) and calculating (using the measured parallax), signal depths can be approximately located to depths of 30-400 nm, which is a considerable increase in Z-resolution compared to that of LM (2–0.7 μm).

Phosphorylated histone H3 (serine 10)

Phosphorylated histone H3 at serine 10 (H3P) is a post-transcriptional histone modification found globally in eukaryotes. It is a “dynamic” modification, in that the state of histone phosphorylation changes in a cell cycle-dependent fashion; kinases phosphorylate the histone tail at serine 10 at onset of mitosis, and phosphatases remove the phosphate residue upon completion of mitosis. The distribution pattern for this modification, however, differs between mammalian and plants (HENDZEL *et al.*, 1997; HOUBEN *et al.*, 1999; MANZANERO *et al.*, 2000, 2002; KASZÁS & CANDE, 2000; GARCIA-ORAD *et al.*, 2001; PEDROSA *et al.*, 2001), and as could be confirmed in this study with LM data for human and for plant chromosomes. It is assumed that H3P is a modification involved in chromosome condensation, sister chromatid cohesion and assembly of the kinetochores (WEI *et al.*, 1999; HOUBEN *et al.*, 1999; VAN HOOSER *et al.*, 2001; ZEITLIN *et al.*, 2001). Recently, it was shown that although inhibition of phosphatase by cantharidin results in H3P distribution over the entire chromosome rather than in the pericentric region, plant chromosomes were still able to condense and separate, but displayed in some cases spindle distortion (MANZANERO *et al.*, 2000; 2002). This contributed to the current view that phosphorylation of H3P at metaphase is involved, but not essential for sister chromatid cohesion and condensation (KASZÁS & CANDE, 2000; MANZANERO *et al.*, 2002). This hypothesis fits well with immunocytological and SEM structural data from barley presented here. Signals are found predominantly in the pericentric region, where sister chromatids are so closely associated that they cannot be distinguished. The structural feature of distinguishable, often separated, chromatids on the distal chromosome arms coincides with areas showing the lowest number of signals, suggesting that chromatids separate where histone H3 phosphorylation is not maintained. However, LM data from immunolabeling of *O. biflora*, which has chromosomes that do not have distinguishable chromatids, shows an equally strong pericentric signal as barley in LM, demonstrating that this structural feature is not necessarily coupled with the H3P distribution.

Structures interpreted as kinetochores have been visualized in SEM investigation of barley and *Tradescantia reflexa* chromosomes (MARTIN *et al.*, 1994; INAGA *et al.*, 2000). LM reports describing the dynamics of Aurora kinases and passenger proteins in several organisms co-localize related proteins accumulated in the centromeric region up to anaphase, and illustrates a mode of progressive cycle-dependent protein assembly at the centromere (ADAMS *et al.*, 2001). Considering the strong pericentric H3P signals in the plants presented this study, it could be speculated that H3P is a participant in an analogous mode of centromeric protein accumulation which is involved in kinetochore assembly (VAN HOOSER *et al.*, 2001; TEN

HOOPEN *et al.*, 2002). Development of antibodies for plant kinetochores for comparative LM and SEM studies would allow clarification of this H3P role. Although there is not yet adequate SEM data for labeling of small chromosomes in *O. biflora* and *A. thaliana*, LM labeling for H3P show that entire chromosomes are labeled. It could be speculated that there is an economy of function for small chromosomes, and that their compact chromatin must assume related functions to those of regions on larger chromosomes. Should high resolution investigations reveal that the signal distribution differs on small and large chromosomes in *O. biflora* it would suggest there are size-dependent modes of the functional manifestations of histone H3 phosphorylation, sister chromatid cohesion and mediation of microtubule attachment.

L. sylvatica differs from barley and *O. biflora* in centromere structure and spindle attachment, and does not have distinguishable sister chromatids. No correlation can yet be made between sister chromatid cohesion and the distribution of H3P for *L. sylvatica*. A continuing goal for SEM analysis, granted that binding efficiency can be improved, will be to investigate whether H3P signals can be located to (or excluded from) chromosome substructures on *L. sylvatica*. It would be interesting to determine if chromomeres with interconnecting residual nucleoplasm, as seen in SE images, are perhaps attachment sites for microtubules. The fact that the plant material is not synchronized and not arrested, but still provides copious chromosomes, is an advantage in comparing different mitotic stages. Since the interruption of spindle assembly by arrestation affects chromosome length and compaction (WANNER *et al.*, 2004), omission of arrestation is advantageous for investigation of structural features that are directly related to microtubule attachment to the chromosomes. With respect to kinetochore assembly, the distribution pattern of H3P on *L. sylvatica* is highly interesting due to its holocentric structure. In this study, LM data, but not SEM data, confirmed the observation of Gernand *et al.* (2003) that H3P is equally distributed over the whole chromosome. It remains to be seen if the LM data reflect the amplification of few actual binding sites detected in SEM, or if the efficiency of the immunogold labeling procedure is lacking. Nonetheless, if the postulation is correct that H3P is involved in kinetochore assembly, it would be expected that accumulation sites for H3P would be observed in SEM, since there is ultrastructural evidence of several microtubule attachment regions/kinetochores along the chromosome (BRASELTON, 1971). Until for *L. sylvatica* the distribution pattern of H3P (S10) is further characterized in SEM, claims on the relevance of signal distribution remain speculative.

H3P “signal gap” at the centromere of barley metaphase chromosomes

High resolution analysis with SEM allowed characterization of the signal gap on barley chromosomes at the centromere. BSE data show a change from early metaphase, during which signals are evenly distributed across the centromere, to late metaphase, at which point the centromere becomes more or less a “signal-free zone” or gap. The simultaneous SE data reveal the corresponding structure to this gap is parallel fibrils, which are exposed at late metaphase. Structurally, this exposed region is not a result of CPD-mediated shrinkage, but of arrestation (WANNER *et al.*, 2004). There are several possibilities to explain the signal gap: i) histone H3 is not phosphorylated in this region during final stages of mitosis, ii) histone H3 is replaced by another centromere-specific histone-like protein, for example CENP (VAN HOOSER *et al.*, 2001), iii) there is simply little chromatin in this region during late metaphase, as proven by Pt-blue and AgNO₃ staining (WANNER & FORMANEK, 1995), and the exposed parallel fibrils represent a chromatin-poor structural entity (matrix fibers, WANNER & FORMANEK, 2000).

Dimethylated histone H3 on lysine 4 and lysine 9

Post-replication histone H3 methylation modifications are also currently the subject of a large body of investigations on chromosomes *in situ*. In particular, histone methylation has been studied various plant and animal species (LITT *et al.*, 2001; NOMA *et al.*, 2001; NAKAYAMA *et al.*, 2001; REUBEN *et al.*, 2002; STRAHL *et al.*, 1999; SOPPE *et al.*, 2002; HOUBEN *et al.*, 2003; LEHNERTZ *et al.*, 2003; PETERS *et al.*, 2003; JACKSON *et al.*, 2004). Two dimethylated positions on lysine 4 and lysine 9 of the histone H3 amino-terminus are postulated to code for euchromatin and heterochromatin, respectively. Hopes of correlating structural features with cytologically-defined heterochromatin and euchromatin by immunogold labeling for H3M(K4) and H3M(K9) have not yet been substantiated. The general assumption that heterochromatin is more compactly condensed than euchromatin in all stages of the cell cycle should have recognizable structural manifestations in SEM. Extensive characterization of signal distribution could not be performed for either H3M(K4) or H3M(K9) due, in general, to weak labeling. In the case of (euchromatic) H3M (K4), the distal regions of the chromosome arms, which correspond to C-band negative regions in barley (LINDE-LAURSEN, 1975; ZOLLER *et al.*, 2001), showed the highest number of signals, but no distinguishing structural characteristic could be determined between chromomeres in proximal and distal regions of the metaphase chromosome arms at this level of magnification. In the case of (heterochromatic) H3M (K9), for

which no specific labeling pattern could be determined, it would be expected that a large percent of the chromosome should be labeled, as approx. 85% of total chromatin is estimated to be heterochromatic repetitive sequences for other large plant species (FUCHS *et al.*, 1998). The signal distributions detected in SEM for both H3M isoforms deviate (to different degrees) from a recent report based on fluorescent LM (HOUBEN *et al.*, 2003).

There are technical and functional aspects to consider in attempts to explain this deviation. One pertains to the difference in the nature of detection of fluorochromes and gold signals. What appears to be an even distribution in LM could be the result of (unspecific) signal amplification of fluorescent molecules. For strong signals, as with H3P, this discrepancy is of little relevance. For epitopes that occur less frequently, this discrepancy can be quite dramatic. If, for example, H3M (K9) should, contrary to expectations, be a less frequently occurring epitope, this could explain the difference in overall impression between LM and SEM data.

A further technical point, is the binding affinity of the H3M (K9) antibody to barley chromatin. Recent publications emphasize the batch variation and cross-reactivity of antibodies, which have very different qualities depending on the length and degree of methylation of the peptide used for inoculation (PEREZ-BURGOS *et al.*, 2004). The product used in our study recognizes a synthetic peptide corresponding to amino acids 6-13 (TAR[dimethyl-K] STGG-C) of histone H3. This antibody was independently compared to other antibodies against methylated histones, and was found to have high affinity for dimethylation at lysine 9 (for mouse), but also a slight affinity for another histone modification, tri-methylated lysine 27 (PEREZ-BURGOS *et al.*, 2004). Thorough control experiments cannot be readily performed because, ideally, specific mono- tri- and di-methylated peptides, which are not commercially available, and a prokaryotic histone, which has no amino-terminal tail modifications, should be tested in addition to the chromosome suspensions (PEREZ-BURGOS *et al.* 2004). In the present study, although H3M (K9) labeling was negligible on chromosomes for LM and SEM, Western blots testing H3M (K9) on fractions from different fixed and unfixed barley cell suspensions proved that the antibody used in this study recognizes a protein in the size range of a histone (17 kDa) in all fractions of fixed chromosome suspensions. Although the Western blot test as it stands is not sufficient to determine the antibody's specificity for dimethylation on lysine 9, it does show that, for the fixations relevant in this study, the antibody recognizes a barley epitope *in vitro*. Clearly there must be a difference in accessibility of epitopes under SDS PAGE conditions and *in situ* conditions. An obvious difference would be the tertiary and quater-

nary structure of the protein, and on a higher level of organization, of nucleosomes and chromatin. Although this packaging of histones logically influences their accessibility, it cannot be considered prohibitive, since other neighboring epitopes, *i.e.* H3P, are readily accessible. It is likely that other histone tail modifications or functional aspects of the mitotic cycle prevent recognition of the H3M (K9) epitope.

One possibility is suggested by the fact that serine (10) neighbors the lysine (9) on the histone amino-terminus. Indeed, all methylatable lysines are neighbored by either a serine or a threonine, both of which allow phosphorylation events (PEREZ-BURGOS *et al.*, 2004). As has been well-documented, serine 10 is phosphorylated in the central region of barley chromosomes throughout mitosis, in particular in the pericentric region in late metaphase (HOUBEN *et al.*, 1999; MANZANERO *et al.*, 2002; GERNAND *et al.*, 2003). These regions are C-band positive (LINDE-LAURSEN, 1975; ZOLLER *et al.*, 2001), which are considered heterochromatic and likely candidates for lysine 9 dimethylation (SOPPE *et al.*, 2002). To what extent phosphorylation may mask methylation epitopes has not yet been studied (PEREZ-BURGOS *et al.*, 2004). This could shed new light on the general observation for mammals (PEREZ-BURGOS *et al.*, 2004), and different plant species (HOUBEN *et al.*, 2003) that an even signal distribution, which differs from cytologically defined heterochromatin distribution, can be detected on chromosomes with the dimethylated H3 (K9) antibody. Houben's group champions a model differentiating heterochromatin distribution in large and small plant genomes, noting an even distribution for barley, which is suggested to be due to amplified repetitive sequences distributed along the chromosome arm. It has been shown in *A. thaliana* that dimethylated H3 (K9) is linked to DNA methylation, and is therefore implicit in one form of gene silencing (SOPPE *et al.*, 2002; JACKSON *et al.*, 2004). For animals, different degrees of methylation appear to be involved in plastic modulation of chromatin states because it is selectively associated with DNA sequences (NAKAYAMA *et al.*, 2001; HAKIMI *et al.*, 2002). It is, however, clear that dimethylation on different amino acid residues alone does not characterize heterochromatin or euchromatin, but is part of a dynamic signaling system, which is described as the "histone code" (STRAHL & ALLIS, 2000; JENUWEIN & ALLIS, 2001). The complexity of the histone code, with interaction of different histone modifications and recruitment of protein players, offers a plausible explanation for the plasticity of chromatin in time and space that cannot be explained by gene coding alone. Correlating different grades of methylation to changes in chromatin organization during the cell cycle remains a relevant topic in understanding nuclear function and architecture.

Conclusion

In summary, SEM offers an important link in investigation of structure and function of chromosomes. With custom modifications of isolation techniques for individual species, it should be possible to continue characterizing chromosomal structural features of different eukaryotic species. Characterization of chromosome similarities as well as variations with high resolution SEM analysis will provide a basis for investigation of structural chromosomal deviations (*i.e.* in mutants), especially those manifested in mitosis. At present, chromatin at all levels of condensation in the cell cycle can be resolved with SEM down to the range of the 10 nm elementary fibril. Modern equipment allowing instrumental resolution of about 1 nm would require thinner metal coating of specimens, enabling a significant improvement of specimen resolution down to 2-3 nm, which is in the range of the DNA molecule.

The established immunogold labeling techniques with Nanogold[®] and AlexaFluor-488 Nanogold[®] can be broadly applied for detection of specific proteins and DNA probes (for *in situ* hybridization) in chromosome studies. In the case of histone modifications, since recognition of dimethylated histone H3 isoforms may be influenced by neighboring histone H3 modifications, it would be of interest to investigate the signal distribution of proteins functionally related to chromatin condensation, euchromatin and heterochromatin (*e.g.* kinetochore components, heterochromatin protein1, or SMC components). The development of antibodies for homologous plant proteins is crucial for further in-depth investigation.

As this study shows, immunogold labeling with Nanogold[®] is a promising method to complement high resolution ultrastructural studies of chromosomes in SEM. At present, with indirect labeling localization of epitopes down to the solenoid level (30 nm) is possible. Critical and essential for further investigations with increased sensitivity is the reduction of background by using alternative secondary antibodies and optimizing enhancement. Developing direct labeling systems, preferentially with Fab' fragments (or avidin molecules for ISH) and 5-8 nm gold markers, which would not require enhancement, localization of markers to the elementary fibril should be possible in routine. Depth resolution would also be improved by such innovations, allowing more precise location of signals from chromosome interior with 3D analysis. Identifying components or modifications of chromatin and locating them in a three dimensional context will contribute to further understanding of chromosome architecture and epigenetics.

Summary

Over the past decade, techniques for high resolution investigation with scanning electron microscopy (SEM) have been established for plant chromosomes. Although the efficient drop/cryo technique for fixation and isolation of chromosomes, as well as other analytical techniques for SEM, have contributed to investigation of chromosome substructures from the chromomere (200-300) to the solenoid (30 nm) and elementary fibril (10 nm), specific detection of protein participants in chromatin condensation has not yet been successful.

The aims of the present study were:

- Application of the drop/cryo technique for fixation and isolation of chromosomes from various plant and animal species;
- Establishment of the “suspension preparation” as an alternative (formaldehyde) fixation and isolation method for chromosomes;
- Scanning electron microscopic investigation of the chromosome structure from selected organisms,
- Development of an efficient immunogoldlabeling protocol appropriate for high resolution detection of specific chromosomal proteins, in particular modified histone H3;
- Quantification of general as well as three dimensional signal distribution from projection images and from stereo-pair images.

“Drop/Cryo” Technique

All plant chromosomes investigated could be isolated with the drop/cryo technique with slight modifications in duration of enzymatic tissue dissociation. The following plant species were investigated: *Hordeum vulgare* (barley), *Vicia faba* (field bean), *Arabidopsis thaliana* (thale cress), *Secale cereale* (rye), *Glycine max* (soybean), *Ozoroë biflora* (formerly *Camassia biflora*), and *Luzula sylvatica* (wood rush).

The spreading of chromosomes is critical for recognition of chromosome substructures in SEM, and is related to the size of chromosomes. Spreading and isolation was better for metaphase spreads composed of moderate to large sized chromosomes or of both large and small chromosomes. Chromosomes in species with exclusively small chromosomes tended to aggregate and were poorly isolated from the nucleoplasm.

Chromosomes from chicken (*Gallus gallus*) and human (*Homo sapiens*) could not be isolated from the nucleoplasm with the drop/cryo technique. The long-standing problem of a concealing nucleoplasmic layer persists. The nucleoplasm could only be removed proteolytically from unfixed chromosomes, which as a result did not remain structurally intact.

“Suspension Preparation”

The “suspension preparation” for fixation and isolation of chromosomes could be established for barley chromosomes. It employs a mild fixation of root tips with formaldehyde, and is considered less denaturing to proteins than the drop/cryo fixation that employs ethanol and acetic acid. “Suspension” chromosomes are found individually rather than with their chromosome complement after isolation. Chromomeres and parallel fibrils could be detected on “suspension” chromosomes in SEM, but the overall structural preservation was inconsistent: chromosomes tended to be flatter (than drop/cryo chromosomes) and/or stretched at the centromere. Nonetheless, suspension chromosomes were included in immunogold labeling assays as crucial parallel controls for antibody recognition of epitopes.

Basic Chromosome Structure

A basic “soft-lobed” structure formed by compact chromomeres is common to metaphase chromosomes of all organisms investigated, regardless of genome size, chromosome size, chromosome number and centromeric orientation. Dependent on the degree of condensation, parallel fibrils can be seen on mitotic metaphase chromosomes at primary and secondary constriction sites and, in particular for holocentric chromosomes investigated, distributed along the chromosome arms. This supports the view that there is a universal basic chromosome structure in eukaryotes.

Immunogoldlabeling with Nanogold®

Good structural preservation requires a good fixation, which potentially hinders access of immunoreagents to epitopes. To counteract this, the drop/cryo technique was modified by postponing glutaraldehyde fixation until after immunolabeling was performed. For specific detection of proteins in SEM by indirect immunogold labeling, employing Fab’ fragments bound with Nanogold® 1.4 nm particles dramatically improves labeling efficiency compared to earlier applications of colloidal gold (10 nm) particles. The small size of Nanogold® labeled

antibodies promotes their accessibility to epitopes. Nanogold particles are, however, at the resolution limit of SEM, and must be metallo-enhanced. Silver-enhancement for 6 min results in a signal diameter of approximately 20 nm that is advantageous for viewing entire chromosomes at moderate magnification in SEM. Enhancement procedure takes a toll, however, on the structural preservation of chromosomes and limits localization of the binding site (dependent on the diameter of signals). Development of more sensitive enhancement procedures and of direct immunolabeling systems with Fab' fragments could improve the resolution of the signals and the binding sites.

Correlative LM and SEM with AlexaFluor®488 Nanogold®

An antibody that is labeled with both Nanogold and the fluorochrome AlexaFluor®488 allows microscopic monitoring of the same labeled chromosome regions in LM and in SEM. Comparative investigations show that AlexaFluor®488 Nanogold® results in higher levels of unspecific labeling than (only) Nanogold®. For detection of epitopes occurring in high numbers, signal distribution can be easily determined in spite of this “background”, but for low-number or single epitopes the specificity of AlexaFluor®488 Nanogold® is inadequate.

Quantification of signal distribution of histone H3 modifications

Individual signals on the back-scattered electron (BSE) image can be counted, therefore enabling the quantification of signal distribution over the entire chromosome. Comparison of signal distribution of phosphorylated histone H3 at serine position 10 (H3P) for barley chromosomes of different fixations and Nanogold® antibodies shows that 3:1 fixation with (only) Nanogold® results in optimal labeling specificity, and that labeling efficiency is decreased, but not inhibited by 3:1 fixation.

BSE signal distribution of dimethylated histone H3 at lysine 4 shows weak signals at the distal chromosome arms and correlates with its LM distribution. The signal distribution of dimethylated histone H3 at lysine 9 indicates unspecific labeling and does not correlate to LM data. This raises some questions about the stability of the immunoreagents, but also about possible masking of the targeted epitopes from neighboring chromatin modifications (*e.g.* H3P).

Localizing signals with high resolution

BSE signals can be localized to chromosome structures by superimposing BSE images with SE images. High resolution SEM analysis of H3P distribution on barley chromosomes, shows

an area of strong labeling on the chromomeres in the pericentric region. Under optimal conditions, individual signals can be located to 30 nm chromosome structures (*e.g.* solenoids, matrix fibers). A signal “gap” at the centromere corresponds to exposed parallel fibrils. The signal gap develops during the transition between early and late metaphase, at which mitotic stage the centromeric constriction and parallel fibrils become visible.

3D Analysis of labeled chromosomes

Stereo pair imaging and anaglyphs show that signals come not only from the chromosome surface but also from different depths. 3D analysis of the BSE signal distribution allows the Z-axis resolution of individual signals in strongly labeled regions and the mutual orientation of neighboring signals (*i.e.* determining which is in foreground and which is in background). Signals can be detected from a depth of up to 300 nm. 3D imaging with high resolution in SEM shows that functional modifications of chromatin can be collocated to structural elements in a three dimensional context.

Zusammenfassung

In den letzten 10 Jahren wurden im Arbeitskreis Techniken für die hochauflösende raster-elektronenmikroskopische (REM) Untersuchung von Pflanzenchromosomen etabliert. Mit Hilfe der effizienten “Tropf/Kryo” Methode zur Fixierung und Isolierung von Chromosomen sowie verschiedener analytischen Techniken der Rasterelektronenmikroskopie, konnten chromosomale Strukturen von Chromomeren (200-300 nm), über Solenoiden (30 nm), bis zu Elementarfibrillen (10 nm) nachgewiesen werden. Der REM Nachweis spezifischer Proteine, die an der Kondensation von Chromatin beteiligt sein könnten, war bisher nicht erfolgreich.

Ziele dieser Arbeit waren:

- die Anwendung der Tropf/Kryo Methode zur Fixierung und Isolierung von Chromosomen bei ausgewählten Eukaryonten;
- die Etablierung der “Suspensions-Präparation” als alternative (Formaldehyd-) Fixierungs- und Isolierungsmethode;
- die rasterelektronenmikroskopische Untersuchung der Chromosomenstruktur von ausgewählten Eukaryonten;
- die Etablierung eines effizienten Immunogoldmarkierungsprotokolls, um im REM spezifische Proteine – insbesondere Modifizierungen von Histon H3 – in hoher Auflösung an Chromosomen nachzuweisen;
- die Quantifizierung der Signalverteilung an der Oberfläche sowie aus der Tiefe von immunmarkierten Chromosomen.

“Tropf/Kryo” Technik

Die Tropf/Kryo-Technik zur Fixierung und Isolierung von Chromosomen konnte, mit Modifizierungen der Verdauungszeit des meristematischen Wurzelspitzen Gewebes, für im folgenden aufgeführten Pflanzenchromosomen erfolgreich eingesetzt werden: *Hordeum vulgare* (Gerste), *Vicia faba* (Saubohne), *Arabidopsis thaliana* (Ackerschmalwandkresse), *Secale cereale* (Roggen), *Glycine max* (Sojabohne), *Oziroë biflora* (syn. *Camassia biflora*), *Luzula sylvatica* (Wald Hainsimse).

Die Spreitung der Chromosomen bei der Isolierung ist kritisch für die Erkennung der chromosomalen Ultrastruktur im REM. Sie ist abhängig von der Größenzusammensetzung

der Chromosomen. Sind mittelgroße bis große Chromosomen beteiligt, zeigt sich eine bessere Spreitung und Isolierung vom Nukleoplasma; sind ausschliesslich kleine Chromosomen vorhanden, bleiben die Chromosomen im Verband.

Huhn (*Gallus gallus*)- und Human (*Homo sapiens*)- Chromosomen konnten nach wie vor nicht von der nukleoplasmatischen Schicht isoliert werden. Die Schicht ließ sich nur unter Beeinträchtigung der Strukturhaltung von Chromosomen proteolytisch entfernen.

“Suspensions-Präparation”

Die “Suspensions-Präparation” zur Fixierung und Isolierung konnte an Gerstechromosomen etabliert werden. Die Suspensions-Präparation gilt als schonende Fixierung weil ausschliesslich eine Formaldehyd-Fixierung der Wurzelspitzen vorgenommen wird. “Suspensions”-Chromosomen liegen nach der Isolierung einzeln statt in Metaphasegruppen vor. REM Untersuchungen zeigen, dass “Suspensions”-Chromosomen Chromomere und parallele Fibrillen aufweisen, in ihrer Strukturhaltung sind sie aber unbeständig – die Chromosomen sind generell flacher (als Tropf/Kryo-Chromosomen) und besonders im Centromer-Bereich häufig gestreckt. Die Suspensions-Präparation wurde parallel zur Tropf/Kryo Technik als wichtige Kontrolle für die Antikörpererkennung der unterschiedlichen Epitopen in Immunomarkierungs-Versuchen eingesetzt.

Grundstruktur der Chromosomen

REM-Untersuchungen zeigen, dass die Chromosomen der in dieser Arbeit untersuchten Organismen eine gemeinsame Grundstruktur aus Chromomere haben, obwohl sie sich in Anzahl, Chromosomengröße, Genomgröße und Orientierung des Centromers unterscheiden. Parallele Fibrillen konnten, abhängig vom Kondensationsgrad des Chromatins, im Centromer und bei holozentrischen Chromosomen an den Chromosomarmen nachgewiesen werden. Diese Ergebnisse unterstützen die Annahme einer universellen chromosomalen Grundstruktur für Eukaryonten.

Immunomarkierung mit Nanogold®

Gute Strukturhaltung setzt eine gute Fixierung voraus, die wiederum den Zugang für Immunoagenzien be-/verhindern kann. Die Tropf/Kryo Präparation wurde dahingehend modifiziert, dass die Glutaraldehyd-Fixierung erst nach der Immunomarkierung durchgeführt wird. Bisher zeigte der spezifische REM Protein- und DNA-Nachweis durch indirekte

Immunogoldmarkierung mit colloidalen Goldpartikeln (6-12 nm) eine extrem niedrige Markierungseffizienz. Mit dem Einsatz von Fab'Fragmenten, die mit 1,4 nm Nanogold® Partikel markiert sind, als sekundäre Antikörper wurde die Markierungseffizienz erheblich verbessert. Die geringere Größe erleichtert ihnen den Zugang zu ihren Epitopen.

Die 1,4 nm Nanogold® Partikeln liegen an der Auflösungsgrenze des Rasterelektronenmikroskops, und müssen daher mit Gold oder Silber verstärkt werden. Eine 6 min Silber-Verstärkung ergibt einen Signaldurchmesser von durchschnittlich 20 nm, der für die Detektion von Signalen bei mittlere Vergrößerung günstig ist. Die Verstärkung bringt allerdings Nachteile mit sich: die Strukturhaltung der Chromosomen wird verschlechtert, und die Bindungsstelle wird "verdeckt". Dadurch wird die Zuordnung des erzielten Epitops zu Strukturelementen (abhängig vom Durchmesser des verstärkten Goldpartikels) begrenzt. Die Entwicklung empfindlichere Verstärkungsreagenzien und direkter Markierungssysteme mit Fab' Fragmenten könnte die Auflösung der Signale und der Bindungsstellen verbessern.

Korrelative LM und REM mit AlexaFluor®488 Nanogold®

Mit einem Antikörper, der sowohl mit Nanogold® als auch mit dem Fluorochrom AlexaFluor®488 markiert ist, können dieselben markierten Chromosomen sowohl im Lichtmikroskop (LM) als auch im REM untersucht werden. Vergleichende REM-Untersuchungen zeigten, dass AlexaFluor®488 Nanogold® zu erhöhten unspezifischen Markierung führt. Für Epitope die in hoher Anzahl vorkommen, kann die Signalverteilung trotz dieses "backgrounds" gut erfasst werden; für die Detektion von Epitopen, die selten oder sogar einzeln vorkommen, ist AlexaFluor®488 Nanogold® nicht geeignet.

Quantifizierung der Signalverteilung von Histonmodifizierungen

Einzelsignale können am Rückstreuielektronen (BSE)-Bild gezählt werden, wodurch die Signalverteilung von Epitope entlang des Chromosoms quantitativ erfasst werden kann. Der Vergleich der Signalverteilung von phosphorylierten Histon H3 (H3P) an Gerstechromosomen verschiedener Fixierungen bzw. verschiedener Nanogold®-Antikörper zeigt, dass 3:1 Fixierung in Kombination mit Nanogold® (ohne AlexaFluor®488) die optimale Markierungsspezifität bietet. Durch 3:1 Fixierung wird die Markierungseffizienz abgeschwächt, aber die Antikörper-Epitop-Erkennung wird dadurch nicht verhindert.

Die BSE Signalverteilung von dimethyliertem Histon H3 am Lysin 4 zeigt eine schwache Markierung an den distalen Chromosomarmen, die mit den lichtmikroskopischen Ergebnisse korrelieren. Bei dimethyliertem Histon H3 am Lysin 9 deutet die BSE-Signalverteilung auf eine unspezifische Markierung hin und stimmt nicht mit der gleichmäßigen LM-Signalverteilung überein. Die Stabilität der Reagenzien, unspezifische Fluoreszenz im LM, aber auch die Inhibitionen der entsprechenden Antikörper durch benachbarte Histonmodifizierungen (z.B. H3P) sind mögliche Ursachen für diese Diskrepanz.

Lokalisierung von Signalen in hoher Auflösung

Signale können durch Überlagerung von Sekundärelektronen- und BSE-Bilder mit chromosomalen Strukturelemente lokalisiert werden. Die Immunogoldmarkierung mit H3P zeigt eine starke Markierung an den Chromomeren in der perizentrischen Region von Gerste-Chromosomen. In diesem Bereich sind die Signale sowohl als Einzelsignale als auch Signalaggregate detektierbar. Bei höherer Vergrößerung und bei optimaler Auflösung können Einzelsignale zu 30 nm großen chromosomalen Strukturen (z.B. Solenoide, Matrixfibrillen) zugeordnet werden. Der perizentrische Signalverlauf wird am Centromer über eine Strecke von ca. 200 nm unterbrochen; die exponierten parallelen Fibrillen im Centromer sind nicht markiert. Die Unterbrechung entsteht beim Übergang von früher bis später Metaphase, wenn mit zunehmender Chromosomenkondensation die Einschnürung und parallele Fibrillen am Centromer sichtbar werden.

3D Darstellung von markierten Chromosomen

Stereo-Aufnahmen und 3D Anaglyphenbilder zeigen, dass Signale nicht nur von der Chromosomenoberfläche, sondern auch aus verschiedenen Tiefen des Chromosoms detektiert werden. Die 3D Analyse der BSE-Signalverteilung ermöglicht die Z-Auflösung von Einzelsignalen in Regionen mit Signalaggregaten und die Orientierung von benachbarten Signalen zueinander. Signale können aus einer Tiefe bis zu 300 nm detektiert werden. Die 3D Darstellung der Signalverteilung und der Chromosomenoberflächenstruktur ermöglicht die Zuordnung funktioneller Modifikationen von Chromatin mit chromosomalen Strukturelementen in einem dreidimensionalen Kontext.

References

- ADAMS, R.R., CARMENA, M., EARNSHAW, W.C. (2001) Chromosomal passengers and the (aurora) ABCs of mitosis. *TRENDS in Cell Biology* 11 (2): 49-54.
- ALLEN, T.D., JACK, E.M., HARRISON, C.J., CLAUGHER, D. (1986) Scanning electron microscopy of human metaphase chromosomes. *Scanning Electron Microscopy* 1: 301-308.
- ALLEN, T. D., JACK, E.M., HARRISON, C.J. (1988) The three-dimensional structure of human metaphase chromosomes determined by scanning electron microscopy. In *Chromosomes and Chromatin*. Ed. K.W. Adolph. CRC Press, Inc.: Florida, USA. pp. 51-72.
- APPELS, R., MORRIS, R., GILL, B.S., MAY, CEDRIC E., eds. (1998) *Chromosome Biology*. Kluwer Academic Publishers, Boston, MA, USA.
- ARENTS, G., BURLINGAME, R.W., WANG, B.C., LOVE, W.E., MOUDRIANANKIS, E.N. (1991) The nucleosomal core histone octamer at 3.1 Å resolution: A tripartite protein assembly and a left-handed superhelix. *Proceedings of the National Academy of Science, USA* 88: 10148-10152.
- BENNETT, M.D. & SMITH, J.B. (1991) Nuclear DNA amounts in angiosperms. *Philosophical Transactions of the Royal Society of London* **B334**: 309-345.
- BENNETT, M.D., BHANDOL, P., LEITCH, I.J. (2000) Nuclear DNA amounts in angiosperms and their modern uses – 807 new estimates. *Annals of Botany* **86**: 859-909.
- BLUMENTHAL, S.S.D., CLARK, G.B., ROUX, S.J. (2004) Biochemical and immunological characterization of pea nuclear intermediate filament proteins. *Planta* **218**: 965-975.
- BRADFORD, M.M. (1976) A rapid sensitive method for the quantification of microgram quantities of protein utilizing the principle of protein-dye binding. *Analytical Biochemistry* **72**: 248-254.
- BRASELTON, J.P. (1971) The ultrastructure of the non-localized kinetochores of *Luzula* and *Cyperus*. *Chromosoma* **36**: 89-99.
- BUSTIN, M., ROBINSON, R.C., FRIEDMAN, F.K. (2004) Immunochemical analysis of chromatin. *Methods in Enzymology* **376**: 209-220.
- CLAUSSEN, U., MICHEL, S., MÜHLING, P.I., WESTERMANN, M., GRUMMT, U.-W., KONMEYER-KAUSCHILD, K., LIEHR, T. (2002) Demystifying chromosome preparation and the implication for the concept of chromosome condensation during mitosis. *Cytogenetic and Genome Research* **98**: 136-146.
- COOK, P.R. (1995) A chromomeric model for nuclear and chromosome structure. *Journal of Cell Science* **108**: 2927-2935.
- DUPRAW, E.J. (1965) molecular organization of nuclei and chromosomes. *Nature* **206**:338-343.

- EARNSHAW, W.C. (1991) large scale chromosome structure and organization. *Current Opinions in Structural Biology* **1**: 237-244.
- FUCHS, J., STREHL, S., BRANDES, A., SCHWEIZER, D., SCHUBERT, I. (1998) Molecular-cytogenetic characterization of the *Vicia faba* genome – heterochromatin differentiation, replication patterns and sequence localization. *Chromosome Research* **6**: 219-230.
- GALLI, D., WIRTH, R., WANNER, G. (1989) Identification of aggregation substances of *Enterococcus faecalis* cells after induction by sex pheromones. An immunological and ultrastructural investigation. *Archives of Microbiology* **151**: 486-490.
- GARCIA-ORAD, A., GOMEZ VARGAS, P., VIG, B.K. (2001) Histone H3 phosphorylation of mammalian chromosomes. *Chromosome Research* **9**: 487-494.
- GAUDIN, V., LIBAULT, M., POUTEAU, S., JUUL, T., GENGCHUN Z., LEFEBVRE, D., GANDJEAN, O. (2001) Mutations in LIKE HETEROCHROMATIN PROTEIN 1 affect flowering time and plant architecture in Arabidopsis. *Development* **128**:4847-4858.
- GERNAND, D., DEMIDOV, D., HOUBEN A. (2003) The temporal and spatial pattern of histone H3 phosphorylation at serine 28 and serine 10 is similar in plants but differs between mono- and polycentric chromosomes. *Cytogenetic and Genome Research* **101**: 172-176.
- GOLDSTEIN, J.I., NEWBURY, D.A., ECHLIN, P., JOY, D.C., ROMIG, A.D. JR., LYMAN, C.E., FIORI, C., LIFSHIN, E. eds. (1992) Scanning electron microscopy and X-ray analysis: A text for Biologists, materials scientists, and geologists. 2nd edition. Plenum press: New York.
- GUAGLIANONE, E.R. & ARROYO-LEUENBERGER, S. (2002) The South American genus *Oziroë* (Hyacinthaceae-Oziroeoideae). *Darwiniana* **40** (1-4): 61-76.
- HAINFELD, JAMES F., POWELL, RICHARD D., STEIN, JOSHUA K., HACKER, GERHARD W., HAUSER-KRONBERGER, CORNELIA, CHEUNG, ANNIE L.M., SCHÖFER, CHRISTIAN (1999) Gold-Based Autometallography. Proceedings of the fifty-seventh Annual Meeting, Microscopy Society of America. Springer-Verlag, New York, NY. pp. 486-487.
- HAINFELD, J.F. & POWELL, R.D. (2000) New frontiers in gold labeling. *Journal of Histochemistry and Cytochemistry* **48** (4): 471-480.
- HAKIMI, M.-A., BOCHAR, D.A., SCHMIESING, J.A., DONG, Y., BARAK, O.G., SPEICHER, D.W., YOKOMORI, K., SCHIEKHATTAR, R. (2002) A chromatin remodeling complex that loads cohesin onto human chromosomes. *Nature* **418**: 994-997.
- HARRISON, C.J., ALLEN, T.D., BRITCH, M., HARRIS, R. (1982) High-resolution scanning electron microscopy of human metaphase chromosomes. *Journal of Cell Science* **56**: 409-22.

- HECK, M.M.S. (1997) Condensins, cohesins, and chromosome architecture: How to make and break a mitotic chromosome. *Cell* **1**: 5-8.
- HENDZEL, M.J., WIE, Y., MANCINI, M.A., VAN HOOSER, A., RANALLI, T., BRINKLEY, B.R., BAZETT-JONES, D.P., ALLIS, C.D. (1997) Mitosis-specific phosphorylation of histone H3 initiates primarily within pericentromeric heterochromatin during G2 and spreads in an ordered fashion coincident with mitotic chromosome condensation. *Chromosoma* **106**: 348-360.
- HERMANN, R., SCHWARZ H., MÜLLER, M. (1991) High precision immuno-scanning electron microscopy using Fab fragments coupled to ultra-small colloidal gold. *Journal of Structural Biology* **107**: 38-47.
- HERMANN, R., WALTHER, P., MÜLLER, M. (1996) Immunogold labeling in scanning electron microscopy. *Histochemistry and Cell Biology* **106**:31-39.
- HOUBEN, A., WAKO, T., FURUSHIMA-SHIMOGAWARA, R., PRESTING, G., KÜNZEL, G. (1999) The cell cycle dependent phosphorylation of histone H3 is correlated with the condensation of plant mitotic chromosomes. *The Plant Journal* **18**(6): 675-679.
- HOUBEN, A., WANNER, G., HANSON, L., VERLIN, D., LEACH C.R., TIMMIS, J.N. (2000) Cloning and characterisation of polymorphic heterochromatic segments of *Brachycome dichromosomatica*. *Chromosoma* **109**: 206-213.
- HOUBEN, A. & SCHUBERT, I. (2003) DNA and proteins of plant centromeres. *Current Opinion in Plant Biology* **6**: 554-560.
- HOUBEN, A. DEMIDOV, D., GERNAND, D., MEISTER, A., LEACH, C.R., SCHUBERT, I. (2003) Methylation of histone H3 in euchromatin of plant chromosomes depends on basic nuclear DNA content. *The Plant Journal* **33**: 967-973.
- INAGA, S., NAGURO, T., KAMEIE, T., IINO, A. (2000) Three-dimensional ultrastructure of in situ chromosomes and kinetochores of *Tradescantia reflexa* anther cells by scanning electron microscopy. 2. Whole mounted chromosomes and kinetochores of pollen mother cells and tapetal cells. *Chromosome Science* **4**: 11-20.
- IRONS, S.L., EVANS, D.E., BRANDIZZI, F. (2003) The first 238 amino acids of the human lamin B receptor are targeted to the nuclear envelope in plants. *The Journal of Experimental Botany* **54**: 943-950.
- JACK, E.M., HARRISON, C.J., ALLEN, T.D., HARRIS, R. (1985) The structural basis for C-banding: A scanning electron microscopy study. *Chromosoma* **91**: 363-368.
- JACKSON, J.P., JOHNSON, L., JASENCAKOVA, Z., ZHANG, X., PEREZ-BURGOS, L., SINGH, P.B., CHENG, X., SCHUBERT, I., JENUWEIN T., JACOBSEN, S.E. (2004) Dimethylation of histone H3 lysine 9 is a critical mark for DNA methylation and gene silencing in *Arabidopsis thaliana*. *Chromosoma* **112**: 308-

315.

Jauris-Heipke, S., Röble, B., Wanner, G., Habermann, C., Rössler, D., Fingerle, V., Lehnert, G., Lobentanzer, R., Pradel, I., Hillenbrand, B., Schulte-Spechtel, U., Wilske, B. (1999) Osp17, a novel immunodominant outer surface protein of *Borrelia afzelii*: recombinant expression in *Escherichia coli* and its use as a diagnostic antigen for serodiagnosis of Lyme borreliosis. *Medical Microbiology and Immunology* **187**: 213-219

Jenuwein, T. & Allis, C.D. (2001) Translating the histone code. *Science* **293**: 1074-1080.

Kaszás, E. & Candé W.Z. (2000) Phosphorylation of histone H3 is correlated with changes in the maintenance of sister chromatid cohesion during meiosis in maize, rather than the condensation of the chromatin. *Journal of Cell Science* **113**: 3217-3226.

Laemmli, U.K. (1970) Cleavage of structural proteins during the assembly of the head of bacteriophage T4. *Nature* **227**: 680-685.

Leitch, A.R., Schwarzacher, T., Jackson, D., Leitch, I.J. eds. (1994) *In situ-Hybridisierung*. Spektrum Akademische Verlag: Heidelberg, Germany.

Lehnertz, B., Ueda, Y., Derjuck, A.A.H.A., Braunschweig, U., Perez-Burgos, L., Kubicek, S., Chen, T., Li, E., Jenuwein, T., Peters, A.H.F.M. (2003) Suv39h-mediated histone H3 lysine methylation directs DNA methylation to mammalian satellite repeats at pericentric heterochromatin. *Current Biology* **13**: 1192-1200.

Linde-Laursen, B. (1975) Giemsa C-banding of the chromosomes of 'Emir' barley. *Hereditas* **81**: 285-289.

Litt, M.D., Simpson, M., Gaszner, M., Allis, C.D., Felsenfeld, G. (2001) Correlation between histone lysine methylation and developmental changes at the chicken beta-globin locus. *Science* **293**: 2453-2455.

Manuelidis, L. & Chen, T.L. (1990) A unified model of eukaryotic chromosomes. *Cytometry* **11**: 8-25.

Manzanero, S., Arana, P., Puertas, M.J., Houben, A. (2000) The chromosomal distribution of phosphorylated histone H3 differs between plants and animals at meiosis. *Chromosoma* **109**: 308-317

Manzanero, S., Rutten, T., Kotscheruba, V., Houben, A. (2002) Alterations in the distribution of histone H3 phosphorylation in mitotic plant chromosomes in response to cold treatment and the protein phosphatase inhibitor cantharidin. *Chromosome Research* **10**: 467-476.

Martin, R., Busch, W., Herrmann, R.G., Wanner, G. (1994) Efficient preparation of plant chromosomes for high-resolution scanning electron microscopy. *Chromosome Research* **2**: 411-415.

- MARTIN, R., BUSCH, W., HERRMANN, R.G., WANNER, G. (1995) In situ hybridization and signal detection by high resolution scanning electron microscopy. Kew Chromosome Conference IV. Royal Botanic Gardens. Eds. Brandham, P.E., Bennett, M.D. Kew, England. pp.159-166.
- MARTIN, R., BUSCH, W., HERRMANN, R.G., WANNER, G. (1996) Changes in chromosome ultrastructure during the cell cycle. *Chromosome Research* **4**: 288-294.
- NAKAYAMA, J., RICE, J.C., STRAHL, B.D., ALLIS, C.D., GREWAL, S.I.S. (2001) Role of histone H3 lysine 9 methylation in epigenetic control of heterochromatin assembly. *Science* **292**: 110-113.
- NOMA, K., ALLIS, C.D., GREWAL S.I.S. (2001) Transitions in distinct histone H3 methylation patterns at the heterochromatin domain boundaries. *Science* **293**: 1150-1155.
- PEDROSA, A., JANTSCH, MF, MOSCONE, EA, AMBROS, PF, SCHWEIZE, R D. (2001) Characterisation of pericentromeric and sticky intercalary heterochromatin in *Ornithogalum longibracteatum* (hyacinthaceae). *Chromosoma* **110**: 203-213.
- PELLING, C. & ALLEN, T.D. (1993) Scanning electron microscopy of polytene chromosomes. *Chromosome Research* **1**(4): 221-237.
- PEREZ-BURGOS, L., PETERS, A.H.F.M., OPRAVIL, M.K., MECHTLER, K., JENUWEIN, T. (2004) Generation and characterization of methyl-lysine histone antibodies. *Methods in Enzymology* **376**: 234-254.
- PETERS, A.H.F.M, UBICEK, S., MECHTLER, K., O'SULLIVAN, R.J., DERIJCK, A.A.H.A., PERER-BURGOS, L., KOHLMAIER, A., OPRAVIL, S., TACHIBANA, M., SHINKAI, Y., MARTENS, J.H.A., JENUWEIN, T. (2003) Partitioning and plasticity of repressive histone methylation states in mammalian chromatin. *Molecular Cell* **12**: 1577-1589.
- POWELL, R.D., HALSEY, C.M., HAINFELD, J.F. (1998) Combined fluorescent and gold immunoprobes: reagents and methods for correlative light and electron microscopy. *Microscopy Research and Technique* **42** (1): 2-12.
- RATTNER, J.B. & LIN, C.C. (1988) Radical loops and helical coils coexist in metaphase chromosomes. *Cell* **42**: 291-296.
- REIMER, L. (1985) Scanning Electron Microscopy: Physics of Image Formation and of Microanalysis. Springer-Verlag, Berlin, FRG.
- REUBEN, M. & LIN, R. (2002) Germline X chromosome exhibit contrast in patterns of histone h3 methylation in *Caenorhabditis elegans*. *Developmental Biology* **245**: 71-82.
- RIS, H. & MALECKI, M. (1993) High-resolution field emission scanning electron microscope imaging of internal cell structures after epon extraction from sections: A new approach to correlative ul-

- trastructural and immunocytochemical studies. *Journal of Structural Biology* **111**: 148-157.
- RÖBLE, B. (2001) Elektronenmikroskopische Untersuchungen an Borrelien: Ultrastruktur und Immunocytologie. Dissertation an der Fakultät für Biologie, Ludwig-Maximilians-Universität München.
- RUHLAND, G., HELLWIG, M., WANNER, G., FIEDLER, F. (1993) Cell-surface location of *Listeria*-specific protein p60-detection for *Listeria* cells by indirect immunofluorescence. *Journal of General Microbiology* **139**: 609-616.
- SCHAPER, A., RÖBLE, M., FORMANEK, H., JOVIN, T.M., WANNER, G. (2000) Complementary visualization of mitotic barley chromatin by field-emission scanning electron microscopy and scanning force microscopy. *Journal of Structural Biology* **129**: 17-29.
- SCHROEDER-REITER, E., HOUBEN, A., WANNER, G. (2003) Immunogold labeling of chromosomes for scanning electron microscopy: A closer look at phosphorylated histone H3 in mitotic metaphase chromosomes of *Hordeum vulgare*. *Chromosome Research* **11**: 585-596.
- SCHUBERT, I., DOLEZEL, J., HOUBEN, A., SCHERTHAN, H., WANNER, G. (1993) Refined examination of plant metaphase chromosome structure at different levels made feasible by new isolation methods. *Chromosoma* **102**: 96-101.
- WANNER, G., FORMANEK, H., GALLI, D., WIRTH, R. (1989) Localization of aggregation substances of *Enterococcus faecalis* after induction by sex pheromones. *Archives of Microbiology* **151**: 491-497.
- WANNER, G., FORMANEK, H., MARTIN, R., HERRMANN, R.G. (1991) High resolution scanning electron microscopy of plant chromosomes. *Chromosoma* **100**: 103-109.
- WANNER, G. & FORMANEK, H. (1995) Imaging of DNA in human and plant chromosomes by high-resolution scanning electron microscopy. *Chromosome Research* **3**: 368-374.
- WANNER, G., & FORMANEK, H. (2000) A new chromosome model. *Journal of Structural Biology* **132**: 147-161.
- WANNER, G., SCHROEDER-REITER, E., FORMANEK, H. (2004) 3D Analysis of chromosome architecture: Advantages and limitations with SEM. *Cytogenetic and Genome Research*, in press.
- WENGENROTH, U., SCHUFFENHAUER, S., FORMANEK, H., MURKEN, J., WANNER, G. (2001) Ultrastructural changes of Dnase-I treated human and plant chromosomes. *Scanning Microscopy*, in press.
- WEI, Y., YU, L., BOWEN, J., GOROVSKY, M.A., ALLIS, C.D. (1999) Phosphorylation of histone H3 is required for proper chromosome condensation and segregation. *Cell* **97**: 99-109.
- WOODCOCK, C.L. & DIMITROV, S. (2001) Higher-order structure of chromatin and chromosomes. *Current Opinion in Genetics & Development* **11**: 130-135.

- WRAY, W., BOULIKAS, T., WRAY, V.P., HANCOCK, R. (1981) Silver staining of proteins in polyacrylamide gels. *Analytical Biochemistry* **118**, 197-203.
- ZEITLIN, S.G., BARBER, C.M., ALLIS, C.D., SULLIVAN, K.E. (2001) Differential regulation of CENP-A and histone H3 phosphorylation in G2/M. *Journal of Cell Science* **114**: 653-661
- ZOLLER, J.F., YANG, Y., HERRMANN, R., HOHMANN, U. (2001) Comparative genomic *in situ* hybridization (cGISH) analysis on plant chromosomes revealed by labeled Arabidopsis DNA. *Chromosome Research* **9**: 357-375.
- ZOLLER, J.F., HERRMANN, R.G., WANNER, G. (2004a) Chromosome condensation in mitosis and meiosis of rye (*Secale cereale* L.). *Cytogenetic and Genome Research* **105**: 134-144.
- ZOLLER, J.F., HOHMANN, U., HERRMANN, R.G., WANNER, G. (2004b) Ultrastructural analysis in meiosis I and II of rye (*Secale cereale* L.). *Cytogenetic and Genome Research* **105**: 145-156.

Websites

Plant DNA C-values Database. Royal Botanical Gardens, Kew.

www.rbgekew.org.UK/cval/homepage.html

"Chromosome numbers of selected organisms", administrated by B. Reid, Kean University, NJ, USA

www.kean.edu/~breid/chromoso.htm

The RCSB Protein Data Bank administrated by the Research Collaboratory for Structural Bioinformatics

www.rcsb.org/pdb/index.html

Acknowledgements

I would like to express my gratitude to Prof. Dr. Gerhard Wanner for making this work possible. His commitment as teacher and advisor, his fine-tuned combination of high standards and generosity in a working atmosphere, and his pragmatic approach to problem solving will always be an example to me.

Many thanks also to the members of his lab: Sabine Steiner, the backbone of chromosome studies, for her generous assistance; Silvia Dobler for instruction on preparing sections; Dr. Eva Facher for her contribution to all things “systematic”, assistance in gathering plant material, and helpful suggestions for the manuscript. Not only their expertise, but also their congeniality made it a pleasure to work with them.

I extend due thanks to Renate Reichinger-Bock for collaboration and execution of schematic drawings.

I am indebted to PD Dr. Helmut Formanek for valuable discussions, and for providing the Pt-blue compound. Thanks to the group of Prof. Dr. Thomas Cremer (Biology Dept. II, Human Genetics, LMU, Munich), in particular Dr. Irina Solovei and Dr. Marion Cremer, for supply of human and chicken chromosome specimens, and especially for the opportunity for regular informal discussion in the field of chromosome research. I also thank PD Dr. Andreas Houben (IPK, Gatersleben) for his suggestions and encouragement, and for providing me with plant suspension preparations when needed.

Sources of plant material, Dr. Christian Lindemayer, Dr. Ute Voteknecht, PD Dr. Uwe Hohmann, Irmgard Reiber, and in particular Prof. Dr. Jürke Grau, are gratefully acknowledged.

Many thanks to Agnes Walter, who performed the SDS PAGE analysis, PD Dr. Axel Mithofer for his review of the procedure, and Ronny Kohl for editing my German.

Finally, my heartfelt gratitude goes to Theresa, Sarah and Walter for their unfailing and enduring moral (and otherwise) support.

Appendix

Stereo viewing

The stereo effect from stereo pairs is obtained by viewing two images of the same area taken with some angular difference (for this study 3°) between them. The perception of depth arises from the parallax, *i.e.* the slightly differing images presented to the brain by our two eyes (GOLDSTEIN *et al.*, 1992). If the viewer can fuse the two images visually, the resulting virtual image is perceived three dimensionally.

The three dimensional effect of stereo pairs can be visualized without a special stereo viewer by holding the stereo pair of micrographs slightly closer than normal viewing distance while “crossing” eyes and simultaneously focusing into an imaginary background. Three images appear: the left and right images that are peripherally perceived as unfocused, and the central fused image “popping” into spatial focus.

Anaglyphs are made by superimposing the stereo images in different color channels, one of which is red and the others of which are green and blue, and must be viewed with red/blue 3D glasses. (3D glasses are provided in the back cover for viewing the anaglyph in this study.)

Curriculum vitae

Elizabeth Schroeder-Reiter

- 17 Sep 1964 born in Honolulu, Hawaii, USA
- 1969-76 Juliet Long Elementary School, Gales Ferry, Connecticut, CT, USA
- 1976-81 Ledyard Junior High School, Ledyard High School, Ledyard, CT, USA
- 1981-82 High School Diploma, London Central High School, High Wycombe, GB
- 1982-83 University of Maryland Munich Campus, Munich, FRG
- 1983-86 Bachelors Degree in Germanistik and Fine Arts
Bryn Mawr College, Bryn Mawr, Pennsylvania, USA
- 1986-87 Photolab Assistant, Max-Planck-Institute for Psychology, Munich, FRG
- 1987-90 Lab Assistant, Dept. Neurophysiology, Max-Planck-Institute for Psychiatry, Martinsried, FRG
- 1990 Marriage to Walter Reiter, Munich, FRG
Admission to undergraduate studies in Biology, Ludwig-Maximilians-Universität, Munich, FRG
- 1991 Birth of daughter Theresa Reiter
- 1993 Birth of daughter Sarah Reiter
Leave of Absence from studies (Erziehungsurlaub)
- 1996 Studies resumed
- Sep 1999-
Jul 2000 Thesis: “Vergleichende Licht- und Elektronenmikroskopische Untersuchungen an Gersten-Chromosomen: Optimierung von *in situ*-Hybridisierung und Immunomarkierung”, advised by Prof. G. Wanner, Department of Biologie I, Electron Microscopy, Ludwig-Maximilians-Universität, Munich, FRG
- Oct 2000 Completion of undergraduate studies (Diplom in Biologie)
Ludwig-Maximilians-Universität, Munich, FRG
- Dec 2000 Begin of postgraduate studies under advisorship of Prof. G. Wanner
- 2001 14th International Chromosome Conference, Würzburg, FRG
Lecture: “A New Chromosome Model”